



Universidad de Concepción
Dirección de Postgrado
Facultad de Ciencias Naturales y Oceanográficas
Programa de Doctorado en Oceanografía

**Influencia de los procesos físicos de mesoescala y submesoescala en
la estructura de tamaños de la comunidad fitoplanctónica en Chile
centro-sur**



Tesis para optar al grado de Doctor en Oceanografía

JULY ANDREA CORREDOR ACOSTA
CONCEPCIÓN-CHILE
2019

Profesor Guía: Dra. Carmen E. Morales Van de Wyngard
Depto. de Oceanografía, Facultad de Ciencias Naturales y Oceanográficas
Universidad de Concepción

Profesor Co-Guía: Dr. Samuel Hormazabal Fritz
Escuela de Ciencias del Mar
Pontificia Universidad Católica de Valparaíso

Universidad de Concepción
Dirección de Postgrado

La Tesis de “*Doctorado en Oceanografía*” titulada “*Influencia de los procesos físicos de mesoescala y submesoescala en la estructura de tamaños de la comunidad fitoplanctónica en Chile centro-sur*”, de la Srta. *JULY ANDREA CORREDOR ACOSTA* y realizada bajo la Facultad de Ciencias Naturales y Oceanográficas, Universidad de Concepción, ha sido aprobada por la siguiente Comisión de Evaluación:

Dra. Carmen E. Morales Van de Wyngard
Profesor Guía
Universidad de Concepción
Concepción – Chile

Dr. Samuel Hormazabal Fritz
Profesor Co-Guía
Pontificia Universidad Católica de Valparaíso
Valparaíso – Chile

Dr. Marco Correa Ramírez
Miembro Comité de Tesis
Instituto de Investigaciones Marinas - INVEMAR
Santa Marta – Colombia



Dr. Ángel Rodríguez Santana
Miembro Comité de Tesis
Universidad de Las Palmas de Gran Canaria
Las Palmas de Gran Canaria – España

Dr. Marcel Ramos Quezada
Evaluador Externo
Universidad Católica del Norte
Coquimbo – Chile

Dra. Pamela Hidalgo
Directora
Programa de Doctorado en Oceanografía
Universidad de Concepción
Concepción – Chile

A mi mami y hermanito



Quiero agradecer a mi familia colombiana y chilena por todo su apoyo incondicional a lo largo de este proceso. A mi mami y hermanito, los motores de mi vida. A Pizarrito, mi compañero de vida y quien llena de amor cada uno de mis días. A mis abuelos, tía y tíos, primas y primos quienes han estado siempre conmigo sin importar la distancia. A la familia de Matías por acogerme como una hija más. Un reconocido agradecimiento a mi profesora Guía Carmen Morales, por su ejemplo, sus enseñanzas, sus consejos y de quien siempre he recibido apoyo. Agradezco también a mi profesor co-guía Samuel Hormazabal y a los investigadores Oscar Pizarro, Rubén Escribano, Ángel Rodríguez, Robert Brewin y Marco Correa por sus conversaciones y enseñanzas. Junto con ellos, agradezco la acogida y el apoyo a los equipos de trabajo en los laboratorios de los profesores Carmen Morales (UdeC) y Samuel Hormazabal (PUCV). Agradezco a mis amigas y amigos de Colombia y Chile quienes me han acompañado a lo largo de esta travesía y de quienes siempre he recibido las mejores energías, especialmente a las rolitas y la caleña, así como también a mis amigos de la cabina 7 y a los que he tenido la oportunidad de conocer en otros rincones del mundo. Agradezco también a Mónica Sorondo, Fabiola Gaete, Gisela Letelier, Alexis Riquelme y al juicioso por toda su colaboración y buena voluntad en todo momento.

Finalmente, agradezco el financiamiento otorgado para mi formación en el doctorado y el desarrollo de esta tesis. A la Beca de Doctorado en Chile para Estudiantes Extranjeros CONICYT, al Instituto Milenio de Oceanografía (IMO) y a los proyectos FONDECYT 1120504, 1151299 y 1171895.

Curriculum Vitae

JULY ANDREA CORREDOR ACOSTA

Nacida el 28 de Abril, 1984, en Bogotá, Colombia

2005-2010: Grado Académico: Licenciatura en Física, Universidad Distrital Francisco José de Caldas, Colombia.

2011-2014: Magíster en Ciencias con mención en Oceanografía, Universidad de Concepción, Chile.

2013-2019: Doctorado en Oceanografía, Universidad de Concepción, Chile.

DISTINCIONES/BECAS

2007-2009. Beca total arancel por rendimiento académico, Universidad Distrital Francisco José de Caldas, Colombia.

2011-2012. Beca para estudios de Magíster, Dirección de Postgrado, Universidad de Concepción, Chile.

2013-2017. Beca Doctorado en Chile para Extranjeros, CONICYT, Chile.

2013. Beca de subsidio de viaje y estadía por parte del grupo “GeoHydrodynamics and Environment Research – GHER” para participar en “The 45th International Liege Colloquium. Primary Production in the ocean: from the synoptic to the global scale”, Bélgica.

2015. Beca de subsidio de viaje y estadía por parte de “Scientific Committee on Oceanic Research – SCOR” para participar en “Second International Ocean Color Science Meeting”, Estados Unidos.

2015. Beca de subsidio de viaje y estadía por parte de “NF-POGO CofE – AWI” para participar del curso “Regional Training. Phytoplankton bio-optical variability: application to the study of coastal systems”, México.

2016. Beca de subsidio de viaje y estadía por parte de “Integrated Marine Biosphere Research – IMBeR Project” para participar en “CLIVAR Open Science Conference and Early Career Scientists Symposium”, China.

2018. Beca finalización de tesis doctoral, Instituto Milenio de Oceanografía – IMO, Chile.

PUBLICACIONES

- Corredor, A., Sandino, M. 2009. Las TIC's como herramienta de investigación científica. Revista Góndola, 4: 25-29. ISSN: 2145-4981.
- Corredor-Acosta, A., Acosta, A., Gaspar, P., Calmettes, B. 2011. Variation in the surface currents in the Panama Bight during El Niño and La Niña events from 1993 to 2007. Bol. Invest. Mar. Cost., 40: 33-56.
- Corredor-Acosta, A., Morales, C. E., Hormazabal, S., Andrade, I., Correa-Ramirez, M. 2015. Phytoplankton phenology in the coastal upwelling region off central-southern Chile (35-38°S): time-space variability, coupling to environmental factors, and sources of uncertainty in the estimates. J. Geophys. Res. Oceans, 120: 813-831. doi: 10.1002/2014JC010330.
- Corredor-Acosta, A., Morales, C. E., Brewin, R. J. W., Auger, P. A., Pizarro, O., Hormazabal, S., Anabalón, V. 2018. Phytoplankton size structure in association with mesoscale eddies off central-southern Chile: The Satellite application of a phytoplankton size-class model. Remote Sens., 10(6): 834. doi:10.3390/rs10060834.
- Corredor-Acosta, A., Morales, C. E., Rodríguez-Santana, A., Anabalón, A., Valencia, L. P., Hormazabal, S. (Sometido en *Frontiers in Marine Science Journal*). Diapycnal nutrient fluxes and phytoplankton distribution in an area of interaction between a mesoscale intrathermocline eddy and a coastal upwelling front.
- Espinosa-Leal, L., Escribano, R., Riquelme-Bugueño, R., Corredor-Acosta, A. (Sometido en *Deep-Sea Research Part I*). Processes and factors shaping up the community structure of hyperiid amphipods across the zonal gradient of the sub-tropical Eastern South Pacific.

ÁREAS DE INVESTIGACIÓN

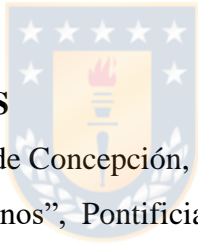
Principal: Oceanografía Física y Biológica

Secundaria: Percepción Remota

EXPERIENCIA DOCENTE

- Docente en estrategias para el desarrollo de pensamiento lógico. Servicio Nacional de Aprendizaje y Secretaria de Educación de Bogotá. Bogotá, Colombia. 2010.
- Ayudante en el curso de Oceanografía Física. Pregrado de Biología Marina, Facultad de Ciencias Naturales y Oceanográficas. Universidad de Concepción. Concepción, Chile. 2012-2016.

- Comisión de titulación para optar al título de Oceanógrafo de Victoria Salas: “Fenología del fitoplancton en el Archipiélago Juan Fernández (33°40'S; 78°40'W), Chile”. Pontificia Universidad Católica de Valparaíso, Escuela de Ciencias del Mar. Valparaíso, Chile. 2016.
- Divulgación Científica del Instituto Milenio de Oceanografía - IMO. Participación en la difusión de la muestra audiovisual itinerante (MACI) y en talleres/charlas para estudiantes de enseñanza básica y media, y docentes. Región Bio Bio, Chile. 2017-2018.
- Co-tutor tesis para optar al grado de Maestría en Ciencias Biológicas de Náyade Cortés Chong: “Caracterización de la variabilidad espacio-temporal del fitoplancton en el Panama Bight”. Pontificia Universidad Javeriana. Bogotá, Colombia. 2018-Actual.
- Co-tutor tesis para optar por el grado de Bióloga de Valentina Echeverry Guerra: “Caracterización de la radiación fotosintéticamente activa (RFA) y temperatura superficial del mar (TSM) en el Panama Bight (Pacífico Este Tropical): Relación con la variabilidad espacio-temporal de la Clorofila-a”. Pontificia Universidad Javeriana. Bogotá, Colombia. 2018-Actual.



CRUCEROS OCEANOGRÁFICOS

- Crucero FRENTEs, Universidad de Concepción, Chile, Febrero 2014.
- Crucero “FIP - Montes Submarinos”, Pontificia Universidad Católica de Valparaíso y Universidad de Concepción, Chile, Septiembre 2015.

ESTADÍAS DE INVESTIGACIÓN O ENTRENAMIENTO

- Plymouth Marine Laboratory (PML), Dr. Robert J. W. Brewin, Reino Unido, Diciembre 2016 – Enero 2017.
- Universidad de Las Palmas de Gran Canaria, Dr. Ángel Rodríguez Santana, España, Septiembre 2017.

Índice de Contenidos

Resumen	i
Abstract	iii
1. INTRODUCCIÓN	5
1.1. Caracterización de la estructura de tamaños del fitoplancton haciendo uso de información de percepción remota	6
1.2. Influencia de los remolinos de mesoescala en la estructura de tamaños de la comunidad fitoplanctónica	8
1.3. Variabilidad espacial de la estructura de la comunidad fitoplanctónica debido a la actividad de sub- y mesoescala en la zona costera y de transición costera.....	10
2. HIPÓTESIS Y OBJETIVOS ESPECÍFICOS	13
3. MATERIAL Y MÉTODOS	14
3.1. Aproximación satelital del fitoplancton por tamaño	14
3.2. Detección de los remolinos de mesoescala y seguimiento de las fracciones de tamaño de fitoplancton en su interior	16
3.3. Flujo diapicno de nutrientes y distribución de fitoplancton en la interacción de un remolino intratermoclina con el frente de surgencia costera (ITE-FSC)	17
4. RESULTADOS	19
4.1. Capítulo 1. Estructura de la comunidad fitoplanctónica en relación con los remolinos de mesoescala en la región centro-sur de Chile: Aplicación de un modelo satelital de fitoplancton por tamaño	19
4.2. Capítulo 2. Flujo diapicno de nutrientes y distribución de fitoplancton en un área de interacción entre un remolino intratermoclina de mesoescala y el frente de surgencia costera.....	43

5. DISCUSIÓN	78
5.1. Estructura de la comunidad fitoplanctónica por tamaños al interior de los remolinos de mesoescala	79
5.2. Distribución del fitoplancton en un área de interacción entre un remolino intratermoclina y el frente de surgencia costera	82
6. CONCLUSIONES	86
7. REFERENCIAS	88



RESUMEN

Influencia de los procesos físicos de mesoescala y submesoescala en la estructura de tamaños de la comunidad fitoplanctónica en Chile centro-sur

July Andrea Corredor Acosta

2019

Dra. Carmen E. Morales, Profesora Guía

Dr. Samuel Hormazabal, Profesor Co-Guía

La estructura de tamaños de la comunidad fitoplanctónica (ECF) en la capa superficial de los océanos está influenciada principalmente por la temperatura, la disponibilidad de luz, el suministro de nutrientes y la estratificación/mezcla de la columna de agua, que a su vez son propiedades moduladas por procesos físicos de submesoescala y mesoescala, tales como frentes y remolinos, con consecuencias en la transferencia de energía a los niveles tróficos superiores, los ciclos biogeoquímicos y la exportación de carbono hacia el océano profundo. El impacto de estas estructuras en el ecosistema pelágico ha sido mayormente estudiado en relación con la biomasa fitoplanctónica (como clorofila-a total) a escala global y en océano abierto, y en menor medida en los Sistemas de Surgencia de Borde Oriental (SSBO). Además, aún son escasos los estudios que han analizado el impacto de los remolinos y otras estructuras de sub- y mesoescala sobre la ECF, debido principalmente a las limitaciones existentes en la obtención de datos de ECF con alta resolución espacio-temporal.

La presente tesis aborda la variabilidad de la ECF a nivel de sub- y mesoescala en la zona costera (ZC) y de transición costera (ZTC) en la región centro-sur de Chile en el SSBO de Humboldt. Las hipótesis propuestas son: (i) La variabilidad temporal de la comunidad fitoplanctónica por clases de tamaño al interior de los remolinos de mesoescala depende de las fases de estos durante su periodo de vida, las que implican cambios en la concentración de nutrientes en la capa superficial; y (ii) La variabilidad espacial de la comunidad fitoplanctónica en la zona costera y de transición costera depende de la magnitud del flujo vertical de nutrientes por procesos de mezcla diapicna turbulenta, lo que implica una ventaja competitiva para las células fitoplanctónicas grandes cuando estos flujos son máximos hacia la capa fótica.

En el primer caso, se evaluaron los cambios en la ECF en asociación con los remolinos de mesoescala en la región, utilizando una aproximación satelital basada en un modelo teórico de tres componentes (micro-, nano- y pico-fitoplancton), parametrizado a partir de datos *in situ* de Clo-a total y fraccionada por tamaño. Los estimados satelitales fueron superpuestos al interior de distintos tipos de remolinos (cyclónico, anticiclónicos e intratermoclina (ITE)) generados en la ZC y en desplazamiento hacia la ZTC. Los resultados muestran una alta correlación entre los datos *in situ* y los estimados satelitales ($0,64 < r < 0,87$), con mayores valores de incertidumbre en la fracción microplancónica. Los cambios en la ECF tuvieron lugar durante los primeros ~2 meses de trayectoria de los remolinos, con una mayor contribución del micro- (~30-50%) cuando los remolinos se encontraban cerca de la ZC, mientras que el nano- fue dominante (~60-70%) y el pico-fitoplancton casi constante (<20%) durante el periodo de vida de los remolinos. Los resultados sugieren que el modelo utilizado es aplicable a sistemas altamente productivos y que las variaciones espacio-temporales en la ECF en remolinos estarían asociadas con las fases de estos durante su periodo de vida y los cambios en la concentración de los nutrientes, y/o de sus proporciones.

En el segundo caso, se analizó el impacto de la interacción entre remolino y frente de surgencia costera (ITE-FSC) enfocado en los cambios en la ECF en respuesta al flujo vertical de nutrientes por la mezcla diapicna turbulenta, utilizando datos *in situ* de Clo-a total y fraccionada por tamaño, nutrientes y propiedades físicas de la columna de agua durante un crucero corto (3-7 febrero 2014) frente a Concepción. El flujo diapicno de nutrientes fue calculado a través de estimados indirectos de difusividad vertical turbulenta usando el método de escala de Thorpe. Los resultados indican flujos verticales máximos de nutrientes en la capa superficial (10-20 m) del FSC y subsuperficial (30-60 m) del ITE, en respuesta a la distribución de los nutrientes y la alta mezcla turbulenta en ambas zonas, así como también, una abundancia máxima de especies costeras de microdiatomeas en el FSC y oceánicas en el ITE. Estos resultados sugieren que el suministro de nutrientes por mezcla diapicna turbulenta en áreas de interacción ITE-FSC promueve la abundancia de células de micro-fitoplancton, y posiblemente es un mecanismo físico importante para sostener altos valores de productividad primaria en la ZC y ZTC en los SSBO, como por ejemplo en la región centro-sur de Chile.

ABSTRACT

Influence of mesoscale and submesoscale processes on phytoplankton size structure in central-southern Chile

July Andrea Corredor Acosta

2019

Dra. Carmen E. Morales, Profesora Guía

Dr. Samuel Hormazabal, Profesor Co-Guía

Phytoplankton size structure (PSS) in the upper layer in oceans is mainly influenced by temperature, light and nutrient availability, as well as stratification or mixing in the water column, properties which could be modulated by submesoscale and mesoscale physical processes, such as fronts and eddies, with consequences in the energy flow pathways to higher trophic levels, the biogeochemical cycles and the efficiency of ecosystems to export carbon into the deep ocean. The impact that these physical structures have on the pelagic ecosystem has been mostly related to phytoplankton biomass (in terms of total chlorophyll-a) at the global scale and in open ocean waters and, far less, in Eastern Boundary Upwelling Systems (EBUS). In addition, there are still few studies that have analysed the impact of eddies and other sub- and mesoscale structures on PSS, mainly due to limitations in obtaining high spatio-temporal resolution data of PSS.

This thesis evaluates the variability of PSS at sub- and mesoscale level in the coastal zone (CZ) and coastal transition zone (CTZ) in the Humboldt EBUS off central-southern Chile. The proposed hypotheses are: (i) The temporal variability of phytoplankton community by size classes within the mesoscale eddies depends of their developmental stages, which involve changes in nutrient concentrations in the surface layer; and (ii) The spatial variability of the phytoplankton community in the coastal and coastal transition zone depends on the magnitude of the vertical nutrient fluxes by turbulent diapycnal mixing processes, which implies a competitive advantage for large phytoplanktonic cells when these fluxes are maximum towards the photic layer.

In the first case, the changes in the PSS were assessed in association with mesoscale eddies in the region, using a satellite approach of a three-component (micro-, nano- and pico-

phytoplankton) abundance model, tuned and parameterized for the first time in this region, based on total and size-fractionated Chl-a *in situ* data. The satellite estimates of the phytoplankton size classes were then overlaid on different types of eddies (cyclonic, anticyclonic and intrathermocline (ITE)) generated in the CZ and moving towards the CTZ. The results show a high correlation between the satellite estimates and the *in situ* Chl-a size fractions ($0.64 < r < 0.87$), with higher uncertainty values for the microplankton. The largest changes in the PSS structure took place during the early life of eddies (~2 months), with a higher contribution by the micro- (~30-50%) when eddies were located close to the CZ, while the nano- was the dominant fraction (~60-70%) and the pico-phytoplankton almost constant (<20%) throughout the lifetime of eddies. These results suggest that the three-component model is applicable to highly productive systems, such as the one studied, and that the spatio-temporal changes in PSS within eddies are most likely associated with the developmental stages during the eddies lifetime and variations in nutrient concentrations, and/or their ratios.

In the second case, the impact of an eddy - coastal upwelling front (ITE-CUF) interaction on PSS was evaluated in response to the vertical flux nutrients by turbulent diapycnal mixing, based on *in situ* data of total and size-fractionated Chl-a, nutrients and physical properties of the water column collected during a short cruise (3-7 February 2014) off Concepción. The diapycnal flux of nutrients were calculated through indirect estimates of vertical eddy diffusivity using the Thorpe scale method. The results show a maximum surface (10-20 m) and subsurface (30-60 m) upward injection of nutrients in the CUF and ITE areas, respectively, in association with the underlying nutrient field and high turbulent mixing in these two areas, as well as, maxima of microdiatoms abundance dominated by coastal species in the CUF and oceanic species in the ITE. These findings suggest that diapycnal nutrient supply in areas of ITE-CUF interaction contributes to promote the presence of large phytoplankton cells, and could be an important mechanism to support primary productivity in the CZ and CTZ of EBUS systems, such as off central-southern Chile.

1. INTRODUCCIÓN

El fitoplancton puede ser clasificado según su tamaño celular, su composición taxonómica y/o su función, y de acuerdo a ello es posible evaluar su rol en los ciclos biogeoquímicos marinos (Le Queré et al., 2005; Finkel et al., 2010). El tamaño celular ha sido asociado con la tasa de incorporación de nutrientes, la absorción de luz, las tasas metabólicas, la trama trófica y la exportación de carbono al océano profundo (Morel y Bricaud, 1981; Bricaud et al., 2004; Guidi et al., 2009; Karl et al., 2012). Las clases de tamaño comúnmente utilizadas (Sieburth et al., 1978) que incluyen a componentes fitoplanctónicos son tres: el picoplancton (0.2-2.0 μm de diámetro), el nanoplancton (2.0-20 μm de diámetro) y el microplancton (20-200 μm de diámetro) y sus distribuciones en la capa superficial del océano depende de una serie de factores, entre los cuales se han enfatizado las condiciones físico-químicas del medio (Margalef, 1978; Cullen et al., 2002; IOCCG, 2014).

Las células fitoplanctónicas grandes (microplancton) tienden a dominar en regiones con altas concentraciones de nutrientes (ej. zonas de surgencia) e incluso con baja disponibilidad de luz en la picnoclina (Goldman y McGillicuddy, 2003), mientras que, las células pequeñas han sido usualmente asociadas con regiones de bajo contenido de nutrientes y baja biomasa (ej. Giros subtropicales; Crisholm, 1992; Platt et al., 2005; Aiken et al., 2009). Además de la disponibilidad de nutrientes en la columna de agua, otros factores tales como la luz, la temperatura y la mezcla/estratificación pueden afectar la estructura de la comunidad fitoplanctónica o ECF (Aiken et al., 2008; Macías et al., 2013). De acuerdo a esto, las células pequeñas son capaces de adaptarse tanto en superficie (<50 m) como en profundidad (100-200 m), en ambientes cálidos, estratificados y con alta exposición a la luz (Agustí, 2004; Sathyendranath y Platt, 2007), a diferencia de las células grandes que tienden a predominar en ambientes altamente mezclados y con altos flujos verticales de nutrientes (Bruland et al., 2001).

Las estructuras de submesoescala (~0.1-10 km, pocos días) y mesoescala (~10-100 km, días a meses), tales como frentes y remolinos, han sido consideradas características ubicuas y frecuentes, capaces de modificar las propiedades físico-químicas de la columna de agua y la

composición de la comunidad fitoplanctónica (McGillicuddy, 2016). Varios estudios en regiones oceánicas (ej. Claustre et al., 1994; Lima et al., 2002; McGillicuddy et al., 2007) y costeras (ej. Reul et al., 2005; Barth et al., 2005; Morales et al., 2007; Letelier et al., 2009; Correa-Ramírez et al., 2012; Li et al., 2012) se han focalizado en comprender la respuesta biológica a la variabilidad oceánica de sub- y mesoescala pero con limitaciones debido a la falta de mediciones frecuentes y de alta resolución espacial (Rodríguez et al., 2001). Esta tesis doctoral es una contribución para entender la variabilidad espacio-temporal de la estructura de la comunidad fitoplanctónica a nivel de sub- y mesoescala en la zona costera (ZC) y de transición costera (ZTC) en la región centro-sur de Chile haciendo uso de datos *in situ* y aproximaciones satelitales.

1.1. Caracterización de la estructura de tamaños del fitoplancton haciendo uso de información de percepción remota

Las propiedades ópticas del océano han sido exploradas mediante percepción remota, con la ventaja de obtener información de alta resolución espacial (4 km o menos) y alta frecuencia temporal (diaria), permitiendo capturar y analizar las variaciones en el material biológico del océano (Platt y Sathyendranath, 2008). Durante la última década, se ha dado un mayor énfasis al desarrollo de aproximaciones satelitales para diferenciar el fitoplancton según su tamaño, basadas principalmente en la abundancia y en las propiedades ópticas inherentes del fitoplancton.

Los métodos basados en las propiedades ópticas se fundamentan en las características espectrales del fitoplancton o de la materia particulada total, y pueden ser asociadas con las variaciones en el tamaño. Estas aproximaciones se dividen en las que usan coeficientes de absorción y las que usan coeficientes de retro-dispersión. En el caso por absorción, el tamaño celular es asociado con los cambios en la forma espectral de absorción de luz por parte del fitoplancton, encontrando que las células pequeñas muestran coeficientes de absorción altos a bajas longitudes de onda (~450 nm) y pronunciados máximos (peaks) al compararlos con las células grandes (Ciotti et al., 2002; Ciotti y Bricaud, 2006; Devred et al., 2006; 2011; Uitz et

al., 2008). Los resultados basados en estos estudios son similares al presentar formas espectrales con peaks agudos en las fracciones nano- y picoplanctónica, y curvas espectrales achatadas para la fracción del microplancton. En el caso de los métodos por retro-dispersión, el tamaño celular es estimado para el conjunto total de partículas en el océano (no sólo fitoplancton), asumiendo que las células pequeñas dispersan la luz hacia longitudes de onda cortas, y que las células grandes exhiben un espectro achatado de dispersión (IOCCG, 2014).

Por otra parte, en los métodos basados en abundancia, las células fitoplanctónicas grandes son asociadas con alta biomasa, mientras que las células pequeñas prevalecen en condiciones de baja biomasa (Platt et al., 2005; Aiken et al., 2009). Este tipo de aproximaciones estiman las fracciones de tamaño de fitoplancton en relación a una concentración dada de Clorofila-a (Clo-a) total, y sus principales diferencias dependen de los métodos de obtención de dichas concentraciones, es decir, vía Cromatografía Líquida de Alta Eficacia (HPLC) o vía Clo-a total y fraccionada por sistema de filtración (Uitz et al., 2006; Brewin et al., 2010; 2015; Hirata et al., 2011; Devred et al., 2011). Los métodos por abundancia, tales como el de Brewin et al. (2010) e Hirata et al. (2011), se basan en el modelo conceptual de Sathyendranath et al. (2001) según el cual la concentración total de Clo-a es la suma de las concentraciones parciales de Clo-a por las fracciones de micro-, nano-, y pico-fitoplancton. Además, este modelo asume que la fracción del microplancton (picoplancton) incrementa (disminuye) monótonicamente en función de la Clo-a total, y que las células fitoplanctónicas pequeñas alcanzan una concentración específica de Clo-a, a partir de la cual valores superiores a dicha concentración son asociados con las células grandes.

La mayoría de estas aproximaciones han sido implementadas en océano abierto (ej. Uitz et al., 2006; 2008; Brewin et al., 2010; 2012; 2017), y solo algunos estudios han incluido información de aguas costeras, utilizando datos *in situ* basados en análisis finos de pigmentos fotosintéticos (HPLC) y curvas espectrales de absorción (Ciotti et al., 2006; Brotas et al., 2013; Brito et al., 2015). En el presente estudio, varias campañas oceanográficas llevadas a cabo en el periodo 2004-2015, han permitido coleccionar datos *in situ* de Clo-a total y fraccionada por tamaño en la ZC (~100 km desde la costa) y ZTC (~600 a 800 km costa afuera) en la región centro-sur de Chile. Por tanto, en este estudio y por primera vez, el modelo de tres

componentes (micro-, nano- y pico-fitoplancton) basado en datos de abundancia vía filtración es parametrizado para un sistema altamente productivo, permitiendo obtener estimados satelitales por clases de tamaño de fitoplancton con resolución espacial de 4 km y frecuencia temporal diaria en este Sistema de Surgencia de Borde Oriental (SSBO) de Humboldt.

1.2. Influencia de los remolinos de mesoescala en la estructura de tamaños de la comunidad fitoplanctónica

Los remolinos de mesoescala ocupan ~30% de la superficie del océano y contienen más del 80% de la energía cinética de la circulación oceánica (Grachev et al., 1979; Chaigneau et al., 2009; He et al., 2016). Estas estructuras pueden generar cambios en la disponibilidad de nutrientes en la columna de agua por procesos de advección horizontal y por la mezcla/estratificación debido al desplazamiento vertical de las isopícnas, lo que implica cambios en la biomasa fitoplanctónica superficial (en términos de Clo-a total) y en la composición de la comunidad fitoplanctónica (Gaube et al., 2014; Cotti-Rausch et al., 2016). Los procesos de advección horizontal implican el intercambio de nutrientes y plancton en la periferia de los remolinos y su posterior atrapamiento al interior de éstos (Gaube et al., 2014). Mientras que, la elevación o hundimiento de las isopícnas y con esto los procesos locales de surgencia/subsidencia al interior de los remolinos, depende de la dinámica física del tipo de remolino y de las fases de desarrollo de éstos durante su periodo de vida. Dos fases han sido propuestas: la fase de formación e intensificación (~12 primeras semanas de vida de los remolinos) y la fase de decaimiento o relajación (posterior a las ~12 primeras semanas; Flierl y McGillicuddy, 2002; McGillicuddy, 2016).

Los remolinos pueden ser ciclónicos o anticiclónicos en la capa superficial (McGillicuddy et al., 2007; McGillicuddy, 2016). Durante la fase de formación e intensificación, los remolinos ciclónicos (anticiclónicos) se caracterizan por una anomalía negativa (positiva) del nivel del mar causada por una divergencia (convergencia) superficial, una elevación (hundimiento) de las isopícnas, y por ende eventos de surgencia (subsistencia) local con entrada (pérdida) de nutrientes a la capa fótica (McGillicuddy et al., 1998; Sweeney et al., 2003; Wang et al.,

2016). En el caso de los remolinos anticiclónicos, son además comunes los subsuperficiales, denominados intratermoclina, los cuales representan entre 30 y 55% de la totalidad de los remolinos anticiclónicos en los SSBO. Este tipo de remolinos se caracterizan por tener un radio de ~20-60 km y una extensión vertical de ~500 m de profundidad, junto con una elevación (hundimiento) de las isopícnas en la parte superior (inferior), un núcleo de mínimo oxígeno y altas tasas de productividad primaria (Mourino-Carballido y McGillicuddy, 2006; Hormazabal et al., 2013; Pegliasco et al., 2015; Barceló-Llull et al., 2017).

En contraste, durante la fase de decaimiento de los remolinos la dirección del movimiento vertical de las isopícnas es contrario al de la fase de formación e intensificación, es decir, las perturbaciones en las isopícnas van en dirección contraria resultando en eventos de subsidencia local al interior de los remolinos ciclónicos e intratermoclina, y surgencia al interior de los remolinos anticiclónicos (Flierl y McGillicuddy, 2002; McGillicuddy, 2016). Sin embargo, otro mecanismo estaría promoviendo un patrón similar, denominado el bombeo tipo remolino-Ekman, el cual modifica las isopícnas al interior de los remolinos debido a la interacción del campo de viento con las corrientes superficiales, generando subsidencia (surgencia) local al interior de los remolinos ciclónicos (anticiclónicos). Este último mecanismo ha sido asociado con el periodo de vida completo de los remolinos y con velocidades verticales menores a las reportadas durante el bombeo por tipo de remolino en la fase de formación e intensificación (Gaube et al., 2014), además de estar influenciado por la distancia entre la nutriclina y la profundidad de la capa de mezcla según la estacionalidad (He et al., 2016).

La mayoría de los estudios enfocados en evaluar el impacto de los remolinos de mesoescala sobre el ecosistema pelágico se han llevado a cabo a escala global y en océano abierto, en tanto que sólo algunos se han focalizado en los SSBO. Los impactos indican que se favorece el intercambio de propiedades físicas, químicas y biológicas entre aguas costeras y oceánicas durante la fase inicial de propagación de los remolinos (Arístegui et al., 2004; Pelegrí et al., 2005; Correa-Ramirez et al., 2007; Gruber et al., 2011). En términos de la Clo-a total, su distribución superficial en forma de un dipolo ha sido asociada con la advección horizontal de biomasa fitoplanctónica debido al sentido de rotación y dirección de propagación de los

remolinos, principalmente durante la fase de formación. Mientras que, un monopolio de anomalías positivas/negativas de Clo-a ha sido asociado con los mecanismos físicos de surgencia o subsidencia local que involucran un intercambio vertical de propiedades en la columna de agua, tales como el bombeo tipo remolino y el bombeo tipo remolino-Ekman (Chelton et al., 2011; Gaube et al., 2014; He et al., 2016; McGillicuddy, 2016). Sin embargo, pocos estudios han evaluado la variabilidad temporal de la Clo-a total durante las distintas etapas de vida de los remolinos (Gaube et al., 2014; He et al., 2016; Frenger et al., 2018) y/o los cambios en la ECF asociados a este tipo de estructuras de mesoescala (Karrasch et al., 1996; Moore et al., 2007; Morales et al., 2012; 2017; Lin et al., 2014; Lamont et al., 2018), en donde la principal limitación es la restricción espacio-temporal de datos de alta resolución sobre ECF.

Por tanto, las siguientes preguntas quedan abiertas, ¿Cómo es la variabilidad temporal de la estructura de la comunidad fitoplanctónica al interior de los distintos tipos de remolinos de mesoescala?, ¿Cómo varía la estructura de la comunidad fitoplanctónica debido a los distintos tipos de mecanismos propuestos de advección y/o bombeo al interior de los remolinos?, ¿Existen cambios en la estructura de la comunidad fitoplanctónica asociados a las fases del periodo de vida de los remolinos?.



1.3. Variabilidad espacial de la estructura de la comunidad fitoplanctónica debido a la actividad de sub- y mesoescala en la zona costera y de transición costera

Los SSBO son regiones caracterizadas por una intensa actividad de sub- y mesoescala (ej. frentes, remolinos, filamentos, jets) en la ZC y ZTC, sujetas a constantes interacciones entre estas estructuras físicas y a modificaciones en la configuración de la columna de agua, con efectos en la biomasa y composición de la comunidad fitoplanctónica (Rodríguez et al., 2001; Macías et al., 2013). En estos sistemas, el transporte de Ekman perpendicular a la costa debido al estrés del viento favorable a la surgencia es balanceado por un flujo vertical de agua hacia la superficie, conllevando al ascenso de la piconclina cerca de la costa, en donde la intensificación y persistencia de los vientos contribuye al sostenimiento pronunciado de un

frente superficial con fuertes gradientes en temperatura, salinidad y densidad (Mahadevan, 2016). Este se conoce como el frente de surgencia costera (FSC) y es considerado un rasgo típico de los SSBO al separar aguas frías costeras de aguas cálidas oceánicas (Brink y Cowles, 1991; Franks y Walstad, 1997; Johnston et al., 2011). Asociados a estos gradientes laterales se producen inestabilidades baroclínicas capaces de incrementar la cizalla vertical del flujo geostrofico en la zona frontal y, por ende, favorecer la mezcla turbulenta (Boccaletti et al., 2007; Mahadevan y Archer, 2000; Mahadevan, 2016). Dado que la distribución de los nutrientes está altamente correlacionada con el campo de densidad y con la presencia de distintas masas de agua, los cambios en la estratificación estarían promoviendo el flujo advectivo de nutrientes a lo largo de las isopicnas (mezcla isopicna) y/o el flujo turbulento por difusión a través de éstas (mezcla diapicna) (Ledwell et al., 1998; Mahadevan y Tandon, 2006; Ascani et al., 2013; José et al., 2017).

Previos estudios han reportado la dominancia de diatomeas en el lado costero del FSC y de células pequeñas en el lado oceánico (Furnas, 1990; Marañón y Fernández, 1995). No obstante, aumentos en la abundancia de células fitoplanctónicas grandes han sido recientemente encontrados alrededor de la picnoclina en zonas frontales, debido a un alto gradiente en la concentración de nutrientes y alta mezcla diapicna turbulenta (Sàngra et al., 2014; Landeira et al., 2014; Zhang et al., 2015). En el SSBO en la región centro-sur de Chile, el FSC ha sido reportado como una barrera para la advección de las altas concentraciones de Clo-a total de aguas costeras (Letelier et al., 2009), sin embargo, cuando el FSC interactúa con un remolino intratermoclina (ITE) esta dinámica tipo barrera puede cambiar. Morales et al. (2017) basados en datos *in situ* de Clo-a total y fraccionada por tamaño, nutrientes y propiedades físicas de la columna de agua durante un crucero corto (3-7 febrero 2014) en la ZC y ZTC frente a Concepción (36°-37°S), registraron un evento de interacción remolino-frente (ITE-FSC). Los autores sugieren que esta dinámica favorece el intercambio de diferentes especies de microdiatomeas desde y hacia la ZC, en asociación con una intensa variabilidad de submesoescala en los nutrientes.

Dado que los procesos físicos de submesoescala y de turbulencia de pequeña escala asociado a este tipo de interacciones son relevantes por ser similares a las escalas temporales de

crecimiento del fitoplancton (Davies et al., 2008; Li et al., 2012; Mahadevan, 2016) las siguientes preguntas quedan abiertas, ¿Cómo es el flujo vertical de nutrientes por mezcla diapirna turbulenta en la ZC y ZTC en la región centro-sur de Chile?, ¿Cuál es el impacto de la magnitud de estos flujos verticales de nutrientes en la estructura de la comunidad fitoplanctónica en la ZC y ZTC durante una interacción ITE-FSC?.



2. HIPÓTESIS Y OBJETIVOS ESPECÍFICOS

La estructura de las comunidades fitoplanctónicas responde a varios factores, incluyendo el contenido de nutrientes y la estratificación/mezcla de la columna de agua. A escala global, el micro-fitoplancton (nano- y pico-fitoplancton) ha sido usualmente asociado a regiones con alta (baja) concentración de nutrientes y alta (baja) turbulencia. Sin embargo, a nivel de sub- y mesoescala, se desconocen los impactos de estos factores sobre la estructura comunitaria. Por tanto, se postulan dos hipótesis para dos casos distintos de procesos de sub- a mesoescala que explicarían la estructura de tamaño de la comunidad fitoplanctónica en la región centro-sur de Chile.

Hipótesis I: La variabilidad temporal de la comunidad fitoplanctónica por clases de tamaño al interior de los remolinos de mesoescala depende de las fases de éstos durante su periodo de vida, las que implican cambios en la concentración de nutrientes en la capa superficial.

Hipótesis II: La variabilidad espacial de la comunidad fitoplanctónica en la zona costera y de transición costera depende de la magnitud del flujo vertical de nutrientes por procesos de mezcla diapicna turbulenta, lo que implica una ventaja competitiva para las células fitoplanctónicas grandes cuando estos flujos son máximos hacia la capa fótica.

Objetivos específicos:

- 1) Evaluar los cambios en la estructura de la comunidad fitoplanctónica durante el periodo de vida de distintos tipos de remolinos de mesoescala en la región centro-sur de Chile.
- 2) Caracterizar la estructura de la comunidad fitoplanctónica debido al flujo vertical de nutrientes por mezcla turbulenta en la zona costera y de transición costera en la región centro-sur de Chile.

3. MATERIAL Y MÉTODOS

La región centro-sur de Chile (32-38°S, 72-81°W) se encuentra ubicada en el Pacífico Sureste y se caracteriza por una surgencia costera estacional durante el periodo de primavera-verano austral en respuesta a la intensificación de los vientos del suroeste, promoviendo la generación de un frente de surgencia con extensión vertical de ~100 m de profundidad y posición espacial variable (~50-150 km desde la costa) en relación a la circulación del jet costero (Shaffer et al., 1999; Sobarzo et al., 2007; Letelier et al., 2009; Oerder et al., 2018). Durante el periodo de surgencia, la variabilidad de la Corriente Subsuperficial Perú-Chile y la formación de meandros a partir del jet costero, en conjunto con la orientación de la línea de costa y la batimetría promueven la generación de filamentos y remolinos superficiales/subsuperficiales de mesoescala con altos valores de energía cinética (Correa-Ramirez et al., 2007; Morales et al., 2012; Hormazabal et al., 2004; 2013).

3.1. Aproximación satelital del fitoplancton por tamaño

Datos in situ: 227 muestras de Clo-a total y fraccionada por tamaño (micro: >20 µm, nano: 2-20 µm y picoplancton: <2 µm) fueron colectadas en la ZC y ZTC durante diferentes campañas oceanográficas en la región centro-sur de Chile: i) Cruceros FIP de monitoreo en la VIII región (~35-38°S, 72-78°W; noviembre 2004 a enero 2009; N°2004-20, N°2005-01, N°2006-12, N°2007-10, N°2008-20, N°2009-39), ii) Serie de tiempo de la estación fija del centro FONDAP COPAS (St. 18; 36,5°S, 73,13°W; julio 2004 a noviembre 2009), iii) crucero oceanográfico “Frentes” (FONDECYT N°1120504) en Concepción (~36.5-36.75°S, 73.10-74.50°W; 3-7 febrero 2014), y iv) crucero “FIP-Montes Submarinos N°2014-04-2” (~33-34°S, 74-80°W; 14-22 septiembre 2015). Las muestras fueron colectadas con botellas Niskin en la capa superficial de la columna de agua (<100 m) y filtradas usando filtros GF/F y/o sistemas de filtración secuencial con filtros de policarbonato. Las muestras fueron analizadas por fluorometría siguiendo la metodología de Anabalón et al. (2007, 2016). *Datos satelitales:* Datos diarios de Clo-a total para el periodo enero 2004 a diciembre 2015 en el área de estudio

fueron obtenidos de la versión 3.0 del producto “Ocean Colour Climate Change Initiative (OC-CCI)” con resolución espacial de 4 km.

La parametrización del modelo de tres componentes se llevó a cabo siguiendo la metodología de Brewin et al. (2012). El modelo se basa en: i) la concentración de Clo-a total (C) es la suma de las concentraciones de Clo-a por las fracciones de tamaño micro- (C_M), nano- (C_N) y picoplancton (C_P), esto es $C = C_M + C_N + C_P$; y ii) la concentración de Clo-a por las células más pequeñas es estimada mediante funciones exponenciales, una combinando el nano- y el picoplancton (C_{NP}) y la otra considerando sólo la fracción picoplanctónica (C_P):

$$C_{NP} = C_{NP}^m \left[1 - \exp \left(- \left(\frac{D_{NP}}{C_{NP}^m} \right) C \right) \right] \text{ y } C_P = C_P^m \left[1 - \exp \left(- \left(\frac{D_P}{C_P^m} \right) C \right) \right]$$

Los parámetros C_{NP}^m y C_P^m son los máximos valores asintóticos asociados a estas fracciones de tamaño, mientras que D_{NP} y D_P reflejan el porcentaje de contribución de estas fracciones a la Clo-a total cuando ésta última tiende a cero. Estos parámetros son obtenidos a partir de los datos *in situ* de Clo-a total y fraccionada por tamaño, y el procedimiento de ajuste usado es el método no lineal por mínimos cuadrados de Levenberg-Marquardt (Brewin et al., 2012). Adicionalmente, con el propósito de calcular la incertidumbre de los parámetros y validar el modelo, los datos *in situ* es decir las 227 muestras, fueron aleatoriamente separadas usando el 80% para la parametrización y el remanente 20% para la validación. En base a la matriz de parametrización, la mediana y los intervalos de confianza al 95% fueron calculados para obtener la distribución de los parámetros. Posteriormente, se usaron los datos satelitales de Clo-a total y los parámetros obtenidos como variables de entrada para las ecuaciones anteriormente descritas, estimando así las concentraciones satelitales de Clo-a para las células pequeñas (C_{NP} y C_P). En el caso de la Clo-a satelital para el microplancton, los datos fueron obtenidos mediante la relación $C_M = C - C_{NP}$. Finalmente, estos estimados satelitales fueron comparados con los datos *in situ* de la matriz de validación, en donde el dato satelital fue contrastado para el mismo día y con los nueve pixeles más cercanos a la ubicación geográfica de la muestra *in situ*, asegurando un coeficiente de variación <0,15 y un mínimo de 50% de datos válidos al interior de los pixeles considerados. La mediana de las concentraciones de Clo-a de los nueve pixeles fue tomado como el dato satelital final en cada caso.

3.2. Detección de los remolinos de mesoescala y seguimiento de las fracciones de tamaño de fitoplancton en su interior

Datos satelitales: i) datos diarios de anomalías del nivel del mar (ANM) para el periodo enero 2014 a diciembre 2015 fueron obtenidos del producto “two-sat SLA Ssalto/Duacs AVISO”, y ii) estimados de Clo-a por tamaño obtenidos en la sección 3.1.

La detección y seguimiento de los remolinos se basó en contornos cerrados de ANM siguiendo la metodología de Mason et al. (2014). Los campos diarios de ANM fueron espacialmente filtrados con un filtro Gaussiano de radio zonal ~1000 km y meridional ~500 km. Los contornos fueron computados a intervalos de 0,2 cm identificando los remolinos ciclónicos (anticiclónicos) a partir de variaciones de 100 cm (-100 cm). Para asegurar un perímetro efectivo, los contornos debían cumplir los siguientes criterios: i) amplitud >0,1 cm, ii) el número de extremo local limitado a 1, y iii) radio del remolino en un rango de ~30 a 446 km. Cuatro remolinos fueron detectados desplazándose desde la ZC y seguidos por ~7,5 a 11 meses: un ciclón superficial, un anticiclón superficial y dos anticiclones intratermoclina, el primero detectado frente a Punta Lavapié y el segundo en Punta Nugurne. Los remolinos intratermoclina o subsuperficiales fueron previamente registrados por cortos periodos a través de mediciones *in situ* durante el crucero “FIP-Montes Submarinos” y el crucero “Frentes”.

Para la proyección de los estimados satelitales de Clo-a por tamaño al interior de los remolinos detectados, las frecuencias de variabilidad diferentes a la mesoescala fueron removidas primero sustrayendo el ciclo estacional y segundo haciendo imágenes compuestas promedio de 8 días. Las imágenes de Clo-a resultantes fueron llevadas a coordenadas polares con distancia radial definida por el radio (R) del remolino, de forma tal que los valores de Clo-a a cualquier distancia r fueron proyectados según la relación r/R . Los campos de Clo-a debían cubrir al menos el 50% de la extensión espacial de los remolinos durante todo el periodo de seguimiento, evitando incluir aquellas semanas que no cumplieran este criterio. Finalmente, la variabilidad de la ECF fue evaluada tanto en el centro ($r/R \leq 1$) como en la periferia ($1 < r/R \leq 2$) de los remolinos de acuerdo con la metodología propuesta por He et al. (2016), y comparados con sus valores promedios cuando éstos se encontraban en su posición más cercana a la costa.

3.3. Flujo diapicno de nutrientes y distribución de fitoplancton en la interacción de un remolino intratermoclina con el frente de surgencia costera (ITE-FSC)

Datos in situ: En el crucero oceanográfico “Frentes” en Concepción (~36.5-36.75°S, 73.10-74.50°W; 3-7 febrero 2014; 2 transectas y 26 estaciones) los siguientes datos fueron obtenidos en los primeros 100 m de profundidad: i) muestras de Clo-a total y fraccionada por tamaño analizadas siguiendo el procedimiento descrito en la sección 3.1, ii) muestras de plancton colectadas para análisis de abundancia de la fracción microplanctónica siguiendo el procedimiento de Morales et al. (2017), y iii) muestras de nutrientes (nitrato, fosfato y silicato) a los 0, 5, 10, 15, 20, 30, 40, 60, 80 y 100 m de profundidad, analizadas siguiendo el protocolo de Atlas et al. (1971). Además, perfiles de conductividad y temperatura en los primeros 300 m de la columna de agua obtenidos con el equipo CTD Sea-Bird SBE 911plus (24 Hz). Datos satelitales para el mismo periodo del crucero “Frentes”: i) temperatura superficial del mar del producto “MUR-SST” con resolución temporal diaria y espacial de 1 km, ii) datos diarios de ANM y corrientes geostróficas de “Copernicus-CMEMS” con resolución espacial de ~25 km, y iii) datos diarios de Clo-a total del producto “OC-CCI” con resolución espacial de 4 km.

Los datos satelitales fueron utilizados para caracterizar las condiciones bio-físicas superficiales promedio durante el crucero “Frentes”. Los datos *in situ* obtenidos con el CTD fueron procesados con el software Sea-Bird y utilizados para caracterizar la estructura física de la columna de agua, y para estimar el coeficiente de difusividad vertical turbulenta mediante la escala de Thorpe con la metodología de Park et al. (2014). Para obtener perfiles verticales de escala fina a partir de los datos de CTD, se minimizó el desfase en la medición de temperatura y se removieron los peaks en la salinidad causados por el desajuste entre las mediciones de conductividad y temperatura. De igual forma, se eliminaron las inversiones en los perfiles de presión, las cuales son el producto del efecto del movimiento del barco mientras el CTD desciende en la columna de agua. Los perfiles finales de temperatura y salinidad fueron utilizados para calcular la densidad potencial usando las subrutinas para matlab TEOS-10 del producto “Gibbs-SeaWater” (McDougall y Barker, 2011), y en todos los casos y sólo para los

cálculos de la escala de Thorpe, los primeros 20 m de profundidad fueron removidos para eliminar el efecto de la turbulencia generada por el barco.

Los perfiles de densidad fueron submuestreados a intervalos regulares de 10 cm y ordenados para obtener perfiles estables, a partir de los cuales los desplazamientos de Thorpe fueron calculados como los cambios verticales necesarios para alcanzar la estabilidad, y la escala de Thorpe (L_T) estimada como la media cuadrática del conjunto sucesivo de desplazamientos de Thorpe distintos de cero en toda la columna de agua y para cada estación (Park et al., 2014; Sàngra et al., 2014). Posteriormente, el coeficiente de difusividad vertical turbulenta (K_z) fue estimado para cada estación mediante la parametrización de Osborn (1980), esto es $K_z = 0,128L_T^2N$, siendo N la frecuencia Brunt-Vaisala. El flujo diapicno de nutrientes fue calculado con el gradiente vertical de la concentración de los nutrientes, siguiendo la metodología de Girault et al. (2015) mediante la ecuación:

$$F_{\text{Nutriente}} = -K_z \left(\frac{\partial \text{Nutriente}}{\partial z} \right)$$

Los perfiles de temperatura, salinidad y densidad fueron además usados para generar diagramas de Temperatura-Salinidad (T-S), calcular la velocidad geostrófica meridional (Pond y Pickard, 2013), y estimar la profundidad de la capa de mezcla mediante valores umbrales de temperatura ($\Delta T=0,2^\circ\text{C}$) y densidad ($\Delta\rho=0,03 \text{ kg m}^{-3}$) siguiendo los procedimientos de Kara et al. (2000) y de Boyer Montégut et al. (2004).

Por último, con el propósito de evaluar la distribución del fitoplancton por tamaño en asociación con los estimados del flujo diapicno de nutrientes, la profundidad de las concentraciones máximas de Clo-a por las fracciones de micro-, nano- y picoplancton fueron comparadas con la profundidad del máximo flujo de nutrientes para cada estación, y se evaluó la coincidencia espacial entre las estaciones que presentaron los mayores valores de mezcla diapicna y flujo de nutrientes con aquellas que presentaron las máximas concentraciones de Clo-a por la fracción microplanctónica. Adicionalmente, se analizó la distribución espacial de las distintas especies de microdiatomeas dominantes a lo largo de la interacción ITE-FSC en respuesta al flujo diapicno de nutrientes y a la proporción nitrato:silicato (N:Si).

4. RESULTADOS

Artículo publicado en *Remote Sensing Journal* (<https://www.mdpi.com/2072-4292/10/6/834>).

4.1. Capítulo 1: Estructura de la comunidad fitoplanctónica en relación con los remolinos de mesoescala en la región centro-sur de Chile: Aplicación de un modelo satelital de fitoplancton por tamaño


Andrea Corredor-Acosta, Carmen E. Morales, Robert J. W. Brewin, Pierre-Amaël Auger, Oscar Pizarro, Samuel Hormazabal y Valeria Anabalón.

Resumen

La influencia de los procesos de sub- y mesoescala en la estructura del fitoplancton es importante para evaluar su impacto en los ciclos biogeoquímicos marinos y en los intercambios costa-océano de plancton en los Sistemas de Surgencia de Borde Oriental. En este estudio, la evolución espacio-temporal del fitoplancton por tamaño es evaluada al interior de los remolinos de mesoescala en la región centro-sur de Chile. Datos *in situ* de Clo-a total y fraccionada por tamaño colectados en múltiples campañas oceanográficas en la zona costera y de transición costera, fueron usadas para parametrizar un modelo de tres componentes (micro-, nano-, y picoplancton), y aplicados a datos satelitales de Clo-a total para obtener estimados satelitales de Clo-a por tamaño. Un algoritmo basado en anomalías del nivel mar fue usado para hacer la detección y seguimiento de un remolino ciclónico superficial y tres remolinos anticiclónicos entre enero 2014 y octubre 2015. Los estimados satelitales de Clo-a por tamaño mostraron una alta correlación con los datos *in situ*, con valores de incertidumbre moderados a altos para el microplancton. Los mayores cambios en la estructura de la comunidad fitoplanctónica se observaron en los primeros ~2 meses de vida de los remolinos. La contribución de la fracción microplanctónica fue de ~30-50% cuando los remolinos se encontraban cerca de la costa, mientras que el nanoplancton fue dominante (~60-70%) y el picoplancton casi constante (~20%) durante la trayectoria de los remolinos. Los resultados sugieren que el modelo de tres componentes es aplicable a un sistema de surgencia altamente productivo, y que los cambios en la distribución del fitoplancton al interior de los remolinos estarían respondiendo a variaciones en la concentración de los nutrientes y/o sus proporciones.

Article

Phytoplankton Size Structure in Association with Mesoscale Eddies off Central-Southern Chile: The Satellite Application of a Phytoplankton Size-Class Model

Andrea Corredor-Acosta^{1,2}, Carmen E. Morales^{2,3,*}, Robert J. W. Brewin^{4,5},
Pierre-Amaël Auger^{2,6} , Oscar Pizarro^{2,7,8}, Samuel Hormazabal^{2,6} and Valeria Anabalón^{2,9}

- ¹ Programa de Postgrado en Oceanografía, Departamento de Oceanografía, Facultad de Ciencias Naturales y Oceanográficas, Universidad de Concepción, Casilla 160-C, Concepción 4070386, Chile; jcorredor@oceanografia.udec.cl
 - ² Instituto Milenio de Oceanografía (IMO), Universidad de Concepción, Concepción 4030000, Chile; pierreamael.auger@gmail.com (P.A.A.); oscar.pizarro@imo-chile.cl (O.P.); samuel.hormazabal@pucv.cl (S.H.); vanabalo@gmail.com (V.A.)
 - ³ Departamento de Oceanografía, Facultad de Ciencias Naturales y Oceanográficas, Universidad de Concepción, Barrio Universitario s/n, Concepción 4070386, Chile
 - ⁴ Plymouth Marine Laboratory, Prospect Place, The Hoe, Plymouth PL1 3DH, UK; robr@pml.ac.uk
 - ⁵ National Centre for Earth Observation, Plymouth Marine Laboratory, Prospect Place, The Hoe, Plymouth PL1 3DH, UK
 - ⁶ Escuela de Ciencias del Mar, Pontificia Universidad Católica de Valparaíso, Valparaíso 2340000, Chile
 - ⁷ Departamento de Geofísica, Universidad de Concepción, Barrio Universitario s/n, Concepción 4070386, Chile
 - ⁸ COPAS-Sur Austral, Universidad de Concepción, Concepción 4030000, Chile
 - ⁹ Instituto de Oceanografía y Cambio Global, Universidad de las Palmas de Gran Canaria, Las Palmas de Gran Canaria 35017, Spain
- * Correspondence: camorale@udec.cl; Tel.: +5-641-266-1234

Received: 17 April 2018; Accepted: 22 May 2018; Published: 25 May 2018



Abstract: Understanding the influence of mesoscale and submesoscale features on the structure of phytoplankton is a key aspect in the assessment of their influence on marine biogeochemical cycling and cross-shore exchanges of plankton in Eastern Boundary Current Systems (EBCS). In this study, the spatio-temporal evolution of phytoplankton size classes (PSC) in surface waters associated with mesoscale eddies in the EBCS off central-southern Chile was analyzed. Chlorophyll-a (Chl-a) size-fractionated filtration (SFF) data from in situ samplings in coastal and coastal transition waters were used to tune a three-component (micro-, nano-, and pico-phytoplankton) model, which was then applied to total Chl-a satellite data (ESA OC-CCI product) in order to retrieve the Chl-a concentration of each PSC. A sea surface, height-based eddy-tracking algorithm was used to identify and track one cyclonic (sC) and three anticyclonic (ssAC1, ssAC2, sAC) mesoscale eddies between January 2014 and October 2015. Satellite estimates of PSC and in situ SFF Chl-a data were highly correlated ($0.64 < r < 0.87$), although uncertainty values for the microplankton fraction were moderate to high (50 to 100% depending on the metric used). The largest changes in size structure took place during the early life of eddies (~2 months), and no major differences in PSC between eddy center and periphery were found. The contribution of the microplankton fraction was ~50% (~30%) in sC and ssAC1 (ssAC2 and sAC) eddies when they were located close to the coast, while nanoplankton was dominant (~60–70%) and picoplankton almost constant (<20%) throughout the lifetime of eddies. These results suggest that the three-component model, which has been mostly applied in oceanic waters, is also applicable to highly productive coastal upwelling systems. Additionally, the PSC changes within mesoscale eddies obtained by this satellite approach are in agreement with results on phytoplankton size distribution

in mesoscale and submesoscale features in this region, and are most likely triggered by variations in nutrient concentrations and/or ratios during the eddies' lifetimes.

Keywords: phytoplankton size classes; remote sensing; mesoscale eddies; coastal upwelling system; size-fractionated filtration data; Eastern Boundary Current Systems

1. Introduction

Physical dynamics in oceans promote processes of change and adaptation in biological systems at global and regional scales [1,2]. In the case of mesoscale structures (10–100 km, day-months), such as fronts and eddies, their movement through the ocean causes modifications in the physical properties (i.e., light, temperature) of the water column, changing nutrient conditions and, consequently, the phytoplankton community structure [3–5]. Mesoscale eddies occupy 25–30% of the surface ocean, contain more than 80% of the kinetic energy of oceanic circulation, and can generate different biological responses depending on eddy type (i.e., surface cyclonic/anticyclonic or subsurface anticyclonic eddy) [6–8]. Surface cyclonic (anticyclonic) eddies have been characterized by a negative (positive) sea level anomaly (SLA), a dome (bowl) shape of the isopycnals inducing upwelling (downwelling) at the eddy center, accompanied with an input (loss) of nutrients to the euphotic layer and a surface enhancement (diminishment) of chlorophyll-a (Chl-a) [9–12]. There is also a particular type of anticyclonic eddy, called intrathermocline (ITE) or subsurface mode water eddy, which represents 30–55% of the anticyclonic eddy population in Eastern Boundary Current Systems (EBCS) [13]. These eddies (ITEs) are characterized by a typical radius of ~20–60 km and have a vertical extent of ~500 m, together with dome-shaped isopleths in the upper layers and a bowl shape in the lower layers, a minimum in oxygen, and high rates of phytoplankton productivity [14–17].

Several mechanisms associated with mesoscale eddies have been proposed to modify primary production, carbon fluxes, and/or phytoplankton patterns (in terms of Chl-a). They include eddy trapping and stirring, which can lead to a dipole-like distribution of Chl-a at the eddy periphery associated with the trap and horizontal advection of waters with high or low Chl-a, caused by the rotation and direction of eddy propagation [11,18,19]. Other mechanisms involve a strong vertical exchange of waters, such as eddy pumping during eddy formation, generating a positive (negative) Chl-a monopole centered on the core of cyclonic (anticyclonic) eddies [10,20]. An opposite pattern is observed after the development phase, mainly in association with eddy-Ekman pumping due to the relative movement of the wind curl and eddy current velocity field [4,8,21–23]. Other important vertical exchanges of waters can be attributed to eddy-eddy interactions, which may also lead to frontogenesis, resulting in a convergent front between eddies and in an enhancement of Chl-a in the warm (anticyclonic) side and isopycnal subduction of Chl-a in the cold (cyclonic) side [24–27]. The impact that eddies have on the pelagic ecosystem has been mostly studied at the global scale and in open ocean environments [4,8] and, far less, in EBCS regions. Studies in EBCS have reported an exchange of chemical and biological properties between coastal and oceanic waters associated with the propagation of mesoscale eddies, e.g., [28–31]. Most of these studies are based on total Chl-a, and only a few have analyzed phytoplankton community structure within mesoscale eddies or other submesoscale features, e.g., [32–35]. The later, however, are restricted in space and time, mainly due to the difficulty in obtaining high-resolution, in situ data associated with the complete trajectory of eddies.

Over the last decade, a growing emphasis has been placed in the development of approaches to differentiate phytoplankton size classes (PSC) using satellite products, since phytoplankton size structure is an important indicator of the state of pelagic ecosystems and is strongly related to ocean carbon cycle, marine biogeochemistry, nutrient uptake, light absorption, primary production, and transfer of energy to higher trophic levels, e.g., [36–41]. These approaches have been based on (i)

the optical signatures of phytoplankton groups using the spectral shape of phytoplankton absorption (a_{ph} : Phytoplankton Absorption spectra) to characterize the PSC, e.g., [36,42]; (ii) the relationship between Chl-a concentration by each PSC with total Chl-a (as an index of phytoplankton abundance or biomass) using high performance liquid chromatography [HPLC] pigment and/or size-fractionated filtration (SFF) in situ data e.g., [43–45]; and (iii) the relationship between the phytoplankton groups and environmental factors (sea surface temperature or irradiance) e.g., [41,46]. Most of these approaches have been applied to open ocean waters, e.g., [41–45,47,48], while fewer ones have been including more information of coastal waters and have been mainly based on pigments or absorption spectra from in situ data [49–51]. Furthermore, only one recent study has used satellite estimates of PSC to infer shifts in the phytoplankton community related to a cyclonic eddy in oceanic waters [52].

In this study, for the first time, the three-component abundance-based model of Brewin et al. [43], developed for satellite ocean colour observations, was tuned for the highly productive coastal upwelling region off central-southern Chile, based on SFF in situ data, in order to estimate the Chl-a concentration of three phytoplankton size-groups [micro-, nano-, and pico-phytoplankton]. Additionally, we assess the changes in phytoplankton size structure throughout the lifetime of four different mesoscale eddies moving from the coastal zone (CZ; ~100 km from the coast) to the coastal transition zone (CTZ; coast to ~600 to 800 km offshore). We discuss the advantages/disadvantages of implementing an abundance-based model using SFF data in this EBCS, and we explore shifts in PSC associated with mesoscale features. We expect this study to contribute to improving regional biogeochemical models, since biological processes at the sub- and mesoscale levels are a key aspect of marine biogeochemistry, carbon export, and transfer of energy to higher trophic levels.

2. Data and Methodology

2.1. Study Area

The selected study region off central-southern Chile (33–38°S, 72–80°W; Figure 1) is located in the Eastern South Pacific and includes several topographic features, in particular the following capes: Point Curaumilla (33°00'S), Point Topocalma (34°10'S), Point Nugurne (35°57'S), and Point Lavapié (37°15'S) [53]. The region between ~35–38°S is characterized by a strong seasonal coastal upwelling during the austral spring-summer months in response to the intensification of southwesterly winds [54,55]. Coastal upwelling and solar radiation promote the generation of an upwelling front in this region. Variations in the coastline orientation, bathymetry, general circulation, and mesoscale activity also influence front and eddy generation [56–58]. In the area off Point Lavapié, several cyclonic and surface/subsurface anticyclonic eddies are persistently generated in association with higher levels of eddy kinetic energy, and these features move seaward through the CTZ at a relatively low speed (~1.7 km d⁻¹) [15,30,32,59].

2.2. Satellite Model of Phytoplankton Size Classes

2.2.1. In Situ Chlorophyll-a Size-Fractionated Data

A total of 227 Chl-a size-fractionated data collected in the CZ and CTZ off central-southern Chile were used to tune and validate the three-component model of Brewin et al. [43]. Total and size-fractionated Chl-a in the micro- (C_M , >20 μm), nano- (C_N , 2 to 20 μm), and pico-phytoplankton (C_P , <2 μm) range were collected during different oceanographic campaigns in the region of study: (i) FIP Bio-Bio monitoring cruises (35.30–38°S, 72.38–78.29°W), between November 2004 and January 2009; (ii) PHYTOFRONT cruise (36.50–36.75°S, 73.10–74.51°W) from 3 to 7 of February 2014; (iii) FIP Seamounts cruise (33–34°S, 73.82–80°W), between 14 and 22 of September 2015; and (iv) COPAS (Centro de Investigación Oceanográfica Pacífico Sur-Oriental) time series at a fixed coastal station (St. 18; 36.50°S–73.13°W) from July 2004 to November 2009 (Figure 1).

The procedure for Chl-a SFF consisted in the following steps for analyses before 2015: (i) filtration (~250 mL) of water samples using GF/F glass fiber filters (<0.7 μm pore diameter) for total Chl-a; (ii) pre-filtration (~250 mL) through cellulose-ester filter (3 μm pore diameter) and then by GF/F glass fiber filters for the C_p ; (iii) pre-filtration (~250 mL) through a NYTEX[®] type of mesh (20 μm pore diameter) and then by GF/F glass fiber filters to obtain a combined C_N and C_p fraction. After this, the C_N and C_M fractions were obtained by subtracting C_p from the combined C_N and C_p fraction and the latter from total Chl-a, respectively [60]. In 2015 (FIP Seamount cruise), sequential filtration systems were used, consisting of three different sizes of polycarbonate filters: 20 μm , 2 μm , and 0.2 μm allowing the derivation of C_M , C_N , and C_p [61]. Pigment extraction was carried out in vials with a known volume of 90% acetone and maintained at $-20\text{ }^\circ\text{C}$ for 24 h, after which the samples were analyzed by fluorometry (Turner Design AU-10, Turner Design TD-700, or a Turner Design Trilogy). Fluorometer calibration was done before and after each cruise using a pure Chl-a standard. In all cases, duplicate or triplicate samples were taken at different depths within the upper 100 m depth; samples collected within the first 10 m of the upper layer were used in this study. Total in situ Chl-a concentration for the subsequent analyses was calculated as the sum of the Chl-a values contributed by each PSC [41,43,44].

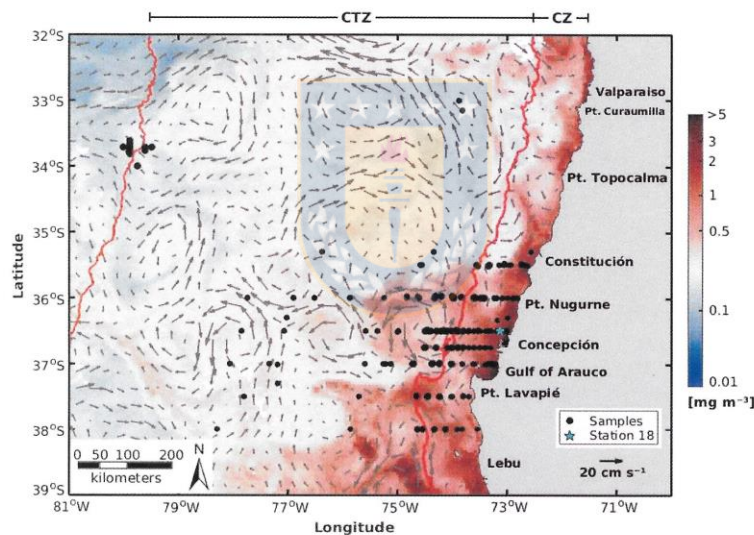


Figure 1. Study area in central-southern Chile. An eight-day composite (25 January 2014–1 February 2014) of surface total chlorophyll-a (Chl-a), obtained from version 3.0 of the Ocean Colour Climate Change Initiative (OC-CCI; 4 km resolution) product, is represented in red-blue color scale. The geostrophic velocity, obtained from Ssalto/Duacs multimission altimeter AVISO product (<http://www.aviso.altimetry.fr>), is shown in gray arrows. The blue star indicates the location of the COPAS coastal time series Station 18 and, together with the black dots, indicates the locations of the size-fractionated filtration (SFF) Chl-a in situ data (≤ 10 m depth), during different campaigns (November 2004–September 2015). The red lines indicate the offshore limit of the coastal zone (CZ; ~100 km from the coast) and the coastal transition zone (CTZ; coast to ~800 km offshore), respectively.

2.2.2. Parameterization of the Three-Component Model

The two-component model of Sathyendranath et al. [62] was extended to a three-component model by Brewin et al. [43] to estimate the Chl-a concentration contributed by three PSC (C_M , C_N , and C_p)

as a function of total Chl-a. The model is abundance-based and assumes that (i) the micro-(pico-) phytoplankton fraction increases (decreases) monotonically as a function of total Chl-a and (ii) smaller cells achieve a given Chl-a concentration, beyond which total Chl-a increases only by the addition of larger size cells. The model is based on the following relationships: (i) total Chl-a concentration (C) is derived from the sum of the three PSC,

$$C = C_M + C_N + C_P \quad (1)$$

and (ii) two exponential functions are used to estimate the Chl-a concentration of the smaller PSC as a function of total Chl-a (C) [62]: one which combines the nano- and picoplankton groups (C_{NP} , [63]), and one for the picoplankton (C_P),

$$C_{NP} = C_{NP}^m \left[1 - \exp\left(-\left(\frac{D_{NP}}{C_{NP}^m}\right)C\right) \right] \quad (2)$$

$$C_P = C_P^m \left[1 - \exp\left(-\left(\frac{D_P}{C_P^m}\right)C\right) \right] \quad (3)$$

in which C_{NP}^m and C_P^m are the asymptotic maximum values for the associated size classes; D_{NP} and D_P reflect the fraction contributed by each size-class to total Chl-a as total Chl-a tends to zero, and they should take values in the range between 0 and 1 to ensure size-fractionated Chl-a does not increase faster than total Chl-a [41]. Equations (2) and (3) can also be expressed in terms of the fractions of each associated size class (F_{NP} and F_P), i.e., the size-specific fractional (relative) contributions to total Chl-a, and can be calculated by dividing the size-specific Chl-a concentration (C_{NP} and C_P) by C [47,64]. Model parameters (C_{NP}^m , C_P^m , D_{NP} , and D_P) were derived from Equations (2) and (3) in terms of the fractions fitted to C , C_{NP} , and C_P , using the in situ SFF Chl-a data. The fitting procedure used a standard, nonlinear least-squares method of Levenberg-Marquardt [43].

In order to compute the uncertainties in the parameters and to validate the model, the in situ SFF Chl-a data (227 samples) were randomly split, using 80% of the measurements (182 samples) for parameterization and the remaining 20% (45 samples) as the validation dataset (see Section 2.2.3). A bootstrapping method [65] was used to compute the model parameters and their uncertainties, so the 182 measurements were randomly sub-sampled with replacement (1000 times) and Equations (2) and (3) were re-fitted for each sub-sample by minimizing the squared difference in the fractions (F). Then, the median and 95% confidence intervals were calculated for the obtained parameter distribution [41].

2.2.3. Validation of the Model, Application to Satellite Data, and Match-Up between In Situ and Satellite Size-Fractionated Chlorophyll-a Estimates

Total Chl-a from the parameterization dataset together with the model parameter values (C_{NP}^m , C_P^m , D_{NP} , and D_P) were used as input variables in Equations (2) and (3) to calculate model estimates of C_{NP} and C_P , after which C_N and C_M were derived from the following relationships $C_N = C_{NP} - C_P$ and $C_M = C - C_{NP}$ [41,43,48]. Modelled and in situ size-fractionated Chl-a data were compared to evaluate the PSC model performance [41,48]. The same procedure was carried out to calculate satellite size-fractionated Chl-a based on daily satellite-derived total Chl-a (January 2004 to December 2015) for the region of study. These data were obtained from version 3.0 of the Ocean Colour Climate Change Initiative (OC-CCL, a merged product available at <http://www.oceancolour.org/>), at processing level 3 and spatial resolution of 4 km. The in situ size-fractionated Chl-a validation dataset (45 samples) was compared with the obtained size-fractionated Chl-a satellite estimates [41,48]. Each in situ sample was matched with a daily satellite dataset using the nine pixels closest to the location of the sample, and only match-ups with a coefficient of variation <0.15 and 50% of valid data in the nine pixels were considered. The median Chl-a concentration of these pixels was taken as the satellite estimate and compared with in situ data [41,66]. Finally, the Pearson linear correlation coefficient (r), root mean square (RMS) error, and bias (δ) were calculated in \log_{10} space as statistical metrics for model and

satellite model validation following Brewin et al. [48], in order to compare them with those from previous studies. Recently Seegers et al. [67] have queried the use of RMS as an error metric in the case of Chl-a data and have instead recommended the use of the mean/median absolute error (MAE and MdAE) and the median bias (δ). In addition, these authors recommend that these metrics be back-transformed from the \log_{10} space for interpretation. For this reason, we have also included the metrics and procedures suggested by Seegers et al. [67].

2.3. Eddy Detection and Tracking

Eddy detection and tracking was based on the freely-available sea surface height (SSH) approach of Mason et al. [68] (<http://imedea.uib-csic.es/users/emason/py-eddy-tracker>), which is based in the detection of closed contours of sea level anomaly (SLA), following the procedures described by Chelton et al. [19], Kurian et al. [69], and Penven et al. [70]. Daily delayed-time “two-sat” SLA data from the Ssalto/Duacs AVISO 2014 altimetry product (<http://www.aviso.altimetry.fr>), from January 2014 to December 2015, were used to represent the surface current in the study region, with the advantage that these data offer homogeneous quality in space and time, and enhance the description of mesoscale activity in coastal regions of EBCS [71].

Daily SLA fields were spatially high-pass filtered by removing a smooth field, obtained from a Gaussian filter with a zonal (meridional) major (minor) radius of 10° (5°) or ~ 1000 km (~ 500 km). SLA closed contours computed at 0.2 cm intervals and searched from 100 (–100) cm downward (upward) were used to identify cyclonic (anticyclonic) eddies. To be selected as the effective perimeter of an eddy, an identified closed contour should meet the following criteria: (i) the amplitude has to be >0.1 cm, (ii) the number of local extreme limited to 1, and (iii) the radius of the eddy has to range from 0.3° (~ 30 km) to 4.461° (~ 446 km) [68]. The lower value differs from that established by Chelton et al. [19], where eddies with radius $<0.4^\circ$ (~ 40 km) were filtered out. In this sense, the method of Mason et al. [68] has a natural tendency to identify more and smaller eddies than that of Chelton et al. [19], presumably due to stricter identification criteria and sharper SLA gradients in the version of the AVISO data (DT14) compared with the DT10 version used by Chelton et al. [19,71]. Moreover, we were interested in following specific eddies, including those subsurface-intensified but with limited surface signature, which justifies our choice of a minimum valid radius of 0.3° (~ 30 km). Also, in order to keep tracking an eddy even when punctually distorted, we chose not to use a shape test that aimed to filter out highly irregular closed contours [68], so the position of an eddy center and the speed-based eddy radius (the radius of the circle with the same area as the region within the contour of SLA with maximum rotational speed) were then followed along the eddy-track path of interest.

One cyclonic and three anticyclonic eddies were detected and tracked in the study region in the period between January 2014 and December 2015. Two of the anticyclones were found to be subsurface-intensified anticyclonic eddies, one of which interacted with an oceanic seamount at some point, as revealed by satellite and CTD (conductivity, temperature and depth) data collected during the FIP Seamount cruise [61], while the other interacted with an upwelling front, as observed in CTD data during the PHYTOFRONT cruise [33]. Specifically, the studied eddies are composed of (i) a subsurface anticyclone (ssAC1), which was born in the coastal region south of Point Lavapié ($\sim 38.04^\circ\text{S}$, 74.30°W) and propagated westward to the Juan Fernandez Ridge (27 December 2014 to 13 August 2015; 7.5 months of tracking); (ii) a subsurface anticyclone (ssAC2), which was initially detected off Point Nugurne ($\sim 36.21^\circ\text{S}$, 73.83°W ; 1 January 2014 to 21 August 2014; 7.5 months of tracking); (iii) a surface anticyclone (sAC), which was born off Lebu ($\sim 38.67^\circ\text{S}$, 74.45°W ; 10 February 2014 to 1 November 2014; 8.5 months of tracking); and iv) a surface cyclone (sC) detected close to Constitución ($\sim 35.14^\circ\text{S}$, 72.83°W ; 9 November 2014 to 8 October 2015; ~ 11 months of tracking; Figure 1).

2.4. Size-Fractionated Chlorophyll-*a* Satellite Estimates in Mesoscale Eddies

Based on the spatial dimension of the study region (5° latitude \times 8° longitude; $33\text{--}38^\circ\text{S}$, $72\text{--}80^\circ\text{W}$) and in order to remove unwanted small and large-scale features unrelated with mesoscale variability [8,19,22], the following procedure was carried out: (i) the seasonal cycle of the satellite estimates of size-fractionated Chl-*a* concentrations (C_M , C_N , and C_P) was removed by subtracting the monthly climatology (linearly interpolated to daily values) from the daily size-fractionated Chl-*a* data and (ii) eight-day composites of the satellite estimates resulting from the previous step were produced (for further details see Appendix A). For this purpose, the monthly climatology and the averages were calculated in \log_{10} space, considering that Chl-*a* concentration is approximately log-normally distributed over the global ocean [72]. Also, an eight-day average of the radius (km) and the displacement speed (km week^{-1}) of eddies were calculated in order to have the same temporal resolution as the Chl-*a* data.

The obtained mesoscale size-fractionated Chl-*a* fields, sampled on a square grid (longitude \times latitude), were placed in a framework of polar coordinates with a radial distance from the eddy center defined by the eddy radius (R), so the associated size-fractionated Chl-*a* fields were projected into an eddy frame and the Chl-*a* values at any distance r were projected to r/R . However, to be able to construct a standard scale based on the eddy radius of each eddy, we normalized the Chl-*a* fields by twice the radius ($2R$) in each case [8,22,73]. Then, we ensured that during the tracking period of eddies, the size-fractionated Chl-*a* fields covered at least 50% of their spatial extension, screening out the periods (weeks) when this was not achieved. Finally, the variability of PSC was evaluated from the average fraction fields (F_M , F_N , and F_P) in the eddy center ($r/R \leq 1$) and in the periphery ($1 < r/R \leq 2$), and these values were compared with the mean of the fractions in the CZ when eddies were located closer to the coast.

A flow-diagram of the methods described above and a list of symbols and abbreviations are presented in Appendixes B and C, respectively.

3. Results

In situ data of total and size-fractionated Chl-*a* concentrations analyzed in this study were mainly obtained in the CZ (77%), with total Chl-*a* values ranging between 0.20 and 17.76 mg m^{-3} , while the remaining (23%) correspond to the CTZ, with values between 0.15 and 1.66 mg m^{-3} (Figure 1). The ~90% of the data were obtained during the spring-summer months, when the southwesterly winds favor the coastal upwelling. For this dataset, the contribution of each PSC in the study region was 35.4% by the microplankton fraction, with a mean (maximum) Chl-*a* concentration of 1.62 mg m^{-3} (16.42 mg m^{-3}); 53.7% by nanoplankton, with a mean (maximum) Chl-*a* concentration of 0.84 mg m^{-3} (4.42 mg m^{-3}); and 10.9% by picoplankton, with mean (maximum) Chl-*a* values of 0.12 mg m^{-3} (0.87 mg m^{-3}).

3.1. Satellite Model of Phytoplankton Size Classes

In situ Chl-*a* concentration by size (C_M , C_{NP} , C_N , and C_P), and by fractions (F_M , F_{NP} , F_N , and F_P), as a function of in situ total Chl-*a*, together with the re-tuned three-component model of Brewin et al. [43], are shown in Figure 2. The general trends of these relationships were captured by the model based on the calculated regional parameters (Table 1), according to which the nano- and picoplankton reached asymptotic values of $C_{NP}^m \sim 2.12 \text{ mg m}^{-3}$ and $C_P^m \sim 0.19 \text{ mg m}^{-3}$, while Chl-*a* concentrations higher than these were only achieved by the micro-phytoplankton (Figure 2a-d). In terms of fractions, the model also captured the trends of the in situ dataset, with large (small) cells increasing (decreasing) their contribution to total Chl-*a* as its values became higher (Figure 2e-h). The parameter D also reflects the higher contribution by the smaller fractions when total Chl-*a* tends to zero ($D_{NP} \sim 0.92$ and $D_P \sim 0.21$; Table 1 and Figure 2f,h).

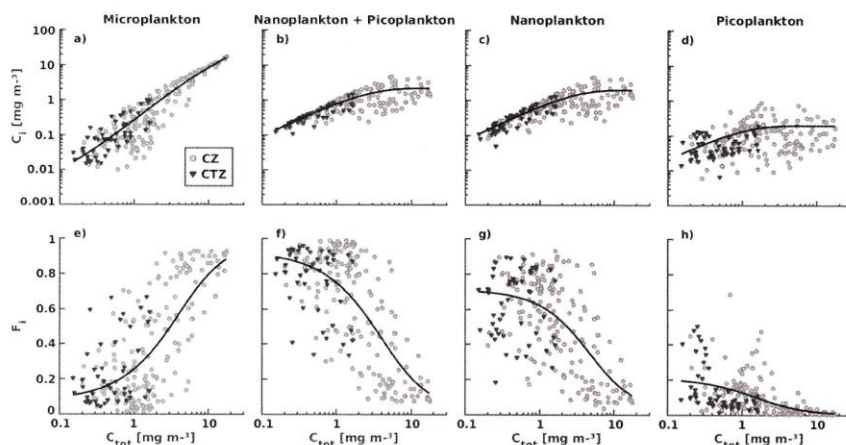


Figure 2. In situ concentrations of size-fractionated Chl-a for micro- (C_M), nano- and pico- (C_{NP}), nano- (C_N), and picoplankton (C_P) (upper panels: a–d), and their contribution to total in situ Chl-a (lower panels: e–h) as a function of total in situ Chl-a concentration (C). The fitted three-component model of Brewin et al. [43] is overlaid in each case (solid black line). The subscript ‘i’ indicates the different Chl-a size classes. The location of the samples in the CZ and CTZ is differentiated by grey dots and black triangles, respectively.

Table 1. Parameter values for the three-component model based on in situ size-fractionated chlorophyll-a (Chl-a) concentrations off central-southern Chile and comparison with those derived from previous studies in different systems.

	Area	Method	Model Parameters			
			C_{NP}^m (mg m^{-3})	D_{NP}	C_P^m (mg m^{-3})	D_P
Brotas et al. [50] [§]	EA	HPLC	0.36	0.92	0.07	0.77
Lin et al. [52]	SCS	HPLC	0.95	0.94	0.26	0.90
Brewin et al. [44]	AO	SFF	2.78 (2.23–3.56)	—	0.66 (0.55–0.80)	—
Brewin et al. [41]	Global	HPLC	0.77 (0.72–0.84)	0.94 (0.93–0.95)	0.13 (0.12–0.14)	0.80 (0.78–0.82)
Brito et al. [51] [§]	NEA	a_{ph} , HPLC	0.26–0.50	0.86	0.09	0.16
Ward [46]	Global	SFF	0.79	0.97	0.16	0.84
Brewin et al. [48]	NA	HPLC, SFF	0.82 (0.76–0.88)	0.87 (0.86–0.89)	0.13 (0.12–0.13)	0.73 (0.71–0.76)
This study	CSC	SFF	2.12 (1.75–2.54)	0.92 (0.88–0.96)	0.19 (0.11–0.27)	0.21 (0.16–0.33)

C^m indicates the asymptotic maximum of Chl-a for a given size class (P = pico-phytoplankton; NP = nano- + pico-phytoplankton), and D reflects the fraction contributed by a given size class to total Chl-a as total Chl-a tends to zero. In brackets are the 95% confidence intervals calculated for the obtained parameters distribution. In situ methods to derive size-specific Chl-a concentrations: HPLC = High Performance Liquid Chromatography, SFF = Size-Fractionated Filtration, and a_{ph} = Phytoplankton Absorption spectra. Study areas: EA = Eastern Atlantic, SCS = South China Sea, AO = Atlantic Ocean, NEA = North-East Atlantic, NA = North Atlantic, and CSC = Central-Southern Chile. [§] Studies that include coastal stations for in situ size-specific Chl-a measurements.

The PSC model validation with regard to in situ size-fractionated Chl-a concentrations was assessed with statistical metrics (r , RMS error, MdAE, and MAE) without back-transformation from \log_{10} space, and the results are presented in Table 2 and compared with previous studies. Higher correlation coefficients (r) were obtained for the micro-, nano-, and the combined nano- and picoplankton groups (>0.80), while that of picoplankton was (<0.4). Low uncertainties values were obtained for the nano- and the combined nano- and picoplankton groups, whereas those of the micro- and picoplankton were moderate. Biases (δ) were mostly low for the different PSC (0.04 for nano- and pico, 0.17 for pico-, 0.05 for nano-, and 0.13 for microplankton). Our correlation and uncertainty values are similar to those reported in previous studies (Table 2), except for the low r value in the case of

the picoplankton. The latter value is, however, higher than that obtained by Ward [46]. In applying the back-transformation procedure recommended by Seegers et al. [67], we considered the metrics MdAE and bias for comparison (Table 3). In the interpretation of these metrics (MdAE(t) and $\delta(t)$), values closer to unity indicate lower relative errors and bias, with biases higher (lower) than unity implying that the model overestimates (underestimates) in situ measurements [67]. In terms of the MdAE(t) results, the highest uncertainties were associated with the micro- (~69%) and picoplankton (~97%) size classes in comparison with the other PSC (<30%); bias values were close to unity, except for picoplankton (Table 3).

Table 2. Statistical relations between modelled and in situ size-fractionated Chl-a concentrations and comparison with those obtained in previous studies.

		Metrics		
		r	RMS	MAE
Micro	Brotas et al. [50] §	—	—	0.32
	Lin et al. [52]	0.99	0.46	—
	Brewin et al. [41]	0.91	0.34	—
	Ward [46]	0.83	0.47	—
	Brewin et al. [48]	0.93	0.32	—
	This study	0.88	0.41	0.30 (0.23)
Nano	Brotas et al. [50] §	—	—	0.19
	Lin et al. [52]	0.94	0.17	—
	Brewin et al. [41]	0.93	0.24	—
	Ward [46]	0.78	0.30	—
	Brewin et al. [48]	0.88	0.30	—
	This study	0.80	0.22	0.16 (0.11)
Pico	Brotas et al. [50] §	—	—	0.18
	Lin et al. [52]	0.89	0.39	0.04
	Brewin et al. [41]	0.64	0.26	—
	Ward [46]	0.21	0.43	—
	Brewin et al. [48]	0.56	0.34	—
	This study	0.37	0.42	0.33 (0.29)
Nano + Pico	Brotas et al. [50] §	—	—	0.11
	Lin et al. [52]	—	—	0.03
	Brewin et al. [41]	0.94	0.13	—
	Ward [46]	0.88	0.12	—
	Brewin et al. [48]	0.90	0.19	—
	This study	0.81	0.20	0.14 (0.10)

r = Pearson linear correlation coefficient, RMS = root mean square error, MAE = mean absolute error, and MdAE = median absolute error in brackets. Statistical test in \log_{10} space. § Studies that include coastal stations for in situ size-specific Chl-a measurements.

Table 3. Statistical relations between modelled and in situ size-fractionated Chl-a concentrations back-transformed from \log_{10} space.

	Metrics	
	MdAE (t)	δ (t)
Micro	1.69	1.07
Nano	1.30	0.98
Pico	1.97	1.36
Nano + Pico	1.27	0.97

MdAE(t) = median absolute error and $\delta(t)$ = median bias, both back-transformed from \log_{10} space (t).

Satellite total Chl-a and model PSC estimates against in situ Chl-a concentrations are displayed in Figure 3. Together with this, the PSC satellite model validation with regard to in situ Chl-a concentrations was assessed with statistical metrics (r and RMS error without back-transformation from \log_{10} space; MdAE and bias with and without back-transformation), and the results are presented in Table 4 and compared with previous studies. Satellite and in situ total Chl-a displayed the highest correlation and lowest uncertainties. Similar values were obtained for nano- and picoplankton groups ($r > 0.70$; RMS < 0.30 ; MdAE < 0.18 ; Figure 3c–e). In the case of the metrics without back-transformation, the microplankton value for r was relatively high, but the uncertainty values were moderate compared to the smaller PSC. The latter is in coherence with a higher data dispersion for this fraction when Chl-a values are $< 0.1 \text{ mg m}^{-3}$ (Figure 3b). Biases (δ) were close to zero for total Chl-a and PSC. In addition, the PSC satellite model validation was performed considering meridional (Northern, Center, and Southern areas of the study region), zonal (CZ and CTZ), and seasonal (calendar seasons) differences. However, no changes were detected in data dispersion (not shown). In comparison with the statistical metrics from previous studies, similar values for r and uncertainty were observed for total Chl-a and PSC; Brotas et al. [50] have reported a similar uncertainty value for the microplankton (48%) compared to ours. In the case of the statistical back-transformed metrics (MdAE(t) and $\delta(t)$), moderate uncertainties ($\sim 50\%$) were observed for total Chl-a and the smaller PSC, whereas those of the microplankton were higher ($> 100\%$). The bias values were mostly low ($< 30\%$).

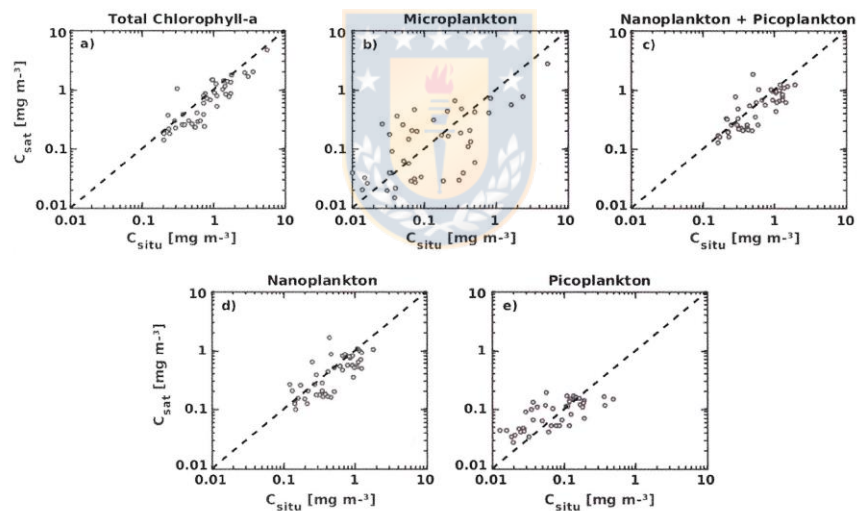


Figure 3. Total satellite Chl-a concentration (OC-CCI product; 4 km resolution) and size-fractionated Chl-a estimates obtained from the regional three-component model, as a function of in situ total and size fractionated Chl-a concentration. The black dotted line represents the 1:1 line (perfect relationship between in situ and satellite estimates).

Table 4. Statistical relations between the satellite estimates of phytoplankton size classes (PSC) from the regional re-tuned three-component model and in situ size-fractionated Chl-a concentrations and comparison with those obtained in previous studies.

	Brewin et al. [41]		Brewin et al. [48]		This Study					
	r	RMS	r	RMS	r	RMS	MdAE	δ	MdAE (t)	δ (t)
Total	0.88	0.25	0.86	0.29	0.87	0.22	0.15	−0.12	1.42	0.73
Micro	0.86	0.41	0.85	0.45	0.64	0.50	0.36	−0.01	2.34	0.92
Nano	0.80	0.38	0.76	0.43	0.79	0.22	0.17	−0.09	1.49	0.79
Pico	0.57	0.28	0.49	0.35	0.72	0.28	0.18	0.06	1.54	1.14
Nano + Pico	0.79	0.27	0.76	0.30	0.76	0.24	0.16	−0.08	1.45	0.77

r = Pearson linear correlation coefficient, RMS = root mean square error. Median absolute error and bias without back-transform from \log_{10} space (MdAE and δ) and back-transformed (MdAE(t) and δ (t)).

An example of the spatial distribution of the satellite estimates for each PSC in the study region is presented in Figure 4. The highest Chl-a concentrations (5.56 mg m^{-3}) are contributed by the microplankton fraction in accordance with the model, and they are mostly observed in the CZ (Figure 4a,d). In contrast, intermediate and lower Chl-a values ($< 5 \text{ mg m}^{-3}$) are mainly achieved by the nano- and picoplankton groups, which are widely distributed in the study region, but with a clear spatial dominance of the nanoplankton (Figure 4b,c,e,f).

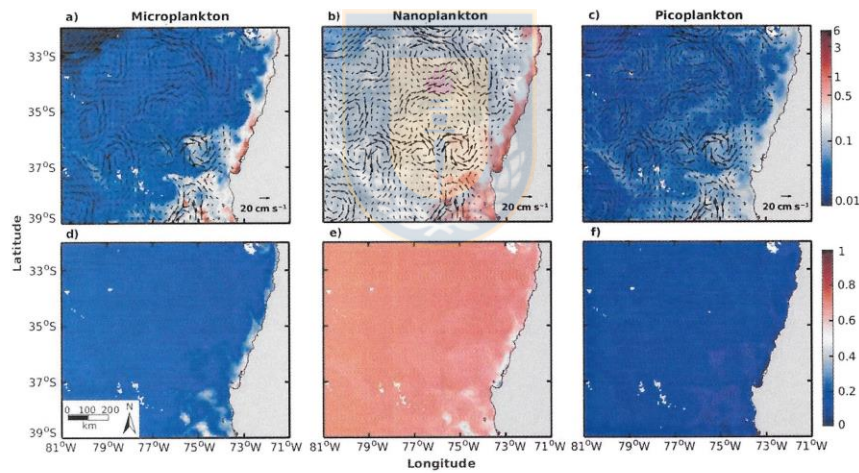


Figure 4. Spatial distribution of the satellite Chl-a estimates for size-fractionated concentrations (a–c; mg m^{-3}) obtained from the regional three-component model applied to the total Chl-a satellite data, and their relative contribution to total Chl-a (d–f; dimensionless). The geostrophic velocity field is shown (black arrows). Data in this figure are an example of an eight-day composite for the same dates included in Figure 1.

3.2. Spatio-Temporal Evolution of Phytoplankton Size Classes within Mesoscale Eddies

The main features and trajectory of the studied eddies, such as the radius and the seaward velocity of displacement, are shown in Figure 5. These eddies move offshore at mean speeds of $\sim 20 \text{ km week}^{-1}$ ($\sim 2.5 \text{ km d}^{-1}$) and have mean radius of $\sim 40\text{--}60 \text{ km}$ ($\sim 80\text{--}120 \text{ km}$ in diameter). For the study period, the trajectories of the four eddies were independent of each other, except for ssAC2 and sAC, which were found to interact with each other during 25 weeks (~ 6 months; 10 February 2014

to 28 August 2014; data not shown). Also, the sAC eddy was detected and tracked farthest from the coast ($\sim 75^\circ\text{W}$) in comparison with the other eddies (upper panels in Figure 5).

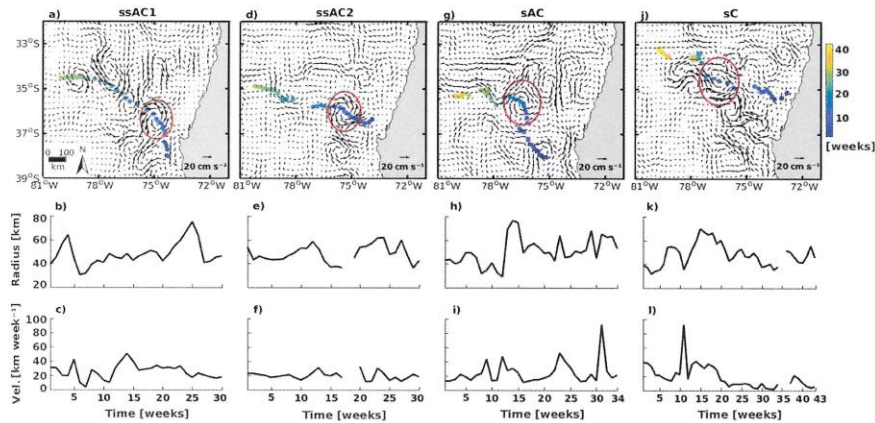


Figure 5. The geostrophic velocity field (black arrows) and the trajectories of the tracked mesoscale eddies (upper panels: a,d,g,j), together with radius (b,e,h,k) and displacement velocity (c,f,i,l) through time (in weeks). The red circles in the upper panels represent the eddies in a time step of their complete trajectories (blue–yellow color scale). Four eddies were analyzed: subsurface anticyclone 1 (ssAC1; 27 December 2014 to 13 August 2015, 30 weeks), subsurface anticyclone 2 (ssAC2; 1 January 2014 to 21 August 2014, 30 weeks), surface anticyclone (sAC; 10 February 2014 to 1 November 2014, 34 weeks), and surface cyclone (sC; 9 November 2014 to 8 October 2015, 43 weeks). Gaps in the data for some periods (weeks) were created after screening out size-fractionated Chl-a fields that did not cover at least 50% of the spatial extent of an eddy.

Eight-day composites of surface total Chl-a anomalies for three different time steps of the eddy trajectories, together with the mean surface currents, are shown in Figure 6, in order to visualize and compare total Chl-a anomalies within the eddies and those in the surrounding waters. High positive Chl-a anomalies ($>1 \text{ mg m}^{-3}$) were mainly observed in ssAC1 and sC when they were located closer to the coast (Figure 6a,j), while lower values were found in ssAC2 and sAC for the first evaluated time step in comparison with those in the surrounding waters (Figure 6d,g). For the other time steps (middle and bottom panels in Figure 6), positive values were observed within and outside the eddies, except for the second evaluated time step in ssAC1, which showed negative anomalies ($\sim -0.2 \text{ mg m}^{-3}$; Figure 6b) and for sC, where positive anomalies values were found ($\sim 0.6 \text{ mg m}^{-3}$; Figure 6k).

The evolution of each phytoplankton size fraction (as fractions of total Chl-a) within the eddies (center and periphery) is shown in Figure 7, along with the mean contribution by each fraction in the CZ for the first week of the eddy tracking period (red dots). No major differences in PSC were found between the center and the periphery of the eddies. The picoplankton fraction was in almost constant proportion ($\sim 0.10\text{--}0.20$) with respect to the other groups, and a clear dominance of the nanoplankton was found in all the eddies (~ 0.50 to 0.70). For ssAC1 and sC eddies, the highest values by the microplankton fraction were of ~ 0.50 within the first 5 to 10 weeks of tracking (Figure 7a,j), in association with their closer proximity to the CZ (Figure 5a,j), while the nanoplankton display values of ~ 0.50 and the picoplankton fraction reached values <0.1 (Figure 7b,c,k,l). Inside these eddies, 20% more of the microplankton fraction is observed when compared with the CZ values (~ 0.33 and 0.26 , respectively). For the subsurface anticyclone ssAC2, the microplankton (nano- and picoplankton) fraction showed a tendency to decrease (increase) along the tracking period (30 weeks;

Figure 7d,f), while for the surface anticyclone sAC, a decrease (increase) of the microplankton (nano- and picoplankton) fraction was detected during the first 10 weeks (Figure 7g–i).

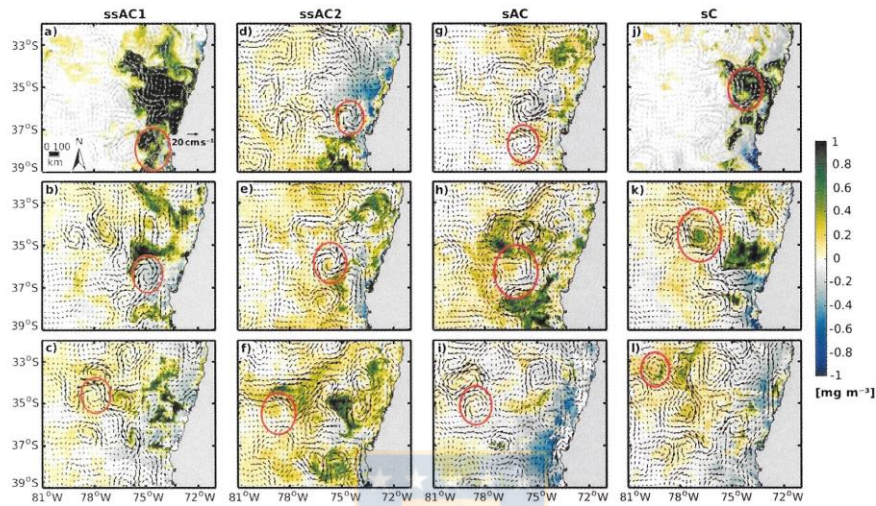


Figure 6. Eight-day composites of surface total Chl-a anomalies (green-blue color scale) for three different time steps of eddies trajectories. The position and radius of the eddies in each composite (red circles) and the geostrophic velocity field (gray/black arrows) are also shown. The dates of the composites are ssAC1 (a–c) 9–16 January 2015, 14–21 March 2015 and 2–9 June 2015; ssAC2 (d–f) 25 January to 1 February 2014, 22–29 March 2014 and 10–17 June 2014; sAC (g–i) 14–21 March 2014, 17–24 May 2014 and 29 August to 5 September 2014; and sC (j–l) 1–8 January 2015, 26 February to 5 March 2015 and 29 August to 5 September 2015.

After the first week of eddy-tracking, a decrease (increase) of the microplankton (nano- and picoplankton) fraction in the surface and subsurface anticyclones (ssAC1, ssAC2, and sAC) was found. A decrease (~15%) in the contribution of larger cells was found at the end of the tracking period for ssAC2 and sAC when compared with their initial CZ values (0.28–0.30; Figure 7d,g), and a larger reduction (~40%) when compared with the highest contribution achieved by the microplankton fraction (~0.50) in ssAC1 (Figure 7a). In terms of smaller fractions, an increase (~10%) was found between the initial CZ values and their final contribution (Figure 7b,c,e,f,h,i). Moreover, in the sC a decrease (increase) of the microplankton (nano- and picoplankton) fraction was also observed after the first ~10 weeks of tracking, but then the fractions were almost constant through the remaining period (Figure 7j–l). Specifically, a ~10% reduction in the microplankton contribution was found at the end of the 43 weeks when compared with the CZ value (0.26), and a ~40% decrease when compared with the highest contribution achieved by the microplankton inside the sC eddy (~0.50; Figure 7j). As well as in the anticyclones, the smaller fractions in the sC showed an increase (~10%) in comparison with the CZ values (~0.60 for nano- and ~0.10 for picoplankton; Figure 7k,l).

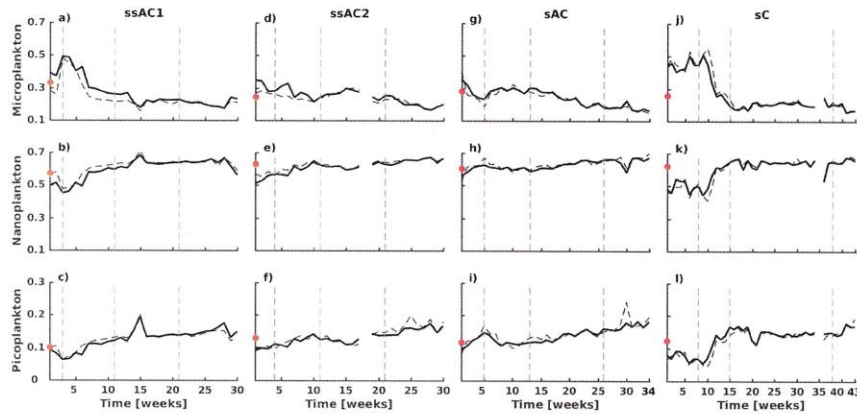


Figure 7. Temporal variability of phytoplankton size classes (PSC) in terms of the size-specific fractional (relative) contributions to total Chl-a (dimensionless) in the four selected eddies (center: continuous black line; periphery: dashed black line) during the period indicated in Figure 5. The mean contribution by each fraction in the CZ for the first week of eddy tracking is denoted by the red dots. The vertical dashed gray lines indicate the weeks of the composites of surface total Chl-a anomalies presented in Figure 6. Gaps in the data are explained in Figure 5.

4. Discussion

4.1. Application of a Three-Component Abundance-Based Model to Retrieve Satellite Estimates of Phytoplankton Size Classes in the Region off Central-Southern Chile

Most of the previous studies using the three-component model have been based on Chl-a data from oceanic waters, e.g., [41,43,44,48,52] and very few have included data from coastal waters [50,51]. Total Chl-a values in this study (0.1 to 18 mg m⁻³) include coastal and coastal transition waters in the Humboldt EBCS [74]. Our in situ dataset supports the model assumptions, i.e., that size-fractionated Chl-a co-varies with total Chl-a and that smaller cells achieve a given Chl-a concentration beyond, which total Chl-a increases only by the addition of larger size cells [43]. Differences between the model parameters obtained in our study with those from previous ones are mainly explained by regional characteristics (i.e., coastal vs oceanic) and/or the technique used to obtain size-fractionated Chl-a concentrations.

The asymptotic maximum of Chl-a for the two smaller PSC in this study ($C_{NP}^m \sim 2.12$ mg m⁻³) is similar to that found in the Atlantic Ocean by Brewin et al. [44] ($C_{NP}^m \sim 2.78$ mg m⁻³), both using the in situ SFF method to derive size-specific Chl-a concentrations (Table 1). In contrast, Ward [46] found a lower asymptotic value (C_{NP}^m : 0.79 mg m⁻³) using the same technique, but the measurements excluded eutrophic and coastal areas. In comparison with studies using HPLC, a_{ph} , or a combination of both techniques, our C_{NP}^m value was almost twice as large as results from oceanic regions ($C_{NP}^m \sim 0.77$ – 0.95 mg m⁻³) [41,48,52] and even larger than those from near-shore or upwelled coastal waters in the North-East/Eastern Atlantic ($C_{NP}^m \sim 0.26$ – 0.50 mg m⁻³) [50,51]. Our estimate of the asymptotic maximum of Chl-a for the picoplankton ($C_P^m \sim 0.19$ mg m⁻³) is in the range of those in previous studies ($C_P^m \sim 0.07$ – 0.26 mg m⁻³) [41,46,48,50–52], except for that of Brewin et al. [44] ($C_P^m \sim 0.66$ mg m⁻³). However, Brewin et al. [44] found higher asymptotic values for SFF data compared with HPLC data in both smaller size fractions (C_{NP}^m : ~ 2.78 mg m⁻³ with SFF and ~ 1.41 mg m⁻³ with HPLC, C_P^m : ~ 0.66 mg m⁻³ with SFF and ~ 0.16 mg m⁻³ with HPLC). Altogether, different techniques generate changes in the computed parameters of the three-component model.

The size-fractionated filtration (SFF) technique directly provides the size classes of phytoplankton, but it has uncertainties associated with inaccurate pore sizes of filters, cell breakage during filtration, and filter clogging, all errors that are very difficult to quantify [41,44,45,48]. In the case of the HPLC technique, size-fractionated Chl-a is inferred indirectly from specific pigments. However, most of these pigments are distributed in different phytoplankton size classes; therefore, a bias can be created [41,43,50]. The biases associated with these two methodological approaches overestimates or underestimates size-specific Chl-a concentrations, e.g., [44,45]. An alternative method, the a_{ph} , has the advantage of being independent of total Chl-a concentration for distinguishing the PSC. However, absorption coefficients that are considered specific to a given PSC may include other size classes as a result of the package effect, which can modify the absorption spectrum, thereby generating uncertainties in the discretization of PSC [75,76]. Future work should focus on intercomparisons of the estimates of PSC in the region of study using different in situ methods and quantifying the uncertainties associated with them, as to improve the accuracy of model parameters [45,77].

In terms of the fractional contribution of the two smaller PSC to total Chl-a when total Chl-a tends to zero, the D_{NP} parameter value obtained in this study (~ 0.92) is very similar to those from previous studies ($\sim 0.86\text{--}0.97$) [41,44,46,48,50–52], without differences among techniques or regions (Table 1). In contrast, the D_P parameter revealed regional differences. High D_P values ($\sim 0.80\text{--}0.90$) have been obtained in open ocean waters, e.g., [41,46,52], in consistency with the expected dominance of the picoplankton fraction in these environments [78–80]. However, Brotas et al. [50] also obtained a high D_P value (0.77) in waters of a wide range of trophic status (from eutrophic to oligotrophic). Microscopic and flow cytometry analysis by these authors indicated that the picoplankton contributed to 90% of total cell abundance, but with a low contribution to total Chl-a ($C_p^m \sim 0.07 \text{ mg m}^{-3}$). Our estimate of D_P (~ 0.21) is low and similar to that obtained in the coastal region off Portugal (D_P of 0.16) [51]. Low D_P values imply a higher contribution by the nanoplankton fraction, i.e., high ($D_{NP}\text{--}D_P$) values. In our study region, the nano- and microplankton fractions have been found to be dominant during the upwelling season [81–84].

The modelled size estimates obtained from the application of the three-component model tuned to the region off central-southern Chile show moderate uncertainty values with in situ Chl-a concentrations for the micro- and picoplankton fractions compared with the other groups (Tables 2 and 3). This could be partially explained by a higher dispersion of the in situ measurements in both PSC. In the case of picoplankton, this problem is detected in the whole range of total Chl-a, making it difficult to adjust an accurate monotonic function for this fraction. This also implies an error in the microplankton model estimates, since they are obtained by subtracting the picoplankton model estimates from in situ total Chl-a measurements. The same problem in the adjustment of a monotonic function for the picoplankton was reported by Ward [46], who used the SFF technique (as in this study) to distinguish in situ PSC. This gives support to the issue that the different in situ methods used to retrieve PSC could imply further uncertainties ([41,44,45,48], this study). Additionally, Ward [46] found a better performance of the three-component model when temperature ranges were incorporated, but reported that this factor is not important for tropical and sub-tropical regions, such as our study region. Altogether, improvements are required in the application of the PSC models, including a wider range of in situ total Chl-a concentrations or direct biomass estimates per size fractions in the region.

Regarding the satellite size model estimates, the moderate to high uncertainty values for the microplankton could be related to a wider dispersion of the satellite estimates for this fraction when total Chl-a reaches values $< 1 \text{ mg m}^{-3}$. In coastal upwelling regions, such as in this study, total Chl-a values reach up to 50 mg m^{-3} [85], implying that the range included here is very narrow. The accuracy in the estimates for all PSC could be also related to (i) deviations in the relationship between the PSC and total Chl-a previously reported for optically complex waters, often found in coastal systems [48]; (ii) the spatial scale when comparing 4 km satellite pixels with specific in situ value obtained from $\sim 250\text{--}300 \text{ mL}$ of water, involving an additional sub-pixel variability in PSC estimates [48]; (iii) the estimation of total Chl-a concentrations from the ocean colour algorithms which

are based on an assumed relationship between the total Chl-a and the remote sensing reflectance, both of which could vary according to cell size [46,67]; and (iv) the optical depth [43,50], an aspect that could be explored in future works.

Finally, the higher uncertainties associated with the microplankton satellite estimates obtained in this and previous studies, which use the same PSC model, represent a limitation in the application of this model. However, there are at least two aspects that support the application of such a model in our case. The first one is that the satellite-derived spatial distribution of the PSC in CZ and CTZ in the study region is consistent with previous reports using in situ data from the same region; that is, nanoplankton dominates in the CTZ, whereas microplankton does so in the CZ, e.g., [30,60,81,84]. The second one is that previous in situ studies on PSC associated with mesoscale eddies have shown that an important fraction of the coastal microplankton in this region appears to be advected by these features during their early stages of development [32,33].

4.2. Shifts on Phytoplankton Size Classes within Mesoscale Eddies

The main features of eddies, mean seaward speed ($\sim 2.5 \text{ km d}^{-1}$) and diameter ($\sim 80\text{--}120 \text{ km}$), are in agreement with previous reports for mid-latitude eddies ($62\text{--}128 \text{ km}$) [7,19] and for eddies off central-southern Chile ($\sim 1\text{--}2 \text{ km d}^{-1}$ and $70\text{--}110 \text{ km}$) [30,32]. Regarding the PSC, the highest contributions of the microplankton fraction during the first 5 to 10 weeks of tracking ssAC1 and sC eddies are associated with their closer proximity to the CZ, characterized by upwelling waters rich in nutrients and in situ high microplankton abundance and Chl-a concentrations [84]. During this first period, the microplankton contribution inside these eddies was higher (about 0.2 difference) in comparison with the surrounding waters in the CZ. This difference could be a response to trapping and stirring of coastal waters within the eddies and/or by the vertical displacement of the isopycnals during eddy formation promoting an influx of nutrients and high phytoplankton productivity rates [10,11,14]. The shift of the phytoplankton community structure towards smaller PSC when the eddies were transiting through the CTZ is in agreement with in situ measurements off central-southern Chile, which indicated that similar eddy types were mostly dominated by smaller cells in the CTZ [32]. In the case of sAC and ssAC2, similar or lower microplankton fraction values were found in comparison with those in the CZ during the first weeks of tracking. For sAC, this could be explained as a response to the physical dynamics of this eddy type, usually characterized by a downward displacement of isopycnals, which forces a flush of nutrients below the euphotic zone and the consequent decrease in primary production [3,9–11]. In the case of ssAC2, Morales et al. [33] have previously described that this eddy was interacting with a coastal front during a relaxation phase of upwelling, time at which the nanoplankton made the largest contributions to total Chl-a.

The observed tendency of the PSC contributions throughout the complete follow-up period of eddies might be explained by factors such as changes in nutrient availability and grazing pressure. In the region off central-southern Chile, waters with high nitrate and silicate concentrations ($\sim 10 \mu\text{M}$) have been associated with the upwelling of the Equatorial Subsurface Waters (ESSW) in the CZ, favoring the dominance of the microplankton fraction (e.g., diatoms) [85,86]. In contrast, waters in the CTZ are often lower in silicate concentration leading to changes in the nitrate:silicate ratios [33]. Ratios close to 1:1 have favored the growth of large phytoplankton cells, whilst higher values ($>3:1$) can produce shifts in the size of diatoms and/or changes towards other small functional groups [33,87,88]. Phytoplankton communities within eddies can also change as a result of predator-prey interactions. Paterson et al. [89] found a lack of phytoplankton biomass accumulation within a surface anticyclone eddy, which was attributed to zooplankton grazing, mostly upon diatoms. They also reported a higher zooplankton biomass inside this type of eddy compared with surface cyclonic eddy. In the region of study, however, it was not possible to test this aspect. Other processes, such as wind-eddy interactions, could favor the transport of phytoplankton below the euphotic zone [11], together with a faster sinking of microplankton cells when the nutrients are depleted [4], which can also generate shifts in the PSC within mesoscale eddies. Future work could be done complementing the three-component

model parameters here calculated together with regional biogeochemical models to better assess the changes of the phytoplankton community structure associated with the mesoscale features off central-southern Chile.

5. Conclusions

A three-component (micro-, nano-, and picoplankton) model for phytoplankton was tuned with in situ Chl-a data from surface waters in CZ and CTZ off central-southern Chile in order to retrieve the satellite estimates of PSC in this highly productive coastal upwelling region. The model was found to capture the trend of in situ SFF Chl-a measurements, and the model assumptions were met. The retrieved model PSC estimates showed the best agreement in the case of the nanoplankton and the combined nano- and picoplankton groups. In contrast, moderate to high uncertainties were found in the case of micro- and picoplankton, in concordance with a higher data dispersion of the picoplankton Chl-a measurements, making it difficult to fit accurate model parameters. The application of the estimated model parameters to total Chl-a satellite data show the best agreement between the satellite estimates of smaller PSC and in situ data measurements. However, the microplankton fraction displayed the highest uncertainty value, which was mainly associated with a larger data dispersion of satellite estimates for this fraction when total Chl-a values were low. Our results show a shift of the PSC from larger to smaller phytoplankton cells in the seaward transit of eddies, changes which appear to be associated with the location of the eddies with regard to the coast, eddy type, nutrient availability, and/or zooplankton grazing upon phytoplankton cells.

Author Contributions: In situ size-fractionated Chl-a data collection: C.E.M., V.A., and A.C.A. Parameterization of the three-component model for the study region: R.J.W.B. and A.C.A. Detection and tracking of eddies: P.A.A. Procedures and data analysis: C.E.M., O.P., S.H., and A.C.A. Manuscript writing: A.C.A. with input from all co-authors.

Funding: This research was funded by FONDECYT Project 1151299 (CONICYT-Chile) to C.E.M. and S.H. Additional support during the writing phase was provided by the Instituto Milenio de Oceanografía (IMO-Chile), funded by the Iniciativa Científica Milenio (ICM-Chile). A.C.A. was supported by a CONICYT-Chile Scholarship (2013–2017).

Acknowledgments: The authors thank the European Space Agency for the production and distribution of the Ocean Colour Climate Change Initiative dataset, Version 3.0, available online at <http://www.esa-oceancolour-cci.org/>. Sea level anomaly data were generated by DUACS and distributed by AVISO (<ftp://ftp.aviso.oceanobs.com>). Cross-Calibrated Multi-Platform (CCMP) Version-2.0 surface wind data were produced by Remote Sensing Systems, and are available at <http://www.remss.com>. We are grateful to the COPAS Center for providing total and size-fractionated Chl-a in situ data from St. 18 time series, and to FIP (Fondo de Investigación Pesquera) projects for providing total and size-fractionated Chl-a in situ data from the area off central-southern Chile (N°2004-20, N°2005-01, N°2006-12, N°2007-10, N°2008-20, N°2009-39 and N°2014-04-2).

Conflicts of Interest: The authors declare no conflict of interest.

Appendix A

Removal of Chlorophyll-a Variability Other than the Mesoscale

In order to remove unwanted small and large-scale features unrelated to mesoscale variability of the size-fractionated Chl-a concentrations, the following procedure was carried out.

Step1: The monthly climatology was linearly interpolated to daily values. For this purpose, the monthly averages were centered on the 15th day of each month (e.g., MA_{m1} and MA_{m2}); then, the interpolated monthly average for a specific day (MA_d) is given by the relationship:

$$MA_d = MA_{m1} \times W_1 + MA_{m2} \times W_2 \quad (4)$$

in which W_1 and W_2 represent the percentage contribution of each monthly average to the date of interest (i.e., W_1 will be 100% if the date of interest corresponds to the 15th of month 1).

Step 2: The daily interpolated climatology was subtracted from the daily size-fractionated Chl-a time series.

Step 3: An eight-day composite of the satellite dataset resulting from the previous step is calculated in \log_{10} space.

Step 4: The spatial median of the whole study region (a box of $\sim 800 \text{ km} \times 800 \text{ km}$; $32\text{--}39^\circ\text{S}$ and $72\text{--}81^\circ\text{W}$) is estimated and removed at each time.

Appendix B

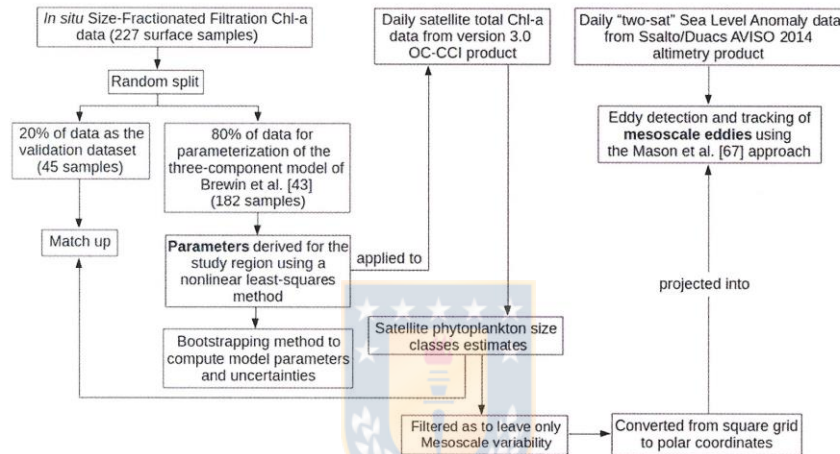


Figure A1. Flow-Diagram of the Methodological Procedures Used in This Study.

Appendix C

Table A1. Symbols and Abbreviations.

Phytoplankton Size-Class Model	
PSC	Phytoplankton size classes
C	Total chlorophyll-a concentration
C_M	Chlorophyll-a concentration by the micro-phytoplankton ($>20 \mu\text{m}$)
C_N	Chlorophyll-a concentration by the nano-phytoplankton ($2\text{--}20 \mu\text{m}$)
C_P	Chlorophyll-a concentration by the pico-phytoplankton ($<2 \mu\text{m}$)
C_{NP}	Chlorophyll-a concentration by the combined nano- and pico-phytoplankton
C_{NP}^{III}	Asymptotic maximum value of C_{NP}
C_P^{III}	Asymptotic maximum value of C_P
D_{NP}	Fraction contribution by the combined nano- and pico-phytoplankton to total chlorophyll-a as total tends to zero
D_P	Fraction contribution by the pico-phytoplankton to total chlorophyll-a as total tends to zero
F_M	Fraction of total chlorophyll-a for micro-phytoplankton
F_N	Fraction of total chlorophyll-a for nano-phytoplankton
F_P	Fraction of total chlorophyll-a for pico-phytoplankton
F_{NP}	Fraction of total chlorophyll-a for the combined nano- and pico-phytoplankton

Table A1. Cont.

In situ methods to characterize the phytoplankton size-classes	
SFF	Size-fractionated filtration
a_{ph}	Phytoplankton absorption spectra
HPLC	High performance liquid chromatography
Statistical metrics	
r	Pearson linear correlation coefficient
RMS	Root mean square error
MAE	Mean absolute error
MdAE	Median absolute error
δ	Bias
Regional abbreviations	
EBCS	Eastern Boundary Current Systems
CZ	Coastal zone
CTZ	Coastal transition zone
EA	Eastern Atlantic
SCS	Southern China Sea
AO	Atlantic Ocean
NEA	North-East Atlantic
NA	North Atlantic
CSC	Central-Southern Chile
Mesoscale features (eddies)	
sC	Surface cyclone
ssAC	Subsurface anticyclone
sAC	Surface anticyclone
ITE	Intrathermocline eddy
R	Eddy radius
r/R	A distance r from eddy center projected to eddy radius
SLA	Sea level anomaly
SSH	Sea surface height

References

- Mann, K.H.; Lazier, J.R. *Dynamics of Marine Ecosystem*; Blakwell Sci.: Michigan, MI, USA, 1991; ISBN 0-86542-082-3.
- Claustre, H.; Kerhervé, P.; Marty, J.C.; Prieur, L. Phytoplankton photoadaptation related to some frontal physical processes. *J. Mar. Syst.* **1994**, *5*, 251–265. [CrossRef]
- Cotti-Rausch, B.E.; Lomas, M.W.; Lachenmyer, E.M.; Goldman, E.A.; Bell, D.W.; Goldberg, S.R.; Richardson, T.L. Mesoscale and sub-mesoscale variability in phytoplankton community composition in the Sargasso Sea. *Deep-Sea Res. I* **2016**, *110*, 106–122. [CrossRef]
- McGillicuddy, D.J., Jr. Mechanisms of physical-biological-biogeochemical interaction at the oceanic mesoscale. *Annu. Rev. Mar. Sci.* **2016**, *8*, 125–159. [CrossRef] [PubMed]
- Garçon, V.C.; Oschlies, A.; Doney, S.C.; McGillicuddy, D.J., Jr.; Waniek, J. The role of mesoscale variability on plankton dynamics in the North Atlantic. *Deep-Sea Res. II* **2001**, *48*, 2199–2226. [CrossRef]
- McGillicuddy, D.J.; Anderson, L.A.; Bates, N.R.; Bibby, T.; Buesseler, K.O.; Carlson, C.A.; Davis, C.S.; Ewart, C.; Falkowski, P.G.; Goldthwait, S.A.; et al. Eddy/wind interactions stimulate extraordinary mid-ocean plankton blooms. *Science* **2007**, *316*, 1021–1026. [CrossRef] [PubMed]
- Chaigneau, A.; Eldin, G.; Dewitte, B. Eddy activity in the four major upwelling systems from satellite altimetry (1992–2007). *Prog. Oceanogr.* **2009**, *83*, 117–123. [CrossRef]
- He, Q.; Zhan, H.; Cai, S.; Zha, G. On the asymmetry of eddy-induced surface chlorophyll anomalies in the southeastern Pacific: The role of eddy-Ekman pumping. *Prog. Oceanogr.* **2016**, *141*, 202–211. [CrossRef]

9. McGillicuddy, D.J., Jr.; Robinson, A.R.; Siegel, D.A.; Jannasch, H.W.; Johnson, R.; Dickey, T.D.; McNeil, J.; Michaels, A.F.; Knap, A.H. Influence of mesoscale eddies on new production in the Sargasso Sea. *Nature* **1998**, *394*, 263–266. [CrossRef]
10. Sweeney, E.N.; McGillicuddy, D.J., Jr.; Buesseler, K.O. Biogeochemical impacts due to mesoscale eddy activity in the Sargasso Sea as measured at the Bermuda Atlantic Time-series Study (BATS). *Deep-Sea Res. II* **2003**, *50*, 3017–3039. [CrossRef]
11. Gaube, P.; McGillicuddy, D.J.; Chelton, D.B.; Behrenfeld, M.J.; Strutton, P.G. Regional variations in the influence of mesoscale eddies on near-surface chlorophyll. *J. Geophys. Res. Oceans* **2014**, *119*, 8195–8220. [CrossRef]
12. Wang, L.; Huang, B.; Chiang, K.P.; Liu, X.; Chen, B.; Xie, Y.; Xu, Y.; Hu, J.; Dai, M. Physical-biological coupling in the western South China Sea: The response of phytoplankton community to a mesoscale cyclonic eddy. *PLoS ONE* **2016**, *11*, e0153735. [CrossRef] [PubMed]
13. Combes, V.; Hormazabal, S.; Di Lorenzo, E. Interannual variability of the subsurface eddy field in the Southeast Pacific. *J. Geophys. Res. Oceans* **2015**, *120*, 4907–4924. [CrossRef]
14. Mourino-Carballido, B.; McGillicuddy, D.J. Mesoscale variability in the metabolic balance of the Sargasso Sea. *Limnol. Oceanogr.* **2006**, *51*, 2675–2689. [CrossRef]
15. Hormazabal, S.; Combes, V.; Morales, C.E.; Correa-Ramirez, M.A.; Di Lorenzo, E.; Nuñez, S. Intrathermocline eddies in the coastal transition zone off central Chile (31–41 S). *J. Geophys. Res. Oceans* **2013**, *118*, 4811–4821. [CrossRef]
16. Pegliasco, C.; Chaigneau, A.; Morrow, R. Main eddy vertical structures observed in the four major Eastern Boundary Upwelling Systems. *J. Geophys. Res. Oceans* **2015**, *120*, 6008–6033. [CrossRef]
17. Barceló-Llull, B.; Sangrà, P.; Pallàs-Sanz, E.; Barton, E.D.; Estrada-Allis, S.N.; Martínez-Marrero, A.; Marrero-Díaz, Á. Anatomy of a subtropical intrathermocline eddy. *Deep-Sea Res. I* **2017**, *124*, 126–139. [CrossRef]
18. Siegel, D.A.; Peterson, P.; McGillicuddy, D.J.; Maritorena, S.; Nelson, N.B. Bio-optical footprints created by mesoscale eddies in the Sargasso Sea. *Geophys. Res. Lett.* **2011**, *38*. [CrossRef]
19. Chelton, D.B.; Gaube, P.; Schlax, M.G.; Early, J.J.; Samelson, R.M. The influence of nonlinear mesoscale eddies on near-surface oceanic chlorophyll. *Science* **2011**, *334*, 328–332. [CrossRef] [PubMed]
20. Klein, P.; Lapeyre, G. The oceanic vertical pump induced by mesoscale and submesoscale turbulence. *Annu. Rev. Mar. Sci.* **2009**, *1*, 351–375. [CrossRef] [PubMed]
21. Martin, A.P.; Richards, K.J. Mechanisms for vertical nutrient transport within a North Atlantic mesoscale eddy. *Deep-Sea Res. II* **2001**, *48*, 757–773. [CrossRef]
22. Gaube, P.; Chelton, D.B.; Strutton, P.G.; Behrenfeld, M.J. Satellite observations of chlorophyll, phytoplankton biomass, and Ekman pumping in nonlinear mesoscale eddies. *J. Geophys. Res. Oceans* **2013**, *118*, 6349–6370. [CrossRef]
23. Gaube, P.; Chelton, D.B.; Samelson, R.M.; Schlax, M.G.; O'Neill, L.W. Satellite observations of mesoscale eddy-induced Ekman pumping. *J. Phys. Oceanogr.* **2015**, *45*, 104–132. [CrossRef]
24. Fielding, S.; Crisp, N.; Allen, J.T.; Hartman, M.C.; Rabe, B.; Roe, H.S.J. Mesoscale subduction at the Almería-Oran front: Part 2. Biophysical interactions. *J. Mar. Syst.* **2001**, *30*, 287–304. [CrossRef]
25. Mahadevan, A.; Tandon, A. An analysis of mechanisms for submesoscale vertical motion at ocean fronts. *Ocean Model.* **2006**, *14*, 241–256. [CrossRef]
26. Nagai, T.; Tandon, A.; Gruber, N.; McWilliams, J.C. Biological and physical impacts of ageostrophic frontal circulations driven by confluent flow and vertical mixing. *Dyn. Atmos. Oceans* **2008**, *45*, 229–251. [CrossRef]
27. Omand, M.M.; D'Asaro, E.A.; Lee, C.M.; Perry, M.J.; Briggs, N.; Cetinić, I.; Mahadevan, A. Eddy-driven subduction exports particulate organic carbon from the spring bloom. *Science* **2015**, *348*, 222–225. [CrossRef] [PubMed]
28. Arístegui, J.; Barton, E.D.; Tett, P.; Montero, M.F.; García-Muñoz, M.; Basterretxea, G.; de Armas, D. Variability in plankton community structure, metabolism, and vertical carbon fluxes along an upwelling filament (Cape Juby, NW Africa). *Prog. Oceanogr.* **2004**, *62*, 95–113. [CrossRef]
29. Pelegrí, J.L.; Arístegui, J.; Cana, L.; González-Dávila, M.; Hernández-Guerra, A.; Hernández-León, S.; Santana-Casiano, M. Coupling between the open ocean and the coastal upwelling region off northwest Africa: Water recirculation and offshore pumping of organic matter. *J. Mar. Syst.* **2005**, *54*, 3–37. [CrossRef]

30. Correa-Ramirez, M.A.; Hormazabal, S.; Yuras, G. Mesoscale eddies and high chlorophyll concentrations off central Chile (29–39 S). *Geophys. Res. Lett.* **2007**, *34*. [CrossRef]
31. Gruber, N.; Lachkar, Z.; Frenzel, H.; Marchesiello, P.; Münnich, M.; McWilliams, J.C.; Plattner, G.K. Eddy-induced reduction of biological production in eastern boundary upwelling systems. *Nat. Geosci.* **2011**, *4*, 787–792. [CrossRef]
32. Morales, C.E.; Hormazabal, S.; Correa-Ramirez, M.; Pizarro, O.; Silva, N.; Fernandez, C.; Torrealba, M.L. Mesoscale variability and nutrient-phytoplankton distributions off central-southern Chile during the upwelling season: The influence of mesoscale eddies. *Prog. Oceanogr.* **2012**, *104*, 17–29. [CrossRef]
33. Morales, C.E.; Anabalón, V.; Berto, J.P.; Hormazabal, S.; Cornejo, M.; Correa-Ramirez, M.A.; Silva, N. Front-Eddy Influence on Water Column Properties, Phytoplankton Community Structure, and Cross-Shelf Exchange of Diatom Taxa in the Shelf-Slope Area off Concepción (~36–37°S). *J. Geophys. Res. Oceans* **2017**, *122*, 8944–8965. [CrossRef]
34. Moore II, T.S.; Matear, R.J.; Marra, J.; Clementson, L. Phytoplankton variability off the Western Australian Coast: Mesoscale eddies and their role in cross-shelf exchange. *Deep-Sea Res. II* **2007**, *54*, 943–960. [CrossRef]
35. Karrasch, B.; Hoppe, H.G.; Ullrich, S.; Podewski, S. The role of mesoscale hydrography on microbial dynamics in the northeast Atlantic: Results of a spring bloom experiment. *J. Mar. Res.* **1996**, *54*, 99–122. [CrossRef]
36. Ciotti, A.M.; Lewis, M.R.; Cullen, J.J. Assessment of the relationships between dominant cell size in natural phytoplankton communities and the spectral shape of the absorption coefficient. *Limnol. Oceanogr.* **2002**, *47*, 404–417. [CrossRef]
37. Guidi, L.; Stemann, L.; Jackson, G.A.; Ibanez, F.; Claustre, H.; Legendre, L.; Gorsky, G. Effects of phytoplankton community on production, size, and export of large aggregates: A world-ocean analysis. *Limnol. Oceanogr.* **2009**, *54*, 1951–1963. [CrossRef]
38. Finkel, Z.V.; Beardall, J.; Flynn, K.J.; Quigg, A.; Rees, T.A.V.; Raven, J.A. Phytoplankton in a changing world: Cell size and elemental stoichiometry. *J. Plankton Res.* **2009**, *32*, 119–137. [CrossRef]
39. Ward, B.A.; Dutkiewicz, S.; Jahn, O.; Follows, M.J. A size-structured food-web model for the global ocean. *Limnol. Oceanogr.* **2012**, *57*, 1877–1891. [CrossRef]
40. Marañón, E. Cell size as a key determinant of phytoplankton metabolism and community structure. *Ann. Rev. Mar. Sci.* **2015**, *7*, 241–264. [CrossRef] [PubMed]
41. Brewin, R.J.; Sathyendranath, S.; Jackson, T.; Barlow, R.; Brotas, V.; Airs, R.; Lamont, T. Influence of light in the mixed-layer on the parameters of a three-component model of phytoplankton size class. *Remote Sens. Environ.* **2015**, *168*, 437–450. [CrossRef]
42. Uitz, J.U.; Huot, Y.; Bruyant, F.; Babin, M.; Claustre, H. Relating phytoplankton photophysiological properties to community structure on large scales. *Limnol. Oceanogr.* **2008**, *53*, 614–630. [CrossRef]
43. Brewin, R.J.; Sathyendranath, S.; Hirata, T.; Lavender, S.J.; Barciela, R.M.; Hardman-Mountford, N.J. A three-component model of phytoplankton size class for the Atlantic Ocean. *Ecol. Model.* **2012**, *221*, 1472–1483. [CrossRef]
44. Brewin, R.J.; Sathyendranath, S.; Tilstone, G.; Lange, P.K.; Platt, T. A multicomponent model of phytoplankton size structure. *J. Geophys. Res. Oceans* **2014**, *119*, 3478–3496. [CrossRef]
45. Brewin, R.J.; Sathyendranath, S.; Lange, P.K.; Tilstone, G. Comparison of two methods to derive the size-structure of natural populations of phytoplankton. *Deep-Sea Res. I* **2014**, *85*, 72–79. [CrossRef]
46. Ward, B.A. Temperature-correlated changes in phytoplankton community structure are restricted to polar waters. *PLoS ONE* **2015**, *10*, e0135581. [CrossRef] [PubMed]
47. Uitz, J.; Claustre, H.; Morel, A.; Hooker, S.B. Vertical distribution of phytoplankton communities in open ocean: An assessment based on surface chlorophyll. *J. Geophys. Res. Oceans* **2006**, *111*. [CrossRef]
48. Brewin, R.J.; Ciavatta, S.; Sathyendranath, S.; Jackson, T.; Tilstone, G.; Curran, K.; Airs, R.L.; Cummings, D.; Brotas, V.; Organelli, E.; et al. Uncertainty in ocean-color estimates of chlorophyll for phytoplankton groups. *Front. Mar. Sci.* **2017**, *4*, 104. [CrossRef]
49. Ciotti, A.M.; Bricaud, A. Retrievals of a size parameter for phytoplankton and spectral light absorption by colored detrital matter from water-leaving radiances at SeaWiFS channels in a continental shelf region off Brazil. *Limnol. Oceanogr. Methods* **2006**, *4*, 237–253. [CrossRef]

50. Brotas, V.; Brewin, R.J.; Sá, C.; Brito, A.C.; Silva, A.; Mendes, C.R.; Diniz, T.; Kaufmann, M.; Tarran, G.; Groom, S.B.; et al. Deriving phytoplankton size classes from satellite data: Validation along a trophic gradient in the eastern Atlantic Ocean. *Remote Sens. Environ.* **2013**, *134*, 66–77. [CrossRef]
51. Brito, A.C.; Sá, C.; Brotas, V.; Brewin, R.J.; Silva, T.; Vitorino, J.; Platt, T.; Sathyendranath, S. Effect of phytoplankton size classes on bio-optical properties of phytoplankton in the Western Iberian coast: Application of models. *Remote Sens. Environ.* **2015**, *156*, 537–550. [CrossRef]
52. Lin, J.; Cao, W.; Wang, G.; Hu, S. Satellite-observed variability of phytoplankton size classes associated with a cold eddy in the South China Sea. *Mar. Pollut. Bull.* **2014**, *83*, 190–197. [CrossRef] [PubMed]
53. Cáceres, M.M. Vórtices y filamentos observados en imágenes de satélite frente al área de surgencia de Talcahuano, Chile central. *Investig. Pesq.* **1992**, *37*, 55–66.
54. Shaffer, G.; Hormazabal, S.; Pizarro, O.; Salinas, S. Seasonal and interannual variability of currents and temperature off central Chile. *J. Geophys. Res. Oceans* **1999**, *104*, 29951–29961. [CrossRef]
55. Sobarzo, M.; Bravo, L.; Donoso, D.; Garcés-Vargas, J.; Schneider, W. Coastal upwelling and seasonal cycles that influence the water column over the continental shelf off central Chile. *Prog. Oceanogr.* **2007**, *75*, 363–382. [CrossRef]
56. Letelier, J.; Pizarro, O.; Nuñez, S. Seasonal variability of coastal upwelling and the upwelling front off central Chile. *J. Geophys. Res. Oceans* **2009**, *114*. [CrossRef]
57. Correa-Ramirez, M.A.; Hormazabal, S.; Morales, C.E. Spatial patterns of annual and interannual surface chlorophyll-a variability in the Peru–Chile Current System. *Prog. Oceanogr.* **2012**, *92*, 8–17. [CrossRef]
58. Morales, C.E.; Hormazabal, S.; Andrade, I.; Correa-Ramirez, M.A. Time-space variability of chlorophyll-a and associated physical variables within the region off Central-Southern Chile. *Remote Sens.* **2013**, *5*, 5550–5571. [CrossRef]
59. Hormazabal, S.; Shaffer, G.; Leth, O. Coastal transition zone off Chile. *J. Geophys. Res. Oceans* **2004**, *109*. [CrossRef]
60. Morales, C.E.; Anabalón, V. Phytoplankton biomass and microbial abundances during the spring upwelling season in the coastal area off Concepción, central-southern Chile: Variability around a time series station. *Prog. Oceanogr.* **2012**, *92*, 81–91. [CrossRef]
61. Fondo de Investigación Pesquera. *Fase II: Levantamiento Oceanográfico para Elaborar la Línea Base de los Montes Submarinos Juan Fernández 5 (JF5), Juan Fernández 6 (JF6) y Monte O'Higgins; Informe final Proyecto FIP 2014-04-2; Chile, 2016; 355p*, Available online: www.subpesca.cl/fipa/613/articles-92055_informe_final.pdf (accessed on 25 May 2018).
62. Sathyendranath, S.; Cota, G.; Stuart, V.; Maass, H.; Platt, T. Remote sensing of phytoplankton pigments: A comparison of empirical and theoretical approaches. *Int. J. Remote Sens.* **2001**, *22*, 249–273. [CrossRef]
63. Devred, E.; Sathyendranath, S.; Stuart, V.; Maass, H.; Ulloa, O.; Platt, T. A two-component model of phytoplankton absorption in the open ocean: Theory and applications. *J. Geophys. Res. Oceans* **2006**, *111*, C03011. [CrossRef]
64. Vidussi, F.; Claustre, H.; Manca, B.B.; Luchetta, A.; Marty, J.C. Phytoplankton pigment distribution in relation to upper thermocline circulation in the eastern Mediterranean Sea during winter. *J. Geophys. Res. Oceans* **2001**, *106*, 19939–19956. [CrossRef]
65. Efron, B. Bootstrap methods: Another look at the jackknife annals of statistics. *Ann. Stat.* **1979**, *7*, 1–26. [CrossRef]
66. Bailey, S.W.; Werdell, P.J. A multi-sensor approach for the on-orbit validation of ocean color satellite data products. *Remote Sens. Environ.* **2006**, *102*, 12–23. [CrossRef]
67. Seegers, B.N.; Stumpf, R.P.; Schaeffer, B.A.; Loftin, K.A.; Werdell, P.J. Performance metrics for the assessment of satellite data products: An ocean color case study. *Opt. Express* **2018**, *26*, 7404–7422. [CrossRef] [PubMed]
68. Mason, E.; Pascual, A.; McWilliams, J.C. A new sea surface height-based code for oceanic mesoscale eddy tracking. *J. Atmos. Ocean. Technol.* **2014**, *31*, 1181–1188. [CrossRef]
69. Kurian, J.; Colas, F.; Capet, X.; McWilliams, J.C.; Chelton, D.B. Eddy properties in the California current system. *J. Geophys. Res. Oceans* **2011**, *116*, C08027. [CrossRef]
70. Perven, P.; Echevin, V.; Pasapera, J.; Colas, F.; Tam, J. Average circulation, seasonal cycle, and mesoscale dynamics of the Peru Current System: A modeling approach. *J. Geophys. Res. Oceans* **2005**, *110*. [CrossRef]

71. Capet, A.; Mason, E.; Rossi, V.; Troupin, C.; Faugere, Y.; Pujol, I.; Pascual, A. Implications of refined altimetry on estimates of mesoscale activity and eddy-driven offshore transport in the Eastern Boundary Upwelling Systems. *Geophys. Res. Lett.* **2014**, *41*, 7602–7610. [CrossRef]
72. Campbell, J.W. The lognormal distribution as a model for bio-optical variability in the sea. *J. Geophys. Res. Oceans* **1995**, *100*, 13237–13254. [CrossRef]
73. Dufois, F.; Hardman-Mountford, N.J.; Greenwood, J.; Richardson, A.J.; Feng, M.; Matear, R.J. Anticyclonic eddies are more productive than cyclonic eddies in subtropical gyres because of winter mixing. *Sci. Adv.* **2016**, *2*, e1600282. [CrossRef] [PubMed]
74. Gutiérrez, D.; Akester, M.; Naranjo, L. Productivity and sustainable management of the Humboldt Current large marine ecosystem under climate change. *Environ. Dev.* **2016**, *17*, 126–144. [CrossRef]
75. Lohrenz, S.; Weidemann, A.; Tuel, M. Phytoplankton spectral absorption as influenced by community size structure and pigment composition. *J. Plankton Res.* **2003**, *25*, 35–61. [CrossRef]
76. Baird, M.; Timko, P.; Wu, L. The effect of packaging of chlorophyll within phytoplankton and light scattering in a coupled physical-biological ocean model. *Mar. Freshw. Res.* **2007**, *58*, 966–981. [CrossRef]
77. Nair, A.; Sathyendranath, S.; Platt, T.; Morales, J.; Stuart, V.; Forget, M.H.; Devred, E.; Bouman, H. Remote sensing of phytoplankton functional types. *Remote Sens. Environ.* **2008**, *112*, 3366–3375. [CrossRef]
78. Hopcroft, R.R.; Roff, J.C. Phytoplankton size fractions in a tropical neritic ecosystem near Kingston, Jamaica. *J. Plankton Res.* **1990**, *12*, 1069–1088. [CrossRef]
79. Gin, K.Y.H.; Lin, X.; Zhang, S. Dynamics and size structure of phytoplankton in the coastal waters of Singapore. *J. Plankton Res.* **2000**, *22*, 1465–1484. [CrossRef]
80. Sathyendranath, S.; Platt, T. Spectral effects in bio-optical control on the ocean system. *Oceanologia* **2007**, *49*, 5–39.
81. Anabalón, V.; Morales, C.E.; Escribano, R.; Varas, M.A. The contribution of nano- and micro-planktonic assemblages in the surface layer (0–30 m) under different hydrographic conditions in the upwelling area off Concepción, central Chile. *Prog. Oceanogr.* **2007**, *75*, 396–414. [CrossRef]
82. González, H.E.; Menschel, E.; Aparicio, C.; Barria, C. Spatial and temporal variability of microplankton and detritus, and their export to the shelf sediments in the upwelling area off Concepción, Chile (~36S), during 2002–2005. *Prog. Oceanogr.* **2007**, *75*, 435–451. [CrossRef]
83. Böttjer, D.; Morales, C.E. Nanoplanktonic assemblages in the upwelling area off Concepción (~36°S), central Chile: Abundance, biomass, and grazing potential during the annual cycle. *Prog. Oceanogr.* **2007**, *75*, 415–434. [CrossRef]
84. Morales, C.E.; González, H.E.; Hormazabal, S.; Yuras, G.; Letelier, J.; Castro, L.R. The distribution of chlorophyll-a and dominant planktonic components in the coastal transition zone off Concepción, central Chile, during different oceanographic conditions. *Prog. Oceanogr.* **2007**, *75*, 452–469. [CrossRef]
85. Anabalón, V.; Morales, C.E.; González, H.E.; Menschel, E.; Schneider, W.; Hormazabal, S.; Escribano, R. Micro-phytoplankton community structure in the coastal upwelling zone off Concepción (central Chile): Annual and inter-annual fluctuations in a highly dynamic environment. *Prog. Oceanogr.* **2016**, *149*, 174–188. [CrossRef]
86. Llanillo, P.J.; Pelegrí, J.L.; Duarte, C.; Emelianov, M.; Gasser, M.; Gourrion, M.J.; Rodríguez-Santana, A. Meridional and zonal changes in water properties along the continental slope off central and northern Chile. *Cienc. Mar.* **2012**, *38*, 307–332. [CrossRef]
87. Harrison, P.J.; Davis, C.O. The use of outdoor phytoplankton continuous cultures to analyze factors influencing species succession. *J. Exp. Mar. Biol. Ecol.* **1979**, *41*, 9–23. [CrossRef]
88. Raven, J.A. Small is beautiful: The picophytoplankton. *Funct. Ecol.* **1998**, *12*, 503–513. [CrossRef]
89. Paterson, H.; Knott, B.; Waite, A. Microzooplankton community structure and grazing on phytoplankton, in an eddy pair in the Indian Ocean off Western Australia. *Deep-Sea Res. Part II* **2007**, *54*, 1076–1093. [CrossRef]



© 2018 by the authors. Licensee MDPI, Basel, Switzerland. This article is an open access article distributed under the terms and conditions of the Creative Commons Attribution (CC BY) license (<http://creativecommons.org/licenses/by/4.0/>).

Artículo enviado a *Frontiers in Marine Science Journal*

4.2. Capítulo 2: Flujo diapicno de nutrientes y distribución de fitoplancton en un área de interacción entre un remolino intratermoclina de mesoescala y el frente de surgencia costera

Andrea Corredor-Acosta, Carmen E. Morales, Ángel Rodríguez-Santana, Valeria Anabalón, Luis P. Valencia y Samuel Hormazabal.

Resumen

Las estructuras de sub- y mesoescala en los Sistemas de Surgencia de Borde Oriental promueven el intercambio de propiedades físico-químicas y de organismos planctónicos entre aguas costeras y oceánicas, promoviendo además inestabilidades en la columna de agua que resultan en procesos turbulentos de pequeña escala. En este estudio, datos *in situ* de Clo-a total y fraccionada por tamaño, nutrientes y propiedades físicas de la columna de agua fueron colectados durante un crucero corto (3-7 febrero 2014) en un área de interacción entre un remolino intratermoclina (ITE) y el frente de surgencia de costera (FSC) en Concepción (36-37°S). Los datos fueron usados para caracterizar la estructura de la comunidad fitoplanctónica por tamaños y para calcular el flujo diapicno de nutrientes mediante una estimación indirecta del coeficiente de difusividad vertical turbulenta usando el método de la escala de Thorpe. Los resultados muestran un máximo flujo de nutrientes hacia arriba en la capa superficial (10-20 m) y subsuperficial (30-60 m) en las áreas del FSC y del ITE, respectivamente, asociados con la distribución espacial de los nutrientes y altos valores de difusividad vertical, es decir, alta mezcla turbulenta en ambas áreas. Los máximos flujos diapicnos de nutrientes mostraron estar asociados con las concentraciones máximas de Clo-a por las fracciones micro- y nanoplanctónica, y con las máximas abundancias de especies costeras de microdiatomeas en el FSC y de especies oceánicas en el ITE. Los resultados sugieren que el suministro diapicno de nutrientes en áreas de interacción ITE-FSC, además de otros mecanismos (ej. advección horizontal), promueve la presencia de células fitoplanctónicas grandes en la zona costera y de transición costera en la región centro-sur de Chile.

Diapycnal nutrient fluxes and phytoplankton distribution in an area of interaction between a mesoscale intrathermocline eddy and a coastal upwelling front

A. Corredor-Acosta^{1,2}, C.E. Morales^{2,3*}, A. Rodríguez-Santana⁴,
V. Anabalón², L. P. Valencia^{2,5}, S. Hormazabal^{2,5}

1 ¹Programa de Postgrado en Oceanografía, Departamento de Oceanografía, Facultad de Ciencias
2 Naturales y Oceanográficas, Universidad de Concepción, Concepción, Chile.

3 ²Instituto Milenio de Oceanografía (IMO), Universidad de Concepción, Concepción, Chile.

4 ³Departamento de Oceanografía, Facultad de Ciencias Naturales y Oceanográficas, Universidad de
5 Concepción, Concepción, Chile.

6 ⁴Departamento de Física, Facultad de Ciencias del Mar, Universidad de las Palmas de Gran Canaria,
7 España.

8 ⁵Escuela de Ciencias del Mar, Facultad de Ciencias Naturales y Geografía, Pontificia Universidad
9 Católica de Valparaíso, Valparaíso, Chile.

10 *** Correspondence:**

11 Carmen E. Morales
12 camorale@udec.cl

13 **Keywords:** Coastal upwelling system, phytoplankton size structure, diapycnal nutrient flux,
14 intrathermocline eddy, coastal upwelling front, vertical eddy diffusivity, Thorpe scale method

15 **Abstract**

16 Mesoscale and submesoscale activity in Eastern Boundary Upwelling Systems (EBUSs) promote the
17 exchange of physical and chemical properties, and of planktonic organisms between coastal and
18 oceanic waters. Such activity generates water column instabilities resulting in small-scale turbulent
19 processes. In this study, *in situ* data on size-fractionated chlorophyll-a (Chl-a), nutrients and physical
20 properties of the water column were collected during a short cruise (3-7 February 2014) in an area of
21 interaction between a mesoscale intrathermocline eddy (ITE) and a coastal upwelling front (CUF) in
22 the area off Concepción (36-37°S). These data were used to characterize phytoplankton size structure
23 and to assess diapycnal nutrient fluxes through indirect estimates of vertical eddy diffusivity using the
24 Thorpe scale method. The results show a maximum surface (10-20 m) and subsurface (30-60 m)
25 upward injection of nutrients in the CUF and ITE areas, respectively, in association with the underlying
26 nutrient field and high vertical eddy diffusivity values which indicated high turbulent mixing in these
27 two areas. Maxima in diapycnal nutrient fluxes were associated with Chl-a maxima in the micro- and
28 nano-phytoplankton fractions, as well as with maxima in microplankton diatom abundance dominated
29 by coastal (oceanic) species in the CUF (ITE) area. These findings suggest that diapycnal nutrient
30 supply in areas of ITE-CUF interaction, besides other mechanisms (i.e. horizontal advection and
31 stirring), contributes to promote the presence of large phytoplankton cells in the coastal transition zone
32 (CTZ) of the central-southern Chile EBUS.

33 **1 Introduction**

34 Phytoplankton can be classified by cell size, taxonomic composition and/or functional groups related
35 to their role in the biogeochemical cycles (Le Queré et al., 2005; Finkel et al., 2010). Cell size has been
36 associated with nutrient uptake, metabolic rates, light absorption and food web structure, making
37 phytoplankton size structure an important aspect to evaluate energy flow pathways and the efficiency
38 of ecosystems to export carbon into the deep ocean (Legendre and Le Fèvre, 1989; Bricaud et al., 2004;
39 Guidi et al., 2009; Karl et al., 2012). Large cells have been associated with eutrophic regions
40 characterized by a higher mixing and large vertical nutrient fluxes, higher exported production and
41 even with low light availability in the pycnocline (Bruland et al., 2001; Goldman and McGillicuddy,
42 2003). In contrast, small cells have been usually associated with oligotrophic, stratified and high light
43 exposure in oceanic waters, in which regenerated production dominates (Eppley and Peterson, 1979;
44 Chisholm, 1992; Agustí, 2004; Platt et al., 2005).

45 Phytoplankton size structure can also be influenced by sub- and mesoscale structures and dynamics,
46 such as fronts and eddies (Semina, 1968; Rodríguez et al., 2001; Macías et al., 2013). Surface
47 cyclonic/anticyclonic and subsurface or mode-water type mesoscale eddies have been related to the
48 trapping and stirring of phytoplankton cells, together with vertical variations in nutrient availability
49 due to eddy pumping and eddy-Ekman pumping dynamics (Chelton et al., 2011; Gaube et al., 2014;
50 McGillicuddy, 2016; Mahadevan, 2016). Eddy pumping has been reported as a transient vertical
51 process with intense upward pulses of nutrient during eddy intensification, while eddy-Ekman pumping
52 has been associated with a persistent nutrient upwelling or downwelling into the euphotic zone during
53 eddies lifetime (O'Neill et al., 2010; Gaube et al., 2014, 2015). These changes in the vertical nutrient
54 supply could alter phytoplankton size structure. For example, Brown et al. (2008), based on *in situ* data
55 from a mesoscale eddy in the subtropical North Pacific, reported the dominance of large cells in the
56 eddy center, where an intense vertical pulse of nutrient was found, in contrast with the dominance of
57 smaller cells in the eddy edges, which were mainly subjected to isopycnal mixing and a continuous
58 low nutrient supply.

59 Frontal structures are also involved in the distribution of phytoplankton size fractions. At fronts,
60 Ekman transport driven by wind stress is balanced by an upward water flux, leading to the elevation of
61 the pycnocline in the nearshore, separating cold and nutrient-rich coastal waters from warm and
62 nutrient-poor oceanic waters (Brink and Cowles, 1991; Franks and Walstad, 1997; Johnston et al.,
63 2011). The lateral gradients of buoyancy resulting from the baroclinic instabilities at the front have
64 been reported to promote diapycnal mixing and nutrient fluxes (Boccaletti et al., 2007; Mahadevan and
65 Archer, 2000; Mahadevan, 2016). Previous studies have shown diatoms on the coastal side of a front
66 and smaller cells on the oceanic side, in accordance with the efficiency for nutrient uptake (Furnas,
67 1990; Marañón and Fernández, 1995). However, increases of large phytoplankton have been recently
68 reported at the front and around the pycnocline, associated with a higher gradient in diapycnal mixing
69 and nutrient concentrations (Sangrà et al., 2014; Landeira et al., 2014; Zhang et al., 2015).

70 Eastern Boundary Upwelling Systems (EBUSs) are regions of intense sub- and mesoscale dynamics,
71 where eddies, filaments, jets, and fronts are typical features in the area extending from the coastal zone
72 (CZ) to oceanic limits of the coastal transition zone (CTZ) (Stramma et al., 2013; Hormazabal et al.,
73 2013; Sabarros, et al., 2014; Pegliasco et al., 2015; Barceló-Llull et al., 2017). In the Humboldt Current
74 System (HCS) EBUS off central-southern Chile, an intensified coastal upwelling front (CUF) has been
75 reported during the summer season, when winds are favorable to upwelling in the CZ; at specific areas,
76 this front is usually flanked on the oceanic side by an intrathermocline eddy (ITE) (Letelier et al.,
77 2009). The intensity of the upwelling-favorable winds constrain the magnitude and width of the

78 upwelling front during the seasonal cycle, and in the long-term trend; in addition, the front position is
79 highly variable, going from being close to a coastal jet when it is nearshore (~25-75 km from coast) to
80 being not co-located with the jet when it is further offshore (>125 km from coast; Oerder et al., 2018).
81 This EBUS region has been also characterized by high mesoscale activity, with surface and
82 intrathermocline type mesoscale eddies reported to be generated near the coast (Hormazabal et al.,
83 2004; Chaigneau and Pizarro, 2005; Vergara et al., 2016). In terms of its effect on phytoplankton
84 biomass, the CUF has been identified as a barrier for the offshore spreading of high chlorophyll-a (Chl-
85 a) values in coastal waters, while mesoscale eddies have been reported as a possible amplifier of the
86 Chl-a annual cycle and as a vehicle for the offshore advection of Chl-a to the CTZ (Morales et al.,
87 2007; Correa-Ramirez et al., 2007, 2012; Letelier et al., 2009).

88 Regarding phytoplankton size structure, the CUF of the central-southern Chile EBUS has been
89 reported to act as a barrier to cross-shelf exchanges of phytoplankton, with the dominance of different
90 groups in the coastal and oceanic sides of it, based on microscopy analyses (Morales et al., 2012;
91 Menschel et al., 2016). In the same area, microscopic analyses within two mesoscale eddies (2 months
92 old) have revealed a dominance of small cells (pico- and nanoplankton), in contrast with a dominance
93 of microplankton cells in the CZ (Morales et al., 2012). Recently, using a satellite approach of
94 phytoplankton size classes, Corredor-Acosta et al. (2018) found a dominance of the microplankton
95 fraction during the early stages of eddy development closer to the coast, and of smaller size fractions
96 as eddies move offshore. In an event of ITE-CUF interaction, in the early stages of ITE formation,
97 Morales et al. (2017) reported that this dynamics favored the cross-shelf exchange of different species
98 of micro-phytoplanktonic diatoms from and towards the CZ, in association with intense submesoscale
99 variability in nutrients, which was probably caused by localized vertical injections of nutrients.

100 Sub- and mesoscale features have been reported to lead to changes in nutrient distributions and in
101 nutrient supply to the euphotic zone through several physical processes, such as, upwelling, subduction,
102 mixing and/or exchange of coastal upwelled waters with oceanic offshore waters (Mooers and
103 Robinson, 1984; Lévy et al., 2001). Ascribing nutrient supply to an individual physical mechanism is
104 a challenging task because of the interdependence among their spatial and temporal scales. However,
105 nutrient supply depends of the underlying nutrient field, which is mostly correlated with the density
106 field and the presence of different water masses (Mahadevan and Tandon, 2006; Mahadevan, 2016;
107 José et al., 2017). Changes in density configuration and in water column stratification could lead to
108 mixing by the vertical movement of isopycnals, promoting an advective flux of nutrients along the
109 isopycnal surfaces (isopycnal mixing), or by turbulent diffusion across them (diapycnal mixing)
110 (Ledwell et al., 1998; Ascani et al., 2013). Fluxes of a property associated with diapycnal mixing are
111 not limited to molecular diffusion and could be applied to a turbulent field in order to estimate vertical
112 input of nutrients into the euphotic zone (King and Devol, 1979; Law et al., 2003; Lund-Hansen et al.,
113 2006; Girault et al., 2015; Zhang et al., 2017).

114 The influence of physical mixing processes on phytoplankton community composition are
115 particularly relevant at the submesoscale level (~0.1-10 km and few days), the same timescale of
116 phytoplankton growth (Mahadevan, 2016). For example, in an area of an oceanic front off southern
117 California, observations from autonomous gliders, field data and diagnostic ecosystem models
118 indicated that the vertical displacement of density fields together with an enhanced diapycnal flux of
119 nutrients by small-scale turbulent forcing could be stimulating net growth of phytoplankton, mainly of
120 diatoms in the frontal zone (Davies et al., 2008; Li et al., 2012). More recently, through observations
121 and modelling approaches, Lévy et al. (2018) found that submesoscale physical forcing can provide
122 nutrient-flux pathways to the euphotic zone leading to changes in the phytoplankton community
123 composition and enhancing phytoplankton growth rates.

124 Changes in phytoplankton size structure in association with nutrient fluxes induced by diapycnal
125 mixing in areas of EBUSs with moderate to high sub- and mesoscale activity remain mostly unknown.
126 In this study, we used *in situ* (the PHYTO-FRONT cruise, 3-7 February 2014) and satellite data to
127 analyze phytoplankton community structure, nutrient distribution, and diapycnal mixing in an area of
128 interaction between a mesoscale intrathermocline eddy (ITE) and a coastal upwelling front (CUF) off
129 Concepción (Chile). For this purpose, the vertical eddy diffusivity, as an indicator of turbulent mixing,
130 was calculated using the Thorpe scale method to estimate diapycnal nutrient fluxes and to compare
131 these results with phytoplankton distribution and composition in terms of size fractions. These are the
132 first results of this nature and, therefore, we have compared them with other few estimates available
133 on diapycnal mixing and its impact on phytoplankton structure.

134 **2 Data and methods**

135 The study area off Concepción (~36-37°S, 73-74.5°W; Figure 1) in the Eastern South Pacific is
136 characterized by a highly seasonal coastal upwelling during the austral spring-summer months in
137 response to the intensification of southwesterly winds (Shaffer et al., 1999; Sobarzo et al., 2007).
138 Coastal upwelling promotes the generation of an upwelling front with a vertical extension up to ~100
139 m depth and a variable offshore location (~50-150 km from the coast), strongly related to a coastal jet
140 circulation (Letelier et al., 2009; Oerder et al., 2018). Additionally, this region is characterized by the
141 presence of filaments and surface/subsurface mesoscale eddies regularly generated during the
142 upwelling season, favored by the Peru-Chile Undercurrent (PCUC) variability and the formation of
143 offshore meanders from the coastal equatorward jet of the upwelling center off Point Lavapié (37°15'S)
144 (Hormazabal et al., 2004, 2013; Correa-Ramirez et al., 2007; Morales et al., 2012).

145 **2.1 Satellite Sea Surface Temperature, total Chl-a and surface circulation field**

146 The mean sea surface temperature (SST) distribution during the cruise time was obtained from the
147 daily Multi-scale Ultra-high Resolution Sea Surface Temperature (MUR-SST;
148 <https://mur.jpl.nasa.gov/>) product with a spatial resolution of 1 km. The mean surface geostrophic
149 velocity field and sea level anomaly (SLA) were obtained from the Copernicus Marine and
150 Environment Monitoring Service (CMEMS; <http://marine.copernicus.eu/>) product with a spatial
151 resolution of 0.25° (~25 km). Finally, the mean surface total Chl-a was obtained from version 3.0 of
152 the Ocean Colour Climate Change Initiative (OC-CCI, a merged product available at
153 <http://www.oceancolour.org/>), at processing level 3 and spatial resolution of 4 km.

154 **2.2 Size-fractionated Chl-a and nutrient *in situ* data**

155 Total and size-fractionated Chl-a samples in the micro-, nano-, and pico-phytoplankton range were
156 collected using Niskin Bottles during the PHYTO-FRONT cruise in the upper layer (<100 m depth)
157 and filtered (~250 mL) using GF/F glass fiber filters (3 to 20 µm pore diameter). All measurements
158 were taken in triplicate and frozen (-20°C) until later analysis by fluorometry (Turner Design AU-10)
159 following standard procedures (Anabalón et al., 2007, 2016). In parallel, nutrient samples were also
160 taken and stored frozen (-20°C) in aseptic high-density polyethylene flasks (60 mL) for subsequent
161 analysis following standard protocols (Atlas et al., 1971). Plankton samples were also collected from
162 the same bottles for composition and abundance analysis in the micro-phytoplankton fraction (detailed
163 procedures in Morales et al., 2017).

164 **2.3 Thorpe scale, vertical eddy diffusivity and diapycnal nutrient fluxes**

165 Conductivity, temperature and depth (CTD) casts (0-300 m depth) were performed during the
 166 PHYTO-FRONT cruise using a Sea-Bird SBE 911plus CTD equipment providing 24 Hz sampling.
 167 Dissolved oxygen and Wetstar fluorescence sensors were also attached to this instrument.

168 To estimate the Thorpe scale, which is an energy-containing vertical overtuning scale, the overturns
 169 generated by turbulence in the stratified part of the water column were detected through inversions in
 170 fine scale vertical density profiles. To do this using CTD data, a minimization in measurement errors
 171 and instrument noise is needed. Therefore, to obtain a fine scale density data, the following steps were
 172 done based on the procedure described by Park et al. (2014). Based on the Sea-Bird processing
 173 software: i) The “Cell Thermal Mass” module was performed to minimize the thermal lag arising,
 174 using the recommended values ($\alpha = 0.03$, $1/\beta = 7.0$) for the SBE 911plus CTD, ii) the “Align” module
 175 was not executed because the CTD includes a deck unit which advances conductivity by 0.073 s
 176 regarding to temperature, removing the salinity spiking caused by the misalignment between these
 177 measurements, and iii) the “Loop Edit” module was performed in order to avoid pressure reversals due
 178 to the effect of the ship while the CTD was falling down. Then, temperature and salinity data were
 179 used to calculate potential density with the TEOS-10 subroutines for matlab of the Gibbs-SeaWater
 180 (GSW) oceanographic toolbox (McDougall and Barker, 2011). The final vertical density profiles were
 181 subsampled at regular depth intervals of 10 cm, each one containing on average three scans, consistent
 182 with a mean fall speed of $\sim 1 \text{ m s}^{-1}$ and the 24 Hz CTD sampling. For all profiles, the first 20 m depth
 183 were removed to avoid surface turbulence generated by the ship.

184 Subsequently, in order to calculate the overturns in the water column for each sampling station, the
 185 vertical density profiles were sorted to obtain a stable monotonic sequence. To do this, an intermediate
 186 density profile was obtained by averaging a downward (top to bottom) and an upward (bottom to top)
 187 constructed profile, maintaining a constant density until it changed over a threshold value (Gargett and
 188 Garner, 2008). Therefore, differences in the intermediate density profile above that threshold level
 189 were considered as real overturns. In this study, the threshold noise value was $5 \times 10^{-4} \text{ kg m}^{-3}$, calculated
 190 as the median of the density differences inside the “well-mixed” layer in all sampling profiles. Finally,
 191 the Thorpe scale (L_T) was estimated by the root-mean-square of an ensemble of vertical displacements
 192 (in meters) necessary to generate the stable vertical density profiles, computed at successive non-zero
 193 Thorpe displacements (Park et al., 2014; Sangrà et al., 2014).

194 Vertical eddy diffusivities (K_z) were then estimated using the Thorpe scale following Ozmidov
 195 (1965) and Dillon (1982), which according to the Osborn parameterization (Osborn, 1980) is obtained
 196 as

$$197 \quad K_z = 0.128 L_T^2 N \quad (1)$$

198 where N is the Brunt-Vaisala frequency or buoyancy frequency at which a fluid parcel oscillates when
 199 it is displaced from the stable state, and was calculated from the relation

$$200 \quad N^2 = \frac{-g}{\rho_0} \frac{\partial \rho}{\partial z} \quad (2)$$

201 where g is the gravitational acceleration, ρ_0 is the mean seawater density and $\partial \rho / \partial z$ is the vertical
 202 density gradient. Maximum frequency values in the water column are expected where the stratification
 203 is strongest.

204 Diapycnal nutrient (nitrate, phosphate and silicate or silic acid) fluxes (F_{Nutrient}) were calculated
 205 through the relation

$$206 \quad F_{\text{Nutrient}} = -K_z \frac{\partial \text{Nutrient}}{\partial z} \quad (3)$$

207 where K_z is the vertical eddy diffusivity obtained in each sampling station and $\partial \text{Nutrient} / \partial z$ is the
 208 vertical nutrient concentration gradient (Girault et al., 2015).

209 The flux of a property in the ocean under turbulent conditions is a useful empirical extension of the
 210 Fickian diffusion equation for molecular diffusivity (Okubo, 1971; King and Devol, 1979). Therefore,
 211 several studies have applied this approximation to calculate nutrient fluxes into the euphotic zone and
 212 have estimated the vertical eddy diffusivity coefficient indirectly through the Thorpe scale method or
 213 directly with microstructure measurements in the water column. However, independent of the method
 214 to estimate this coefficient, it is an important measurement to interpret turbulence dissipation rates and
 215 small-scale mixing processes (Park et al., 2014; Ledwell et al., 2008). This coefficient has been called
 216 in different ways in the literature, for example, vertical diffusivity (Law et al., 2003; Park et al., 2014),
 217 vertical turbulent diffusivity (Girault et al., 2015), diapycnal diffusivity (Ledwell et al., 2008; Li et al.,
 218 2012; Zhang et al., 2017), eddy diffusion coefficient (Lund-Hansen et al., 2006), eddy diffusivity
 219 (Rippeth et al., 2009) and vertical eddy diffusivity (Arcos-Pulido et al., 2014; Doubell et al., 2018;
 220 Henley et al., 2018; Hsu et al., 2019).

221 2.4 Meridional geostrophic velocity and mixed layer depth

222 Previously obtained temperature and absolute salinity profiles were used to calculate potential
 223 density anomaly and meridional geostrophic velocity (Pond and Pickard, 2013). The geostrophic
 224 velocity (V_g) was computed every three stations along each transect and was obtained from the balance
 225 between planetary vorticity and the pressure gradient force as follows

$$226 \quad V_g = \frac{1}{f \rho_0} \frac{\partial P}{\partial x}$$

227 where f is the Coriolis parameter, ρ_0 is the mean seawater density and $\partial P / \partial x$ is the pressure horizontal
 228 gradient from the geopotential anomaly relative to the sea surface. Additionally, the mixed layer depth
 229 was evaluated for each sampling station using a threshold value in temperature ($\Delta T = 0.2^\circ\text{C}$) and density
 230 ($\Delta \rho = 0.03 \text{ kg m}^{-3}$) from a near-surface depth of 10 m, following the procedures of Kara et al. (2000)
 231 and de Boyer Montégut et al. (2004).

232 3 Results and Discussion

233 3.1 Surface bio-physical features and water column structure

234 The mean satellite surface conditions in temperature, geostrophic circulation and total Chl-a during
 235 the PHYTO-FRONT cruise are shown in Figure 1 and have previously been described in detail by
 236 Morales et al (2017). Colder waters ($<15^\circ\text{C}$) were observed near the coast, followed by a strong SST
 237 gradient or thermal front characterized by the $16\text{-}17^\circ\text{C}$ isotherms (Sts. 6-7 and 16-18, $\sim 70\text{-}100$ km from
 238 coast), after which warmer waters ($>17^\circ\text{C}$) in the CTZ were found (Figure 1a). The geostrophic
 239 currents and SLA clearly indicated the presence of an anticyclonic mesoscale eddy (diameter of ~ 150
 240 km) in the sampling area, with the northern transect involving stations closer to eddy center and its east
 241 edge and the southern transect including stations located on the south-east edge of the eddy (Figure
 242 1b). In terms of surface total Chl-a, the highest values ($>3 \text{ mg m}^{-3}$) were observed near the coast, while

243 moderate ($\sim 1\text{-}2\text{ mg m}^{-3}$) and lower Chl-a values ($< 1\text{ mg m}^{-3}$) were found in the CTZ (Figure 1c).
244 Additionally, an abrupt change from moderate to low surface Chl-a concentrations was observed
245 westward from the thermal front (Sts. 7-8 and 18-19), together with an offshore plume of moderate
246 Chl-a strongly associated with a cold filament in the northern part of the identified eddy, and an inshore
247 intrusion towards the coast of low Chl-a and warm waters in the southern part of it (Figures 1a, 1c).
248 These surface SST and Chl-a distributions have been previously reported for the frontal zone off
249 central-southern Chile in summer, together with a lateral advection (stirring) of Chl-a by mesoscale
250 structures, such as eddies and filaments (Correa-Ramirez et al., 2007; Letelier et al., 2009; Morales et
251 al., 2012).

252 Regarding the water column structure, the distribution of temperature, salinity and potential density
253 in the first 100 m depth are shown in Figure 2 and have previously been described in detail by Morales
254 et al. (2017). A strong uplift of isolines towards the coast (up to 80 m) was detected in both transects
255 (Figures 2a-b, 2d-e), with colder ($< 16^{\circ}\text{C}$) and higher salinity (> 34) waters reaching the upper layer in
256 the coastal band, creating a coastal upwelling front (CUF) area (Sts. 5-7 and 16-18), also characterized
257 by a strong horizontal density gradient ($0.5\text{-}1\text{ kg m}^{-3}$ in 10 km; Figures 2c, 2f). In addition, a deepening
258 of isolines associated with the westward side of the frontal area (Sts. 8-9 and 18-19), contributed to
259 clearly separate coastal and CTZ waters. In EBUSs, coastal upwelling fronts are usually defined by
260 strong cross-shore SST and density gradients (Austin and Barth, 2002; Peliz et al., 2002). In the study
261 region, coastal upwelling has been described to induce a surface density gradient which contributes to
262 separate cold upwelled coastal waters and warm open oceanic waters, also with a strong signature in
263 the upper water column ($\sim 0\text{-}50$ m depth) over the shelf-break zone (Hormazabal et al., 2004; Letelier
264 et al., 2009). In the offshore stations (Sts. 10-11 and 21-24), a dome shape subsurface uplifting of the
265 25.7-26.2 isopycnals, together with an intrusion of high salinity waters (> 34.4 ; Figures 2b-c, 2e-f),
266 signaled the presence of an intrathermocline eddy (ITE), which is a mode-water type of eddy
267 recurrently generated in the survey area during the summer, characterized by trapping high salinity,
268 low oxygen subsurface waters from coastal origin (Morales et al., 2012; Hormazabal et al., 2013).
269 Overall, the satellite data and water column configuration indicated the occurrence of an ITE-CUF
270 interaction area during the cruise time (Figure 2a-f). In addition, Morales et al. (2017) reported that
271 this cruise took place during a wind-relaxation event after a strong upwelling episode.

272 The distribution of the Equatorial Subsurface (ESSW) and Subantarctic (SAAW) water masses in the
273 CUF area (Sts. 5-7 and 16-18), and in the stations nearest to it in the coastal (Sts. 4 and 15) and oceanic
274 (Sts. 8 and 19) direction are represented in Figure 3. In the coastal stations, the ESSW was found to
275 dominate in the subsurface layer (~ 30 to 100 m depth), whereas the contribution of the SAAW was
276 limited to the upper layer (< 30 m). In the CUF area, the contribution of the SAAW was slightly higher
277 and reached deeper (0-40 m), while at the subsurface the contribution of the ESSW was dominant (> 40
278 m depth). In contrast, the oceanic stations showed a higher contribution of the SAAW, with a minimum
279 contribution of the ESSW at depth (> 80 m). In addition, a shallow (< 20 m) salinity minimum (< 34.1)
280 was observed in the westward side of the CUF area and in the oceanic stations (Sts. 17-19 and 7-8). In
281 the HCS, the ESSW is a high salinity, nutrient-rich and oxygen depleted water mass, transported along
282 the continental slope by the poleward Peru-Chile Undercurrent (PCUC), and is the main source of
283 upwelling waters in the region. In contrast, the SAAW is a fresh and well oxygenated water mass
284 transported northward by the coastal Humboldt Current (HC), which could be slightly modified in
285 summer by mixing with a fresher water from the intensified runoff and summer melting from the fjord
286 region, originating a shallow salinity minimum (Leth et al., 2004; Silva et al., 2009; Letelier et al.,
287 2009; Llanillo et al., 2012).

288 The vertical structure (0-300 m depth) of the meridional geostrophic circulation during the cruise is
 289 shown in Figure 4. In the area immediately beyond the shelf-break zone (~100 km from the coast), a
 290 predominantly southward flow was registered, with values of 0.2 m s^{-1} in the CUF area of the northern
 291 transect (St. 17; Figure 4a) and maximum values ($\sim 0.4 \text{ m s}^{-1}$) in the oceanic side of the CUF in the
 292 southern transect (Sts. 7-8; Figure 4b). This coastal flow configuration is consistent with the observed
 293 and modelled PCUC current in summer, reaching values close to $\sim 0.5 \text{ m s}^{-1}$ in central Chile (Aguirre
 294 et al., 2012; Vergara et al., 2016). Immediately offshore of this flow, in the area of the ITE-CUF
 295 interaction, a change to a northward flow was detected in both transects (Sts. 9-10 and 19-21). This
 296 flow reached values of $0-0.1 \text{ m s}^{-1}$ in the stations closer to the ITE center in the northern transect (Sts.
 297 21-23; Figure 4a), and higher intensity ($0.1-0.2 \text{ m s}^{-1}$) was observed in the southern transect in the
 298 stations associated with the south-east edge of the eddy (St. 9-10; Figure 4b). These values are similar
 299 in pattern to those measured in an ITE in the Eddy Canary Corridor, in which the vertical velocity
 300 section across the eddy showed values of $\sim 0.45 \text{ m s}^{-1}$, reaching the lowest velocities in the eddy
 301 center compared with the edges (Barceló-Llull et al., 2017).

302 3.2 Nutrient distributions, vertical eddy diffusivity and diapycnal nutrient fluxes

303 The vertical sections (0-100 m depth) of nutrient distributions during the cruise are shown in Figure
 304 5 and have previously been described by Morales et al. (2017). In the CZ of both transects, maximum
 305 nutrient concentrations were located at the subsurface (~20-100 m depth) for nitrate ($>20 \text{ } \mu\text{M}$; Figures
 306 5a, 5d), phosphate ($>2 \text{ } \mu\text{M}$; Figures 5b, 5e), and silicate ($>15 \text{ } \mu\text{M}$; Figures 5c, 5f), associated with the
 307 ESSW nutrient-rich water mass (Llanillo et al., 2012). In the CUF and ITE-CUF interaction areas (Sts.
 308 6-10 and 16-20), a decrease in nutrient concentrations was observed, with maximum values of nitrate
 309 ($>10 \text{ } \mu\text{M}$; Figures 5a, 5d) and phosphate ($1-2 \text{ } \mu\text{M}$; Figures 5b, 5e) between ~40 and 100 m depth,
 310 whereas silicate values were relatively low along the whole column (Figures 5c, 5f), accordingly with
 311 the presence of the SAAW water mass in central Chile (i.e. high nitrate content but depleted in silicate;
 312 Silva et al., 2009; Llanillo et al., 2012). Moreover, this silicate deficit was more intense in the southern
 313 transect than in the northern one, suggesting a mixing of ESSW and SAAW water masses toward the
 314 north (Morales et al., 2017). In the ITE area (Sts. 10-11 and 20-24), increases in nitrate and phosphate
 315 concentrations were found at shallow depth (~30 m), reaching maxima between ~40 and 100 m depth
 316 (nitrate $>15 \text{ } \mu\text{M}$, phosphate $>1.5 \text{ } \mu\text{M}$; Figures 5a-b, 5d-e), while higher silicate values ($\sim 10 \text{ } \mu\text{M}$) were
 317 restricted to the ~60-100 m layer (Figures 5c, 5f). At these stations, nutrient distribution is associated
 318 with the trapping of ESSW waters inside the ITE, and with the offshore displacement of SAAW waters
 319 by the ESSW during upwelling periods (Hormazabal et al., 2013; Morales et al., 2017). Associated
 320 with these nutrient distributions, the maximum nutrient gradients were found at a shallower depth (~10-
 321 20 m) in the CZ and CUF areas, and deeper towards the oceanic side, i.e. ~20-60 m in the ITE-CUF
 322 interaction and ITE areas (Table 1).

323 Estimates of the diapycnal nutrient fluxes for nitrate and silicate are shown in Figure 6. The patterns
 324 of the nitrate and phosphate fluxes were similar, therefore, the latter are not shown. In addition, the
 325 maximum values of the three nutrient fluxes at each station and the depth of these maxima are presented
 326 in Table 2, together with the estimates of vertical eddy diffusivity (K_z) used to obtain the fluxes. Since
 327 there was not direct measurements of turbulence dissipation rates via a microstructure profiler during
 328 the survey, the Thorpe scale method was used to estimate K_z values from CTD profiles. The
 329 performance of the Thorpe scale method compared with microstructure estimates has been reported to
 330 overestimate K_z by one to two orders of magnitude in the Eastern South Pacific (Frants et al., 2013).
 331 However, in a previous oceanographic campaign off central Chile, using CTD and micro-profiler
 332 measurements, both methods matched in the areas of maximum and minimum K_z , with values
 333 oscillating between $\sim 10^{-6}$ and $10^{-4} \text{ m}^2 \text{ s}^{-1}$ (Barahona et al., in prep.). The higher values are in the order

334 of magnitude compared to our estimates (1×10^{-4} to $16 \times 10^{-4} \text{ m}^2 \text{ s}^{-1}$). In both transects, the highest K_z
 335 values were found in the CUF and ITE areas ($\sim 4 \times 10^{-4} \text{ m}^2 \text{ s}^{-1}$ in the northern and $\sim 5\text{--}7 \times 10^{-4} \text{ m}^2 \text{ s}^{-1}$ in the
 336 southern); however, in the southern transect, K_z was also high ($\sim 4 \times 10^{-4} \text{ m}^2 \text{ s}^{-1}$) in the CZ (St. 1), in
 337 addition to a maximum ($\sim 16 \times 10^{-4} \text{ m}^2 \text{ s}^{-1}$) in the ITE-CUF interaction area (St. 9). These values are also
 338 consistent with diapycnal diffusivities reported for other coastal regions (e.g. Hales et al., 2005;
 339 Thompson et al. 2007; Li et al., 2012).

340 The highest nitrate fluxes ($>16 \text{ mmol m}^{-2} \text{ d}^{-1}$) were found in the CZ (Sts. 1 and 26), the CUF (Sts. 5,
 341 7 and 16), and ITE (Sts. 10 and 22) areas in both transects, and in the ITE-CUF interaction area (St. 9)
 342 in the southern transect (Figures 6a, 6c, and Table 2). Regarding silicate fluxes, the highest values were
 343 found in the CUF (Sts. 5-6 and 16) and ITE (Sts. 10 and 22) areas, and higher in the southern transect
 344 ($>20 \text{ mmol m}^{-2} \text{ d}^{-1}$) compared with the northern one ($>11 \text{ mmol m}^{-2} \text{ d}^{-1}$; Figures 6b, 6d, and Table 2).
 345 These flux estimates are in the range of ~ 1 to $40 \text{ mmol m}^{-2} \text{ d}^{-1}$, which are in the same order of magnitude
 346 as those previously reported in North Atlantic coastal waters (Zhang et al., 2018), in mesoscale eddies
 347 (Law et al., 2001), and in frontal zones of the southern California Current system (Li et al., 2012). To
 348 our knowledge, this is the first report of diapycnal nutrient fluxes associated with the interaction of a
 349 CUF and an ITE in the Eastern South Pacific. In order to analyze the location, depth and direction of
 350 these flux estimates, some important aspects should be considered: i) the diapycnal nutrient fluxes
 351 strongly depend on the distribution of the underlying nutrient content, typically increasing with depth
 352 (Garside, 1985; Mahadevan, 2016), and ii) diapycnal mixing can be caused by several small-scale
 353 turbulent processes associated with instabilities in the water column due to the shear of the geostrophic
 354 circulation field, internal wave breaking, ageostrophic instability, among others (Franks and Walstad,
 355 1997; Siegel et al., 1999; Gargett and Garner, 2008; Li et al., 2012).

356 A maximum in nitrate flux in the CZ (St. 26) of the northern transect is associated with a high nitrate
 357 gradient ($>1 \mu\text{M m}^{-1}$), whereas in the CZ (St. 1) of the southern one it appears to be related to a higher
 358 diapycnal mixing value ($K_z: \sim 4 \times 10^{-4} \text{ m}^2 \text{ s}^{-1}$) since the gradient is smaller ($\sim 0.4 \mu\text{M m}^{-1}$; Tables 1 and
 359 2). Moreover, in the CZ (St. 25 and 26) of the northern transect, the intense uplift of isopycnals towards
 360 the coast could also bring nutrients into the upper layer along isopycnal surfaces (Figure 2c), an
 361 advective flux not quantified in this study due to the poor resolution in the velocity field in all directions
 362 (zonal, meridional, and vertical). Maximum nutrient fluxes in the east side of the CUF (Sts. 5 and 16)
 363 and in the ITE (Sts. 10 and 22) areas are associated with maximum in surface ($\sim 10\text{--}20 \text{ m}$) and
 364 subsurface ($\sim 20\text{--}60 \text{ m}$) nutrient gradients ($\sim 0.6\text{--}0.8 \mu\text{M m}^{-1}$ for nitrate and $\sim 0.3\text{--}0.7 \mu\text{M m}^{-1}$ for silicate),
 365 but also with high K_z values ($\sim 4\text{--}7 \times 10^{-4} \text{ m}^2 \text{ s}^{-1}$), suggesting a more intense diapycnal mixing in these
 366 areas (Figure 6a-d, Tables 1 and 2). However, differences between nitrate and silicate fluxes were
 367 found on the west side of the CUF area (Sts. 6-7) in the southern transect, with a maximum in the
 368 nitrate flux at St. 7 and in the silicate flux at St. 6 (Figure 6c-d, Table 2). These differences are mainly
 369 associated with: i) water masses distribution, with a higher contribution of the SAAW in St. 7 and of
 370 ESSW in St. 6 (Figures 2d-f, 3b), involving a higher nitrate gradient at the surface layer (15-20 m
 371 depth) in St. 7 compared with that in St. 6 ($1.43 \mu\text{M m}^{-1}$ and $0.23 \mu\text{M m}^{-1}$, respectively), but a similar
 372 silicate gradient ($0.59 \mu\text{M m}^{-1}$ and $0.51 \mu\text{M m}^{-1}$, respectively; data not shown); and ii) a higher
 373 diapycnal mixing at St. 6, where the K_z value was almost twice that at St. 7 ($\sim 6 \times 10^{-4} \text{ m}^2 \text{ s}^{-1}$ and $\sim 3 \times 10^{-4}$
 374 $\text{m}^2 \text{ s}^{-1}$, respectively; Table 2). Finally, the nitrate flux in ITE-CUF interaction area (St. 9) of the
 375 northern transect is more related to the highest estimated value of K_z ($\sim 16 \times 10^{-4} \text{ m}^2 \text{ s}^{-1}$; Table 2) than to
 376 the nitrate gradient ($\sim 0.1 \mu\text{M m}^{-1}$; Table 1). This pattern is expected from a relatively higher shear of
 377 the geostrophic circulation field in that area (Figure 4b). However, the upward direction of the flux at
 378 this station is in disagreement with the deepening direction of isopycnals (Figure 2f), implying that a
 379 careful interpretation of diapycnal fluxes is required since these fluxes are strongly related to the
 380 nutrient field, which increases with depth.

381 Previous studies based on the impact of physical mixing dynamics on biogeochemical processes in
382 marine ecosystems have shown that instabilities in the water column may lead to small-scale vertical
383 turbulent motions of nutrients at the base of the mixed layer or the euphotic zone, with major
384 implications for the productivity of phytoplankton because the timescales on which nutrients change
385 are similar to those of phytoplankton growth (Lévy et al., 2001; Mahadevan and Tandon, 2006; Li et
386 al., 2012; Mahadevan, 2016). The turbulent energy cascade in the ocean implies an energy flow from
387 large-scale motion fields to smaller-scales, for example, the influence of the wind to promote velocity
388 differences (shear) through the water column or the relative movement between mesoscale structures,
389 which could enhanced turbulent mixing at submesoscale level (~0.1-10 km, few days) or lesser,
390 eroding the stability of the water column and bringing nutrients to the upper layer. This kind of nutrient
391 supply and turbulent mixing is still an area of active research, however, it has been suggested to be a
392 most important issue because it can directly affect phytoplankton growth rates, biomass and the
393 community structure (Falkowski and Oliver, 2007; Mahadevan, 2016; Lévy et al., 2018).

394 3.3 Total and size-fractionated Chl-a, and phytoplankton cross-shore distribution

395 Regarding phytoplankton size structure during the survey (data not shown), the proportion of the
396 micro-phytoplankton fraction was highest (~40-70% of total Chl-a) in the CUF and ITE areas, whereas
397 that of the nano-phytoplankton fraction was dominant (~30-80%) in both transects, and that of the pico-
398 phytoplankton fraction was lowest (<20%). However, the latter was unusually higher in the CZ
399 compared with the CTZ (Figure 7 in Morales et al., 2017) and, overall, the size distribution pattern
400 differs from that previously reported for waters off central Chile, where the contribution of the micro-
401 phytoplankton fraction is highest in the CZ and that of the smaller cells (nano- and pico-) is higher in
402 the CTZ and/or in mesoscale eddies (Morales et al., 2012; Anabalón et al., 2016).

403 In order to evaluate how the phytoplankton size distribution compared with the estimated diapycnal
404 nutrient fluxes, the depth of Chl-a maxima in each size fraction and the spatial distribution of total and
405 micro-phytoplankton Chl-a concentrations obtained from fluorometric measurements are displayed in
406 Figure 7. In addition, the maxima in micro-, nano- and pico-phytoplankton Chl-a concentrations are
407 detailed in Table 3. Related to the depth of the maximum Chl-a values in each size fraction, those in
408 the micro- and nano-phytoplankton fractions displayed a similar pattern to that of the nutrient fluxes,
409 i.e. maxima in the upper layer closer to the coast and deeper towards the oceanic area (Figures 7a, 7d).
410 Regarding total Chl-a, maximum values (>5 mg m⁻³) were detected in the surface layer (<20 m depth)
411 of the CUF area (Sts. 5 and 16), whereas moderate total Chl-a values (~1-3 mg m⁻³) were found in the
412 upper layer of the CZ and at the subsurface (~20-30 m depth) in the ITE area (Sts. 10-11 and 20-24;
413 Figures 7b, 7e).

414 Among the three Chl-a size fractions, only the maxima in the micro-phytoplankton fraction co-occur
415 with the highest values in the diapycnal nutrient fluxes observed in the CUF (Sts. 5 and 16) and ITE
416 areas (Sts. 10 and 22) (Figures 7c, 7f, Tables 2 and 3). This is consistent with previous studies that
417 have reported the presence of microdiatoms in frontal zones, oceanic intrathermocline eddies and
418 around the pycnocline, associated with higher turbulent mixing and nutrient content, which locally
419 contribute to enhance micro-phytoplankton growth and to biomass accumulation (e.g. Lund-Hansen et
420 al., 2006; Ledwell et al., 2008; Li et al., 2012; Landeira et al., 2014; Zhang et al., 2015). Considering
421 that there are two main factors modulating phytoplankton primary production and growth in the oceans,
422 light and nutrients (Mahadevan, 2016), we assume that there was no light limitation during our survey,
423 since the *in situ* climatological values of the photic layer depth oscillate between ~10 and 30 m depth
424 during February in the region of study (Testa et al., 2018). In addition, the maxima in diapycnal nutrient
425 fluxes (thin black lines; Figures 7b-c, 7e-f) are located below the mixed layer, which was between ~10-

426 20 m depth during the survey (yellow lines; Figures 7b-c, 7e-f), suggesting that diapycnal mixing is an
427 important mechanism in controlling the vertical nutrient fluxes to the euphotic zone through turbulent
428 inversions in the stratified parts of the water column (Park et al., 2014) and, in turn, these fluxes would
429 contribute to the development of Chl-a maxima (Richardson et al., 2000; Lund-Hansen et al., 2006).

430 In order to evaluate in further detail the observed spatial coincidence between high diapycnal nutrient
431 fluxes and Chl-a maxima in the micro-phytoplankton fraction, we analyzed the spatial distribution of
432 dominant microdiatom species in Figure 8. As total diatom abundance, the highest values were detected
433 in the CUF and ITE areas (Figures 8a, 8e). In the CUF area of the northern transect (St. 16), a maximum
434 in abundance of the coastal taxa *Skeletonema sp.* and *Chaetoceros debilis* was observed (Figures 8b-
435 c). These species are usually found in the CZ off central-southern Chile, where nitrate:silicate (N:Si)
436 ratios close to 1:1 are favorable to them since they have high nutrient requirements, specially of silicate
437 (Gómez et al., 2007; González et al., 2007; Anabalón et al., 2016). The observed maxima of these
438 species in the CUF area may be favored by moderate nitrate concentrations in the surface layer and a
439 relatively higher silicate flux (Figures 6a-b and Table 2). The lower abundance of these species in the
440 CUF area of the southern transect (Figures 8f-g) compared with the northern one (Figures 8b-c) could
441 be the combined result of a northward advection of waters (including nutrients and phytoplankton) in
442 association with the south-east edge portion of the ITE (Figure 1), a stronger frontal gradient of
443 isopycnals, and a higher area of maxima in diapycnal nutrient fluxes compared to the northern sector
444 (Figure 6), implying a potential delay in the phytoplankton response to nutrient injections in the
445 southern transect.

446 In the case of the ITE area (Sts. 10-11 and 20-24), the dominant oceanic diatom species was *Pseudo-*
447 *nitzschia pseudo-delicatissima* (Figures 8d, 8h), which has been reported to have lower silicate
448 requirements (Sommer, 1994). This distribution is consistent with the occurrence of a relatively higher
449 nitrate flux in the ITE area but weaker in the case of the silicate in both transects (Figure 6 and Table
450 2), implying a deficiency of the latter. These diatoms were more abundant in the northern transect than
451 in the southern one, probably as a response to the nutrient fluxes being maximum at a shallower depth
452 (~30-40 m depth) in the first compared to the second case (~40-60 m depth). In the CTZ off central-
453 southern Chile, the presence of this species has been associated with waters having relatively high N:Si
454 ratios (>3:1) (Gómez et al., 2007; Menschel et al., 2016), as reported previously for the ITE area during
455 the present survey (Figure 5 in Morales et al., 2017). Moreover, the coastal diatom species described
456 above were also found in the ITE area (Sts. 10-11, 20-24; Figures 8b-c, 8f-g) and the oceanic species
457 was abundant in the CUF area (Sts. 7, 16-18; Figures 8d, 8h), suggesting an exchange of diatoms taxa
458 by the mesoscale ITE-CUF interaction, as previously reported in Morales et al. (2017).

459 Quantifying the physical mechanisms responsible for bringing nutrients into the upper euphotic layer
460 is important in terms of the oceanic biological production and nutrient cycles (Arrigo, 2004; Muller-
461 Karger et al., 2005). Previous studies using a modelling approach have shown that diapycnal nutrient
462 fluxes exert a bottom-up control on phytoplankton community structure, locally controlling primary
463 production and carbon export towards deep waters (Allen et al., 2004; Kelly-Gerreyn et al., 2004), but
464 there is still scarce evidence of this aspect. For example, the influence of diapycnal nitrate fluxes and
465 new primary production at a frontal zone in the southern California current system was estimated by
466 Li et al. (2012), using field measurements and a modelling approach. They estimated that new
467 production at the frontal zone was $\sim 0.28 \text{ g C m}^{-2} \text{ d}^{-1}$ and it was associated with a high carbon biomass
468 from diatoms (>50%) and an upward diapycnal nitrate flux of $\sim 4 \text{ mmol m}^{-2} \text{ d}^{-1}$ at the base of the
469 euphotic zone, suggesting this flux supported the observed new production values. In another case for
470 coastal waters in the Baltic Sea, a maximum in subsurface Chl-a (7.5 mg m^{-3}) dominated by diatoms
471 ($\sim 90\%$) was associated with a diapycnal nitrate flux ranging from ~ 7 to $17 \text{ mmol m}^{-2} \text{ d}^{-1}$, sustaining a

472 primary production of $\sim 1.36 \text{ g C m}^{-2} \text{ d}^{-1}$, this value accounting for 17% of new production during the
473 spring bloom (Lund-Hansen et al., 2006).

474 Our results are the first ones of this nature in the Humboldt EBUS to provide evidence of diapycnal
475 mixing, associated with a CUF and an ITE, as an additional mechanism contributing to modulate
476 phytoplankton size structure and, potentially, to influence primary production in the CZ and CTZ off
477 central-southern Chile. During the PHYTO-FRONT survey no direct measurements of primary
478 production were taken, but we used the above reported values as a response to diapycnal fluxes to
479 indirectly estimate it. Based on this, the maximum diapycnal nitrate fluxes (~ 20 to $37 \text{ mmol m}^{-2} \text{ d}^{-1}$;
480 Table 2) in the CUF and ITE areas could support a primary production ranging from ~ 1.4 to 2.9 g C
481 $\text{m}^{-2} \text{ d}^{-1}$ in the area of study. These estimates are similar to those previously reported from *in situ*
482 measurements (~ 1 and $3 \text{ g C m}^{-2} \text{ d}^{-1}$) in the CZ off central-southern Chile during February, which have
483 been mainly associated with the phase of upwelling events (relaxation and active phases, respectively)
484 (Testa et al., 2018). Since the PHYTO-FRONT survey took place during a relaxation upwelling phase
485 (Morales et al., 2017), we suggest that ITE-CUF interactions off central-southern Chile would locally
486 enhance diapycnal nutrient fluxes and with it, enhance primary production in the CTZ waters. Under
487 this scenario, we expect large phytoplankton cells, such as diatoms, to make a higher contribution to
488 the total primary production due to their competitive advantage under turbulent mixing conditions
489 (Reynolds, 1997; Falkowski and Oliver, 2007). Similarly, Pérez-Santos et al. (2018) found a strong
490 relation between turbulent mixing and macro-zooplankton aggregations, favored by local increases in
491 primary production in response to enhanced diapycnal mixing in fjord waters of the southern
492 Patagonian region off Chile.

493 Small-scale turbulent mixing, mesoscale activity, primary production, and phytoplankton size
494 structure in the region off central-southern Chile might be influenced by temporal variability in their
495 forcing processes, however, little is known about their patterns of variability at the lower frequencies.
496 At the interannual scale, El Niño Southern Oscillation (ENSO) events are regular (every ~ 2 -8 years)
497 remote equatorial processes (Torrence and Compo, 1998) in the Pacific Ocean. In the region off
498 central-southern Chile, phytoplankton phenology, total Chl-a, and primary production in the CZ have
499 been shown to have a weak association with warm (El Niño) and cold (La Niña) ENSO phases during
500 the 2002-2016 period (Corredor-Acosta et al., 2015; Testa et al., 2018). At the same time, Combes et
501 al. (2015) found, through a modelling approach, a significant correlation between ITEs variability and
502 ENSO, with a lower number of ITEs during strong El Niño events. Inversely, during La Niña events,
503 an increase in the number of ITEs was related to a higher zonal density gradient, which implies a
504 stronger uplifting of isopycnals towards the coast. In the context of our results, these findings would
505 imply a potential increase (decrease) of small-scale turbulent mixing and of diapycnal nutrient fluxes
506 into the upper layer under La Niña (El Niño) conditions, leading to an increase in diatom abundance
507 and in the Chl-a values of the micro-phytoplankton fraction, at least in the areas associated with the
508 early stages of ITEs lifetime.

509 Finally, under a climate change scenario, the expected increase of alongshore coastal winds off
510 central-southern Chile will enhance coastal upwelling and, with it, stronger zonal temperature and
511 density gradients may develop a stronger coastal upwelling front (Sydeman et al., 2014; Oerder et al.,
512 2018). Associated with this pattern, higher baroclinic instabilities and turbulent mixing, and increases
513 in microplanktonic primary production in the frontal zone would be expected. In areas of ITE-CUF
514 interaction, we expect more intense small-scale turbulence to favor the efficiency of the biological
515 pump in the region. However, larger efforts are required to resolve processes and interactions at the
516 mesoscale-submesoscale level, since small scale processes, such as diapycnal mixing, are frequently
517 avoided in modelling regions closer to the coastal zone (e.g. Marchesiello et al., 2009; Combes et al.,

518 2015). In perspective, climate-driven and turbulent mixing processes are important factors shaping
519 phytoplankton community structure and functioning, and investigating their links in highly productive
520 EBUS systems are a priority in the prediction the impacts of regional and global climate change.

521 **4 Conclusions**

522 EBUS systems are regions of intense mesoscale and submesoscale activities, such as coastal
523 upwelling fronts, filaments, surface and intrathermocline eddies, which have been shown to have an
524 important impact on phytoplankton distribution and community structure. This study focuses on the
525 role of small-scale turbulent diapycnal mixing in phytoplankton size distribution in an area of ITE-
526 CUF interaction off central-southern Chile. Our results suggest that maximum values in vertical
527 nutrient fluxes took place in the CUF and ITE areas in association with higher nutrient gradients and
528 diapycnal mixing, favoring the competitive advantage of larger phytoplankton cells (diatoms). In the
529 CUF area, maximum abundance of coastal diatoms taxa were found in association with their higher
530 nutrient requirements (especially silicate) and higher diapycnal fluxes of nitrate and silicate. In the ITE
531 area, oceanic diatoms species were dominant according to their lower silicate requirements and a higher
532 diapycnal nitrate fluxes compared to that of silicate. These findings suggest that turbulent diapycnal
533 mixing in areas of ITE-CUF interaction can promote the presence of large phytoplankton cells and
534 could be an important mechanism to support primary productivity in coastal and coastal transition
535 zones of EBUSs.

536 **5 Conflict of Interest**

537 The authors declare that the research was conducted in the absence of any commercial or financial
538 relationships that could be considered as a potential conflict of interest.

539 **6 Author Contributions**

540 Data collection during the PHYTO-FRONT cruise: C.E.M., V.A., L.P.V., S.H., and A.C.A. *In situ*
541 size-fractionated Chl-a and diatoms abundance analysis: V.A., C.E.M., and A.C.A. Thorpe scale
542 method and diapycnal nutrient fluxes analysis: L.P.V., A.R.S., C.E.M., and A.C.A. Manuscript writing:
543 A.C.A. with input from all co-authors.

544 **7 Funding**

545 This research was funded by FONDECYT Projects 1120504, 1151299 and 1171895 (CONICYT-
546 Chile). Additional support during the writing phase was provided by the Instituto Milenio de
547 Oceanografía (IMO-Chile), funded by the Iniciativa Científica Milenio (ICM-Chile). A.C.A. was
548 supported by a CONICYT-Chile Scholarship (2013–2017).

549 **8 Acknowledgments**

550 The authors thank the European Space Agency for the production and distribution of the Ocean
551 Colour Climate Change Initiative dataset, Version 3.0, available online at
552 <http://www.oceancolour.org/>. The Multi-scale Ultra-high Resolution Sea Surface Temperature (MUR-
553 SST) data distributed by NASA (<https://mur.jpl.nasa.gov/>). Mean surface geostrophic velocity field
554 and sea level anomaly data distributed by the Copernicus Marine and Environment Monitoring Service
555 (CMEMS; <http://marine.copernicus.eu/>). Nutrient sampling and analyses were undertaken by Dr. M.
556 Cornejo and M.Sc. N. Silva (PUCV), for which we are grateful. The PHYTO-FRONT cruise was

557 successful thanks to the support from the crew in the R/V A. Molina (IFOP) and from the students
558 participating in it.

559 9 References

560 Aguirre, C., Pizarro, O., Strub, P.T., Garreaud, R., and Barth, J.A. (2012). Seasonal dynamics of the
561 near-surface alongshore flow off central Chile. *J. Geophys. Res.* 117, C01006,
562 doi:10.1029/2011JC007379.

563 Agustí, S. (2004). Viability and niche segregation of *Prochlorococcus* and *Synechococcus* cells across
564 the Central Atlantic Ocean. *Aquat. Microb. Ecol.* 36: 53–59.

565 Allen, J.I., Siddorn, J.R., Blackford, J.C., and Gilbert, F.J. (2004). Turbulence as a control on the
566 microbial loop in a temperate seasonally stratified marine systems model. *Journal of Sea
567 Research.* 52(1), 1-20.

568 Anabalón, V., Morales, C.E., Escribano, H.R., and Varas, M.A. (2007). The contribution of nano- and
569 micro-planktonic assemblages in the surface layer (0–30 m) under different hydrographic conditions
570 in the upwelling area off Concepción, central Chile. *Prog. Oceanogr.* 75, 396–414.

571 Anabalón, V., Morales, C.E., González, H.E., Menschel, E., Schneider, W., Hormazabal, S., and
572 Escribano, R. (2016). Micro-phytoplankton community structure in the coastal upwelling zone off
573 Concepción (central Chile): Annual and inter-annual fluctuations in a highly dynamic environment.
574 *Prog. Oceanogr.* 149, 174–188.

575 Arcos-Pulido, M., Rodríguez-Santana, A., Emelianov, M., Paka, V., Aristegui, J., Benavides, M.,
576 Sangrà, P., Machín, F., García-Weil, L and Estrada-Allis, S. (2014). Diapycnal nutrient fluxes on the
577 northern boundary of Cape Ghir upwelling region. *Deep Sea Research Part I: Oceanographic
578 Research Papers.* 84, 100-109.

579 Arrigo, K. R. (2004). Marine microorganisms and global nutrient cycles. *Nature.* 437(7057), 349.

580 Ascani, F., Richards, K.J., Firing, E., Grant, S., Johnson, K.S., Jia, Y., Lukas, R., and Karl, D. M.
581 (2013). Physical and biological controls of nitrate concentrations in the upper subtropical North Pacific
582 Ocean. *Deep Sea Research Part II: Topical Studies in Oceanography.* 93, 119-134.

583 Atlas, E., Hager, S., Gordon, L., and Park, P. (1971). A practical manual for use of the Technicon
584 Autoanalyser in sea water nutrient analyses (Tech. Rep. 215), Corvallis, OR: Department of
585 Oceanography, Oregon State University.

586 Austin, J.A., and Barth, J.A. (2002). Variation in the position of the upwelling front on the Oregon
587 shelf. *J. Geophys. Res. Oceans.* 107(C11), 3180.

588 Barceló-Llull, B., Sangrà, P., Pallàs-Sanz, E., Barton, E.D., Estrada-Allis, S.N., Martínez-Marrero, A.,
589 et al. (2017). Anatomy of a subtropical intrathermocline eddy. *Deep Sea Research Part I:
590 Oceanographic Research Papers.* 124, 126-139.

591 Boccaletti, G., Ferrari, R., and Fox-Kemper, B. (2007). Mixed layer instabilities and restratification. *J.
592 Phys. Oceanogr.* 37: 2228–2250.

- 593 Bricaud, A., Claustre, H., Ras, J., and Oubelkheir, K. (2004). Natural variability of phytoplanktonic
594 absorption in oceanic waters: Influence of the size structure of algal populations. *J. Geophys. Res.* 109:
595 C11010.
- 596 Brink, K.H., and Cowles, T.J. (1991). The coastal transition zone program. *J. Geophys. Res.* 96: 14637-
597 14647.
- 598 Brown, S.L., Landry, M.R., Selph, K.E., Yang, E.J., Rii, Y.M., et al. (2008). Diatoms in the desert:
599 Plankton community response to a mesoscale eddy in the subtropical North Pacific. *Deep Sea Res. II.*
600 55: 1321–1333.
- 601 Bruland, K.W., Rue, E.L., and Smith, G.J. (2001). Iron and macronutrients in California coastal
602 upwelling regimes: Implications for diatom blooms. *Limnol. Oceanogr.* 46: 1661–1674.
- 603 Chaigneau, A., and Pizarro, O. (2005). Eddy characteristics in the eastern South Pacific. *J. Geophys.*
604 *Res.* 110, C06005. doi:10.1029/2004JC002815.
- 605 Chelton, D.B., Gaube, P., Schlax, M.G., Early, J.J., and Samelson, R.M. (2011). The influence of
606 nonlinear mesoscale eddies on near-surface oceanic chlorophyll. *Science.* 334 (6054): 328-332.
- 607 Chisholm, S. (1992). Phytoplankton size. In: Falkowski, P.G., Woodhead, A.D. (Eds.), Primary
608 productivity and biogeochemical cycles in the sea. Plenum Press, New York, pp. 213–237.
- 609 Combes, V., Hormazabal, S., and Di Lorenzo, E. (2015). Interannual variability of the subsurface eddy
610 field in the Southeast Pacific. *J. Geophys. Res. Oceans.* 120(7), 4907-4924.
- 611 Correa-Ramirez, M.A., Hormazabal, S., and Yuras, G. (2007). Mesoscale eddies and high chlorophyll
612 concentrations off central Chile (29°–39°S). *Geophys. Res. Lett.* L12604.
- 613 Correa-Ramirez, M.A., Hormazabal, S., and Morales, C.E. (2012). Spatial patterns of annual and
614 interannual surface chlorophyll-a variability in the Peru-Chile Current System. *Prog. Oceanogr.* 92-
615 95: 8-17. doi:10.1016/j.pcean.2011.07.008.
- 616 Corredor-Acosta, A., Morales, C.E., Hormazabal, S., Andrade, I., and Correa-Ramirez, M.A. (2015).
617 Phytoplankton phenology in the coastal upwelling region off central-southern Chile (35°S-38°S):
618 Time-space variability, coupling to environmental factors, and sources of uncertainty in the
619 estimates. *J. Geophys. Res. Oceans.* 120(2), 813-831.
- 620 Corredor-Acosta, A., Morales, C.E., Brewin, R.J.W., Auger, P.A., Pizarro, O., Hormazabal, S., and
621 Anabalón, V. (2018). Phytoplankton Size Structure in Association with Mesoscale Eddies off Central-
622 Southern Chile: The Satellite Application of a Phytoplankton Size-Class Model. *Remote Sensing.*
623 10(6), 834; doi:10.3390/rs10060834.
- 624 Davis, R.E., Ohman, M.D., Rudnick, D.L., and Sherman, J. T. (2008). Glider surveillance of physics
625 and biology in the southern California Current System. *Limnology and Oceanography.* 53(5part2),
626 2151-2168.
- 627 de Boyer Montégut, C., Madec, G., Fischer, A.S., Lazar, A., and Iudicone, D. (2004). Mixed layer
628 depth over the global ocean: An examination of profile data and a profile-based climatology. *J.*
629 *Geophys. Res. Oceans.* 109(C12).

- 630 Dillon, T. M. (1982). Vertical overturns: A comparison of Thorpe and Ozmidov length scales. *J.*
631 *Geophys. Res. Oceans.* 87(C12), 9601-9613.
- 632 Doubell, M.J., Spencer, D., van Ruth, P.D., Lemckert, C., and Middleton, J.F. (2018). Observations of
633 vertical turbulent nitrate flux during summer in the Great Australian Bight. *Deep Sea Research Part*
634 *II: Topical Studies in Oceanography.* 157, 27-35.
- 635 Eppley, R.W., and Peterson, B.J. (1979). Particulate organic matter flux and planktonic new production
636 in the deep ocean. *Nature*, 282, 677–680.
- 637 Falkowski, P.G., and Oliver, M.J. (2007). Mix and match: how climate selects phytoplankton. *Nature*
638 *reviews microbiology.* 5(10), 813.
- 639 Finkel, Z.V., Beardall, J., Flynn, K.J., Quigg, A., Rees, T.A.V., and Raven, J.A. (2010). Phytoplankton
640 in a changing world: cell size and elemental stoichiometry. *J. Plankton Res.* 32: 119–137.
- 641 Franks, P.J.S., and Walstad, L. (1997). Phytoplankton patches at fronts: A model of formation and
642 response to wind events. *J. Marine Res.* 55: 1-29.
- 643 Frants, M., Damerell, G. M., Gille, S. T., Heywood, K. J., MacKinnon, J., and Sprintall, J. (2013). An
644 assessment of density-based finescale methods for estimating diapycnal diffusivity in the Southern
645 Ocean. *Journal of Atmospheric and Oceanic Technology.* 30(11), 2647-2661.
- 646 Furnas, M.J. (1990). In situ growth rates of marine phytoplankton: approaches to measurement,
647 community and species growth rates. *J. Plankton Res.* 12(6): 1117 – 1151.
- 648 Gargett, A., and Garner, T. (2008). Determining Thorpe scales from ship-lowered CTD density
649 profiles. *Journal of Atmospheric and Oceanic Technology.* 25(9), 1657-1670.
- 650 Garside, C. (1985). The vertical distribution of nitrate in open ocean surface water. *Deep Sea Research*
651 *Part A. Oceanographic Research Papers.* 32(6), 723-732.
- 652 Gaube, P., McGillicuddy, D.J., Chelton, D.B., Behrenfeld, M.J., and Strutton, P.G. (2014). Regional
653 variations in the influence of mesoscale eddies on near-surface chlorophyll. *J. Geophys. Res.* 119(12):
654 8195-8220. doi:10.1002/2014JC010111.
- 655 Gaube, P., Chelton, D.B., Samelson, R.M., Schlax, M.G., and O'Neill, L.W. (2015). Satellite
656 observations of mesoscale eddy-induced Ekman pumping. *Journal of Physical Oceanography.* 45(1),
657 104-132.
- 658 Girault, M., Arakawa, H., Barani, A., Ceccaldi, H.J., Hashihama, F., and Gregori, G. (2015).
659 Heterotrophic prokaryote distribution along a 2300 km transect in the North Pacific subtropical gyre
660 during a strong La Niña conditions: relationship between distribution and hydrological conditions.
661 *Biogeosciences.* 12(11), 3607-3621.
- 662 Goldman, J.C., and McGillicuddy, D.J.Jr. (2003). Impact of large marine diatoms growing at low light
663 on episodic new production. *Limnol. Oceanogr.* 48: 1176–1182.

- 664 Gómez, F., Claustre, H., Raimbault, P., and Souissi, S. (2007). Two High-Nutrient Low-Chlorophyll
665 phytoplankton assemblages: The tropical central Pacific and the offshore Perú-Chile Current.
666 *Biogeosciences*. 4, 1101–1113.
- 667 González, H.E., Menschel, E., Aparicio, C., and Barriá, C. (2007). Spatial and temporal variability of
668 microplankton and detritus, and their export to the shelf sediments in the upwelling area off
669 Concepción, Chile (~36°S), during 2002-2005. *Prog. Oceanogr.* 75, 435-451.
- 670 Guidi, L., Stemmann, L., Jackson, G.A., Ibanez, F., Claustre, H., Legendre, L., Picheral, M., and
671 Gorsky, G. (2009). Effects of phytoplankton community on production, size and export of large
672 aggregates: A world-ocean analysis. *Limnol. Oceanogr.* 54(6): 1951–1963.
- 673 Hales, B., Moum, J.N., Covert, P., and Perlin, A. (2005). Irreversible nitrate fluxes due to turbulent
674 mixing in a coastal upwelling system. *J. Geophys. Res. Oceans*. 110(C10).
675 doi:10.1029/2004JC002685.
- 676 Henley, S.F., Jones, E.M., Venables, H.J., Meredith, M.P., Firing, Y.L., Dittrich, R., Heiser, S., Stefels,
677 J., and Dougans, J. (2018). Macronutrient and carbon supply, uptake and cycling across the Antarctic
678 Peninsula shelf during summer. *Philosophical Transactions of the Royal Society A: Mathematical,
679 Physical and Engineering Sciences*. 376(2122), 20170168.
- 680 Hormazabal, S., Shaffer, G., and Leth, O. (2004). Coastal transition zone off Chile. *J. Geophys. Res.*
681 *Oceans*. 109(C1).
- 682 Hormazabal, S., Combes, V., Morales, C.E., Correa-Ramirez, M.A., Di Lorenzo, E., and Nuñez, S.
683 (2013). Intrathermocline eddies in the coastal transition zone off central Chile (31–41 S). *J. Geophys.*
684 *Res. Oceans*. 118, 4811–4821.
- 685 Hsu, P.C., Cheng, K.H., Jan, S., Lee, H.J., and Ho, C.R. (2019). Vertical structure and surface patterns
686 of Green Island wakes induced by the Kuroshio. *Deep Sea Research Part I: Oceanographic Research
687 Papers*. 143, 1-16.
- 688 Johnston, T.M.S., Rudnick, D.L., and Pallàs-Sanz, E. (2011). Elevated mixing at a front. *J. Geophys.*
689 *Res.* 116: C11033. doi:10.1029/2011JC007192.
- 690 José, Y.S., Dietze, H., and Oschlies, A. (2017). Linking diverse nutrient patterns to different water
691 masses within anticyclonic eddies in the upwelling system off Peru. *Biogeosciences*. 14(6), 1349-1364.
- 692 Kara, A.B., Rochford, P.A., and Hurlburt, H.E. (2000). An optimal definition for ocean mixed layer
693 depth. *J. Geophys. Res. Oceans*. 105(C7), 16803-16821.
- 694 Karl, D.M., Church, M.J., Dore, J.E., Letelier, R.M., and Mahaffey, C. (2012). Predictable and efficient
695 carbon sequestration in the North Pacific Ocean supported by symbiotic nitrogen fixation. *PNAS*.
696 109(6): 1842-1849. doi:10.1073/pnas.1120312109.
- 697 Kelly-Gerreyn, B.A., Anderson, T.R., Holt, J.T., Gowen, R.J., and Proctor, R. (2004). Phytoplankton
698 community structure at contrasting sites in the Irish Sea: a modelling investigation. *Estuarine, Coastal
699 and Shelf Science*. 59(3), 363-383.

- 700 King, F.D., and Devol, A.H. (1979). Estimates of vertical eddy diffusion through the thermocline from
701 phytoplankton nitrate uptake rates in the mixed layer of the eastern tropical Pacific1. *Limnology and*
702 *Oceanography*. 24(4), 645-651.
- 703 Landeira, J.M., Ferron, B., Lunven, M., Morin, P., Marié, L., and Sourisseau, M. (2014). Biophysical
704 interactions control the size and abundance of large phytoplankton chains at the Ushant tidal front.
705 *PLoS ONE*. 9(2): e90507. doi: 10.1371/journal.pone.0090507.
- 706 Law, C.S., Martin, A.P., Liddicoat, M.I., Watson, A.J., Richards, K.J., and Woodward, E.M.S. (2001).
707 A Lagrangian SF6 tracer study of an anticyclonic eddy in the North Atlantic: Patch evolution, vertical
708 mixing and nutrient supply to the mixed layer. *Deep Sea Research Part II: Topical Studies in*
709 *Oceanography*. 48(4-5), 705-724.
- 710 Law, C.S., Abraham, E.R., Watson, A.J., and Liddicoat, M. I. (2003). Vertical eddy diffusion and
711 nutrient supply to the surface mixed layer of the Antarctic Circumpolar Current. *J. Geophys. Res.*
712 *Oceans*. 108(C8), 3272, doi:10.1029/2002JC001604.
- 713 Ledwell, J.R., Watson, A.J., and Law, C.S. (1998). Mixing of a tracer in the pycnocline. *J. Geophys.*
714 *Res. Oceans*. 103(C10), 21499-21529.
- 715 Ledwell, J.R., McGillicuddy Jr, D.J., and Anderson, L.A. (2008). Nutrient flux into an intense deep
716 chlorophyll layer in a mode-water eddy. *Deep Sea Research Part II: Topical Studies in Oceanography*.
717 55(10-13), 1139-1160.
- 718 Legendre, L., and Le Fèvre, J. (1989). In: Berger, W.H., Smetacek, V.S. and Wefer, G. (Eds.),
719 Productivity of the Ocean: Present and Past. John Wiley & Sons Limited, New York, pp. 49–63.
- 720 Le Queré, C., Harrison, S.P., Prentice, C.I., Buitenhuis, E.T., Aumont, O., Bopp, L., Claustre, H., et al.
721 (2005). Ecosystem dynamics based on plankton functional types for global ocean biogeochemistry
722 models. *Global Change Biol.* 11(11): 2016–2040. doi:10.1111/j.1365-2486.2005.1004.x.
- 723 Letelier, J., Pizarro, O., and Nuñez, S. (2009). Seasonal variability of coastal upwelling and the
724 upwelling front off central Chile. *J. Geophys. Res.* 114: C12009.
725 <http://dx.doi.org/10.1029/2008JC005171>.
- 726 Leth, O., Shaffer, G., and Ulloa, O. (2004). Hydrography of the eastern South Pacific Ocean: results
727 from the Sonne 102 cruise, May–June 1995. *Deep Sea Research Part II: Topical Studies in*
728 *Oceanography*. 51(20-21), 2349-2369.
- 729 Lévy, M., Klein, P., and Treguier, A. M. (2001). Impact of sub-mesoscale physics on production and
730 subduction of phytoplankton in an oligotrophic regime. *J. Mar. Res.* 59(4), 535-565.
- 731 Lévy, M., Franks, P.J., and Smith, K.S. (2018). The role of submesoscale currents in structuring marine
732 ecosystems. *Nature communications*. 9(1), 4758.
- 733 Li, Q.P., Franks, P.J., Ohman, M.D., and Landry, M.R. (2012). Enhanced nitrate fluxes and biological
734 processes at a frontal zone in the southern California current system. *J. Plankton Res.* 34(9), 790-801.

- 735 Llanillo, P. J., Pelegrí, J. L., Duarte, C. M., Emelianov, M., Gasser, M., Gourrion, J., and Rodríguez-
736 Santana, A. (2012). Meridional and zonal changes in water properties along the continental slope off
737 central and northern Chile. *Ciencias Marinas*. 38(1B), 307-332.
- 738 Lund-Hansen, L.C., Ayala, P.C.D.A., and Reglero, A.F. (2006). Bio-optical properties and
739 development of a sub-surface chlorophyll maxima (SCM) in southwest Kattegat, Baltic Sea. *Estuarine,
740 Coastal and Shelf Science*. 68(1-2), 372-378.
- 741 Macías, D., Rodríguez-Santana, A., Ramírez-Romero, E., Bruno, M., Pelegrí, J.L., Sangrà, P., Aguiar-
742 González, B., and García, C.M. (2013). Turbulence as a driver for vertical plankton distribution in the
743 subsurface upper ocean. *Sci. Mar.* 77(4): 541-549. doi: 10.3989/scimar.03854.03A.
- 744 Mahadevan, A., and Archer, D. (2000). Modeling the impact of fronts and mesoscale circulation on
745 the nutrient supply and biogeochemistry of the upper ocean. *J. Geophys. Res.* 105: 1209-25.
- 746 Mahadevan, A., and Tandon, A. (2006). An analysis of mechanisms for submesoscale vertical motion
747 at ocean fronts. *Ocean Model.* 14: 241-256.
- 748 Mahadevan, A. (2016). The impact of submesoscale physics on primary productivity of plankton.
749 *Annu. Rev. Mar. Sci.* 8: 161-84.
- 750 Marañón, E., and Fernández, E. (1995). Changes in phytoplankton ecophysiology across a coastal
751 upwelling front. *J. Plankton Res.* 17(10): 1999-2008. doi: 10.1093/plankt/17.10.1999.
- 752 Marchesiello, P., Debreu, L., and Couvelard, X. (2009). Spurious diapycnal mixing in terrain-following
753 coordinate models: The problem and a solution. *Ocean Modelling*. 26(3-4), 156-169.
- 754 McDougall, T.J., and P.M. Barker. (2011). Getting started with TEOS-10 and the Gibbs Seawater
755 (GSW) Oceanographic Toolbox, 28pp. SCOR/IAPSO WG127, ISBN 978-0-646-55621-5.
- 756 McGillicuddy, D.J.Jr. (2016). Mechanisms of physical-biological-biogeochemical interaction at the
757 oceanic mesoscale. *Annu. Rev. Mar. Sci.* 8: 125-159.
- 758 Menschel, E., Gonzalez, H.E., and Giesecke, R. (2016). Coastal-oceanic distribution gradient of
759 coccolithophores and their role in the carbonate flux of the upwelling system off Concepción, Chile
760 (36°S). *J. Plankton Res.* 38(4), 798-817.
- 761 Mooers, C.N., and Robinson, A.R. (1984). Turbulent jets and eddies in the California Current and
762 inferred cross-shore transports. *Science*. 223(4631), 51-53.
- 763 Morales, C.E., González, H.E., Hormazabal, S.E., Yuras, G., Letelier, J., and Castro, L.R. (2007). The
764 distribution of chlorophyll-a and dominant planktonic components in the coastal transition zone off
765 Concepción, central Chile, during different oceanographic conditions. *Prog. Oceanogr.* 75: 452-469.
- 766 Morales, C.E., Hormazabal, S., Correa-Ramírez, M., Pizarro, O., Silva, N., Fernandez, C., Anabalón,
767 V., and Torreblanca, M.L. (2012). Mesoscale variability and nutrient-phytoplankton distributions off
768 central-southern Chile during the upwelling season: The influence of mesoscale eddies. *Prog.
769 Oceanogr.* 104: 17-29. doi:10.1016/j.pocean.2012.04.015

- 770 Morales, C.E., Anabalón, V., Berto, J.P., Hormazabal, S., Cornejo, M., Correa-Ramírez, M.A., and
 771 Silva, N. (2017). Front-Eddy Influence on Water Column Properties, Phytoplankton Community
 772 Structure, and Cross-Shelf Exchange of Diatom Taxa in the Shelf-Slope Area off Concepción (~36–
 773 37° S). *J. Geophys. Res. Oceans.* 122(11), 8944-8965.
- 774 Muller-Karger, F.E., Varela, R., Thunell, R., Luerksen, R., Hu, C., and Walsh, J.J. (2005). The
 775 importance of continental margins in the global carbon cycle. *Geophys. Res. Lett.* 32(1).
- 776 Oerder, V., Berto, J.P., Morales, C.E., Hormazabal, S., and Pizarro, O. (2018). Coastal Upwelling
 777 Front Detection off Central Chile (36.5-37°S) and Spatio-Temporal Variability of Frontal
 778 Characteristics. *Remote Sensing.* 10(5), 690; doi:10.3390/rs10050690.
- 779 O’Neill, L., Chelton, D., and Esbensen, S. (2010). The effects of SST-induced surface wind speed and
 780 direction gradients on midlatitude surface vorticity and divergence. *J. Clim.* 23(2), 255–281.
- 781 Okubo, A.K.I.R.A. (1971). Horizontal and vertical mixing in the sea. *Impingement of Man on the*
 782 *Oceans.* 89, 68.
- 783 Osborn, T. R. (1980). Estimates of the local rate of vertical diffusion from dissipation measurements.
 784 *Journal of Physical Oceanography.* 10(1), 83-89.
- 785 Ozmidov, R. V. (1965). On the turbulent exchange in a stably stratified ocean. *Izv. Acad. Sci. USSR.*
 786 *Atmos. Oceanic Phys.* 1, 861-871.
- 787 Park, Y.H., Lee, J.H., Durand, I., and Hong, C.S. (2014). Validation of Thorpe-scale-derived vertical
 788 diffusivities against microstructure measurements in the Kerguelen region. *Biogeosciences.* 11(23),
 789 6927-6937.
- 790 Platt, T., Bouman, H., Devred, E., Fuentes-Yaco, C., and Sathyendranath, S. (2005). Physical forcing
 791 and phytoplankton distributions. *Sci. Mar.* 69: 55–73.
- 792 Pegliasco, C., Chaigneau, A., and Morrow, R. (2015). Main eddy vertical structures observed in the
 793 four major Eastern Boundary Upwelling Systems. *J. Geophys. Res. Oceans.* 120(9), 6008-6033.
- 794 Peliz, Á., Rosa, T.L., Santos, A.M.P., and Pissarra, J.L. (2002). Fronts, jets, and counter-flows in the
 795 Western Iberian upwelling system. *Journal of marine systems.* 35, 61-77.
- 796 Pérez-Santos, I., Castro, L., Ross, L., Niklitschek, E., Mayorga, N., Cubillos, L., Gutierrez, M.,
 797 Escalona, E., Castillo, M., Alegría, N., and Daneri, G. (2018). Turbulence and hypoxia contribute to
 798 dense biological scattering layers in a Patagonian fjord system. *Ocean Science.* 14(5), 1185-1206.
- 799 Pond, S., and Pickard, G.L. (2013). *Introductory dynamical oceanography.* 2nd edition. Elsevier.
- 800 Reynolds, C.S. (1997). *Vegetation processes in the pelagic: a model for ecosystem theory (Vol. 9).*
 801 Oldendorf/Luhe: Ecology Institute.
- 802 Richardson, K., Visser, A.W., and Pedersen, F.B. (2000). Subsurface phytoplankton blooms fuel
 803 pelagic production in the North Sea. *J. Plankton Res.* 22(9), 1663-1671.

- 804 Rippeth, T.P., Wiles, P., Palmer, M.R., Sharples, J., and Tweddle, J. (2009). The diapycnal nutrient
805 flux and shear-induced diapycnal mixing in the seasonally stratified western Irish Sea. *Cont. Shelf*
806 *Res.* 29(13), 1580-1587.
- 807 Rodríguez, J., Tintoré, J., Allen, J.T., Blanco, J.M., Gomis, D., Reul, A., and Jiménez-Gómez, F.
808 (2001). Mesoscale vertical motion and the size structure of phytoplankton in the ocean. *Nature*.
809 410(6826), 360.
- 810 Sabarros, P.S., Grémillet, D., Demarcq, H., Moseley, C., Pichegru, L., Mullers, R.H., Stenseth, N.C.,
811 and Machu, E. (2014). Fine-scale recognition and use of mesoscale fronts by foraging Cape gannets in
812 the Benguela upwelling region. *Deep Sea Research Part II: Topical Studies in Oceanography*. 107,
813 77-84.
- 814 Sangrà, P., García-Muñoz, C., García, C.M., Marrero-Díaz, A., Sobrino, C., and Mouriño-Carballido,
815 B. (2014). Coupling between upper ocean layer variability and size-fractionated phytoplankton in a
816 non-nutrient-limited environment. *Mar Ecol Prog Ser.* 499: 35-46.
- 817 Semina, H.J. (1968). Water movement and the size of phytoplankton cells. *Sarsia*. 34, 267–272.
- 818 Shaffer, G., Hormazabal, S., Pizarro, O., and Salinas, S. (1999). Seasonal and interannual variability
819 of currents and temperature off central Chile. *J. Geophys. Res.* 104(C12), 29,951-29,961,
820 doi:10.1029/1999JC900253.
- 821 Siegel, D. A., McGillicuddy, D.J.Jr., and Fields, E.A. (1999). Mesoscale eddies, satellite altimetry, and
822 new production in the Sargasso Sea. *J. Geophys. Res. Oceans*. 104(C6), 13359-13379.
- 823 Silva, N., Rojas, N., and Fedele, A. (2009). Water masses in the Humboldt Current System: Properties,
824 distribution, and the nitrate deficit as a chemical water mass tracer for Equatorial Subsurface Water off
825 Chile. *Deep Sea Research Part II: Topical Studies in Oceanography*. 56(16), 1004-1020.
- 826 Sobarzo, M., Bravo, L., Donoso, D., Garcés-Vargas, J., and Schneider, W. (2007). Coastal upwelling
827 and seasonal cycles that influence the water column over the continental shelf off central Chile. *Prog.*
828 *Oceanogr.* 75, 363-382, doi:10.1016/j.pocean.2007.08.022.
- 829 Sommer, U. (1994). Are marine diatoms favored by high Si:N ratios?. *Marine Ecology Progress Series*.
830 115, (3), 309–315.
- 831 Stramma, L., Bange, H.W., Czeschel, R., Lorenzo, A., and Frank, M. (2013). On the role of mesoscale
832 eddies for the biological productivity and biogeochemistry in the eastern tropical Pacific Ocean off
833 Peru. *Biogeosciences*. 10(11), 7293-7306.
- 834 Sydeman, W.J., García-Reyes, M., Schoeman, D.S., Rykaczewski, R.R., Thompson, S.A., Black, B.A.,
835 and Bograd, S.J. (2014). Climate change and wind intensification in coastal upwelling
836 ecosystems. *Science*. 345(6192), 77-80.
- 837 Testa, G., Masotti, I., and Farias, L. (2018). Temporal Variability in Net Primary Production in an
838 Upwelling Area off Central Chile (36°S). *Frontiers in Marine Science*. 5, 179.
- 839 Thompson, A.F., Gille, S.T., MacKinnon, J.A., and Sprintall, J. (2007). Spatial and temporal patterns
840 of small-scale mixing in Drake Passage. *Journal of Physical Oceanography*. 37(3), 572-592.

- 841 Torrence, C., and Compo, G.P. (1998). A practical guide to wavelet analysis. *Bulletin of the American*
842 *Meteorological society*. 79(1), 61-78.
- 843 Vergara, O.A., Echevin, V., Sepulveda, H.H., Colas, F., and Quiñones, R.A. (2016). Modelling the
844 seasonal dynamics of the Peru-Chile Undercurrent off Central Chile (30–40°S). *Cont. Shelf Res.* 123,
845 61–79. <https://doi.org/10.1016/j.csr.2016.04.001>.
- 846 Zhang, Y., Bellingham, J., Ryan, J., and Godin, M. (2015). Evolution of a physical and biological front
847 from upwelling to relaxation. *Cont. Shelf Res.* 108: 55-64. <http://dx.doi.org/10.1016/j.csr.2015.08.005>.
- 848 Zhang, J.Z., Baringer, M.O., and Fischer, C. J. (2017). An estimate of diapycnal nutrient fluxes to the
849 euphotic zone in the Florida Straits. *Scientific reports*. 7(1), 16098.
- 850 Zhang, S., Curchitser, E. N., Kang, D., Stock, C.A., and Dussin, R. (2018). Impacts of mesoscale eddies
851 on the vertical nitrate flux in the Gulf Stream region. *J. Geophys. Res. Oceans*. 123(1), 497-513.

852 1 Data Availability Statement

853 Raw and processed data supporting the conclusions of this manuscript will be available under request
854 to authors.

855 Table legends

856 **Table 1.** Vertical gradients for nitrate, phosphate and silicate at specific stations across both transects.
857 Gradient units are in $\mu\text{M m}^{-1}$.

858 **Table 2.** Maximum diapycnal nutrient fluxes and vertical eddy diffusivity coefficients across both
859 transects. Flux units are in $\text{mmol m}^{-2} \text{d}^{-1}$ and vertical eddy diffusivity (K_z) units in $\text{m}^2 \text{s}^{-1}$. The depth
860 (m) of the maxima in these fluxes is in parentheses.

861 **Table 3.** Maximum values of size-fractionated (micro-, nano- and pico-phytoplankton) Chl-a values
862 across both transects. Chl-a units are in mg m^{-3} . The depth (m) of the maxima is in parentheses.

863 Figure legends

864 **Figure 1.** Study area and satellite mean surface conditions during the PHYTO-FRONT cruise (3-7
865 February 2014). (A) Sea Surface Temperature (MUR-SST), (B) surface geostrophic circulation and
866 Sea Level Anomaly (SLA; CEMS), and (C) total chlorophyll-a (Chl-a) concentration (ESA OC-CCI).
867 The dots represents the sampling stations in the northern (36.5°S, 73.1-74.5°W) and southern transect
868 (36.75°S, 73.3-74.5°W). The magenta dots indicate the coastal upwelling front (CUF) area (Sts. 5-7
869 and 16-18, respectively).

870 **Figure 2.** Spatial vertical distribution of the oceanographic properties in the first 100 m depth during
871 the PHYTO-FRONT cruise. Temperature, salinity and potential density for the northern (A-C), and
872 southern transects (D-F). The dots represents the sampling stations as indicated in Figure 1.

873 **Figure 3.** T-S diagrams in the first 100 m depth for the coastal upwelling front (CUF) area (Sts. 5-7
874 and 16-18), and for the stations nearest to it in the coastal (Sts. 4 and 15) and oceanic (Sts. 8 and 19)
875 direction, in the northern (A) and southern (B) transect of the PHYTO-FRONT cruise. The colors
876 represent depth. The blue and red rectangles indicate the typical temperature – salinity features of the

877 Equatorial Subsurface Water (ESSW) and Subantarctic Water (SAAW) masses, respectively. The
878 rectangles displayed the values reported by Vergara et al. (2016), ESSW: 8.5-10.5°C, 34.4-34.9;
879 SAAW: 11.5-14.5°C, 34.1-34.8.

880 **Figure 4.** Meridional geostrophic velocity derived from conductivity, temperature and depth (CTD) of
881 situ casts in the upper 300 m depth water column for the northern (A) and southern (B) transects of the
882 PHYTO-FRONT cruise. Positive (negative) velocity values represent a northward (southward) flow.
883 The thick black line represents the zero velocity contour. The gray lines correspond to isopycnals. Dots
884 represent the sampling stations detailed in Figure 1.

885 **Figure 5.** Vertical distribution of nitrate, phosphate and silicate concentrations (μM) in the first 100 m
886 depth for the northern (A-C) and southern (D-F) transects of the PHYTO-FRONT cruise. The black
887 lines correspond to isopycnals.

888 **Figure 6.** Vertical distribution of the upward diapycnal fluxes ($\text{mmol m}^{-2} \text{d}^{-1}$) for nitrate (left panel)
889 and silicate (right panel) in the northern (A-B), and southern (C-D) transects of the PHYTO-FRONT
890 cruise. Dashed black lines indicate the maxima in nitrate and silicate fluxes in each sampling station.
891 The gray lines correspond to isopycnals. Triangles are the sampling stations detailed in Figure 1.

892 **Figure 7.** Depth of the maxima in each Chl-a size fraction and distribution of total and micro-
893 phytoplankton Chl-a values in the first 50 m depth in the northern (A-C) and southern (D-F) transects
894 of the PHYTO-FRONT cruise. The yellow line indicates the mixed layer depth obtained by using two
895 different methods ($\Delta T=0.2^\circ\text{C}$ and $\Delta\rho=0.03 \text{ kg m}^{-3}$), following the procedures of Kara et al. (2000) and
896 de Boyer Montégut et al. (2004). The gray lines correspond to isopycnals. Triangles are the sampling
897 stations detailed in Figure 1.

898 **Figure 8.** Spatial distribution of micro-phytoplankton abundance ($\text{cells} \times 10^6 \text{ m}^{-3}$) in the upper 50 m
899 depth for the northern (top panel) and southern (bottom panel) transects of the PHYTO-FRONT cruise.
900 (A and E) Total diatom abundance; (B and F) *Skeletonema sp.*; (C and G) *Chaetoceros debilis*; (D and
901 H) *Pseudonitzschia pseudodelicatissima*. The dashed black line indicates the maximum nitrate flux in
902 each sampling station. The gray lines correspond to isopycnals. Triangles are the sampling stations
903 detailed in Figure 1.

904

905

906

907

908

909

910

911

912

913 **Table 1.** Vertical gradients for nitrate, phosphate and silicate at specific stations across both transects. Gradient units are in $\mu\text{M m}^{-1}$.

Layer (m)	CZ (St. 26)			CUF (St. 16)			ITE-CUF (St. 20)			ITE (St. 22)		
	Grad N	Grad P	Grad Si	Grad N	Grad P	Grad Si	Grad N	Grad P	Grad Si	Grad N	Grad P	Grad Si
0-5	0.034	0.008	0.056	0.116	0.006	0.006	0.010	0.000	0.020	0.009	0.002	0.044
5-10	0.034	0.008	0.056	0.214	0.042	0.032	0.034	0.006	0.016	0.009	0.002	0.003
10-15	0.635	0.046	0.493	0.533	0.069	0.278	0.036	0.003	0.063	0.148	0.024	0.003
15-20	1.236	0.084	0.252	0.852	0.096	0.524	0.036	0.003	0.063	0.304	0.030	0.017
20-30	0.146	0.025	0.010	0.082	0.015	0.063	0.710	0.055	0.087	0.561	0.034	0.009
30-40	0.010	0.005	0.081	0.113	0.008	0.112	0.256	0.010	0.023	0.591	0.030	0.292
40-60	0.010	0.002	0.069	0.056	0.004	0.056	0.128	0.005	0.023	0.237	0.026	0.255

Layer (m)	CZ (St. 1)			CUF (St. 5)			ITE-CUF (St. 9)			ITE (St. 10)		
	Grad N	Grad P	Grad Si	Grad N	Grad P	Grad Si	Grad N	Grad P	Grad Si	Grad N	Grad P	Grad Si
0-5	0.018	0.004	0.090	0.062	0.002	0.002	0.000	0.002	0.000	0.061	0.002	0.020
5-10	0.018	0.004	0.186	0.544	0.056	0.496	0.000	0.010	0.000	0.061	0.000	0.008
10-15	0.274	0.030	0.150	0.578	0.068	0.698	0.000	0.008	0.000	0.062	0.018	0.003
15-20	0.460	0.037	0.354	0.282	0.026	0.184	0.042	0.008	0.000	0.020	0.002	0.003
20-30	0.367	0.034	0.252	0.108	0.015	0.484	0.132	0.001	0.000	0.243	0.015	0.028
30-40	0.087	0.003	0.056	0.108	0.036	0.016	0.136	0.035	0.112	0.665	0.040	0.072
40-60	0.000	0.001	0.156	0.128	0.008	0.008	0.128	0.019	0.038	0.467	0.033	0.423

914

915

916

917

918

919

920

921

Running Title

922 **Table 2.** Maximum diapycnal nutrient fluxes and vertical eddy diffusivity coefficients across both transects. Flux units are in $\text{mmol m}^{-2} \text{d}^{-1}$
 923 and vertical eddy diffusivity (K_z) units in $\text{m}^2 \text{s}^{-1}$. The depth (m) of the maxima in these fluxes is in parentheses.

Longitude ($^{\circ}\text{W}$)	-73.1	-73.2	-73.3	-73.4	-73.5	-73.6	-73.7	-73.8	-73.9	-74.0	-74.1	-74.3	-74.5
	CZ												
North Transect	Sc. 25	Sc. 26	Sc. 12		Sc. 14		Sc. 16		Sc. 18		Sc. 20	Sc. 22	ITE
Nitrate	7.83 (15)	16.51 (20)	13.86 (30)		8.91 (20)		30.20 (20)		5.48 (40)		11.44 (30)	22.62 (40)	4.96 (40)
Phosphate	0.65 (15)	1.12 (20)	1.10 (30)		0.62 (20)		3.40 (20)		0.42 (40)		0.88 (30)	1.30 (30)	0.35 (40)
Silicate	4.68 (30)	6.58 (15)	10.76 (30)		5.44 (15)		18.57 (20)		1.60 (40)		1.39 (30)	11.17 (40)	1.42 (40)
K_z	1.51e-4	1.55e-4	2.41e-4		3.00e-4		4.10e-4		0.73e-4		1.87e-4	4.43e-4	0.80e-4
	CUF												
South Transect	Sc. 1	Sc. 2	Sc. 3	Sc. 4	Sc. 5	Sc. 6	Sc. 7	Sc. 8	Sc. 9	Sc. 10	ITE	Sc. 11	
Nitrate	16.53 (20)	2.04 (20)	7.04 (20)	2.62 (30)	34.70 (15)	13.20 (30)	36.81 (20)	4.43 (40)	19.34 (40)	31.90 (40)	15.09 (30)		
Phosphate	1.33 (20)	0.20 (20)	2.65 (10)	0.48 (15)	4.08 (15)	4.43 (30)	2.05 (20)	0.35 (40)	4.97 (40)	1.91 (40)	1.25 (30)		
Silicate	12.72 (20)	1.60 (20)	15.39 (15)	2.15 (60)	41.90 (15)	29.53 (30)	15.28 (60)	0.70 (60)	15.93 (40)	20.29 (60)	3.06 (30)		
K_z	4.16e-4	0.50e-4	3.29e-4	0.88e-4	6.95e-4	6.59e-4	2.98e-4	0.57e-4	16.4e-4	5.55e-4	2.34e-4		

924

925

926

927

928

929

930

931

932

933

934



935 **Table 3.** Maximum values of size-fractionated (micro-, nano- and pico-phytoplankton) Chl-a values across both transects. Chl-a units are in
 936 mg m^{-3} . The depth (m) of the maxima is in parentheses.

Longitude (°W)	-73.1	-73.2	-73.3	-73.4	-73.5	-73.6	-73.7	-73.8	-73.9	-74.0	-74.1	-74.3	-74.5
	CZ												
North Transect													
Micro	St. 25 0.30 (5)	St. 26 1.63 (5)	St. 12 1.34 (5)		St. 14 0.58 (20)		St. 16 13.74 (10)		St. 18 1.30 (30)		St. 20 1.23 (30)	St. 22 1.99 (30)	St. 24 0.90 (30)
Nano	0.67 (0)	0.58 (5)	1.44 (20)		1.19 (15)		2.89 (10)		0.35 (10)		1.36 (30)	0.66 (30)	0.55 (30)
Pico	0.38 (5)	0.24 (0)	0.69 (15)		0.53 (10)		0.28 (10)		0.08 (10)		0.08 (5)	0.31 (20)	0.05 (10)
	CUF												
South Transect													
Micro	St. 1 0.26 (10)	St. 2 0.54 (5)	St. 3 0.15 (15)	St. 4 0.62 (20)	St. 5 2.25 (10)	St. 6 0.25 (10)	St. 7 0.24 (10)	St. 8 0.10 (30)	St. 9 0.16 (30)	St. 10 1.01 (20)	St. 11 1.09 (30)		
Nano	0.97 (5)	0.94 (5)	1.37 (5)	0.94 (5)	1.23 (10)	1.64 (10)	0.95 (30)	0.95 (30)	0.48 (30)	1.10 (20)	1.09 (30)		
Pico	0.68 (10)	1.05 (0)	1.02 (0)	0.40 (0)	0.59 (5)	0.48 (5)	0.29 (20)	0.09 (10)	0.06 (10)	0.06 (5)	0.31 (5)		
	ITE												

937



FIGURA 1

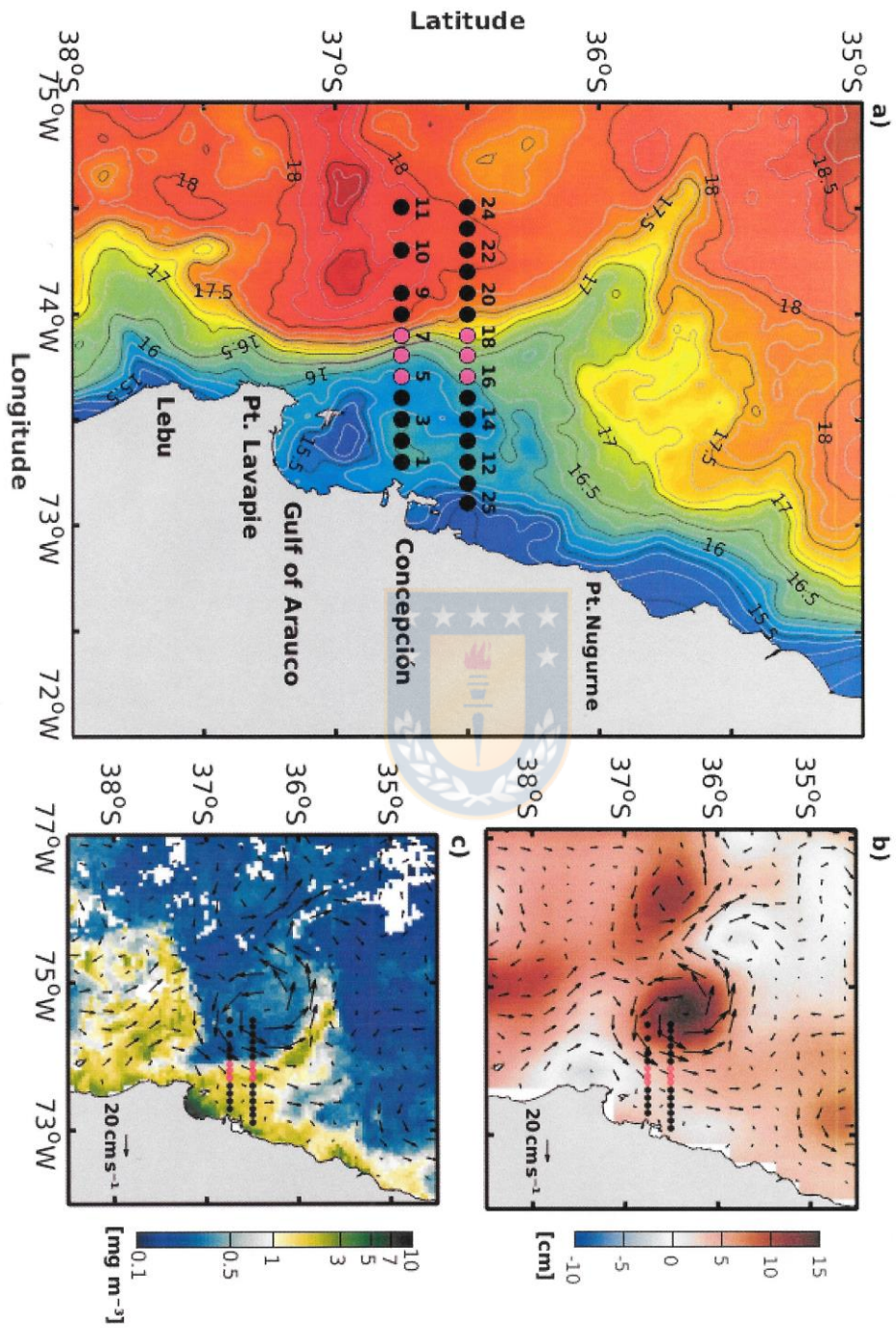


FIGURA 2

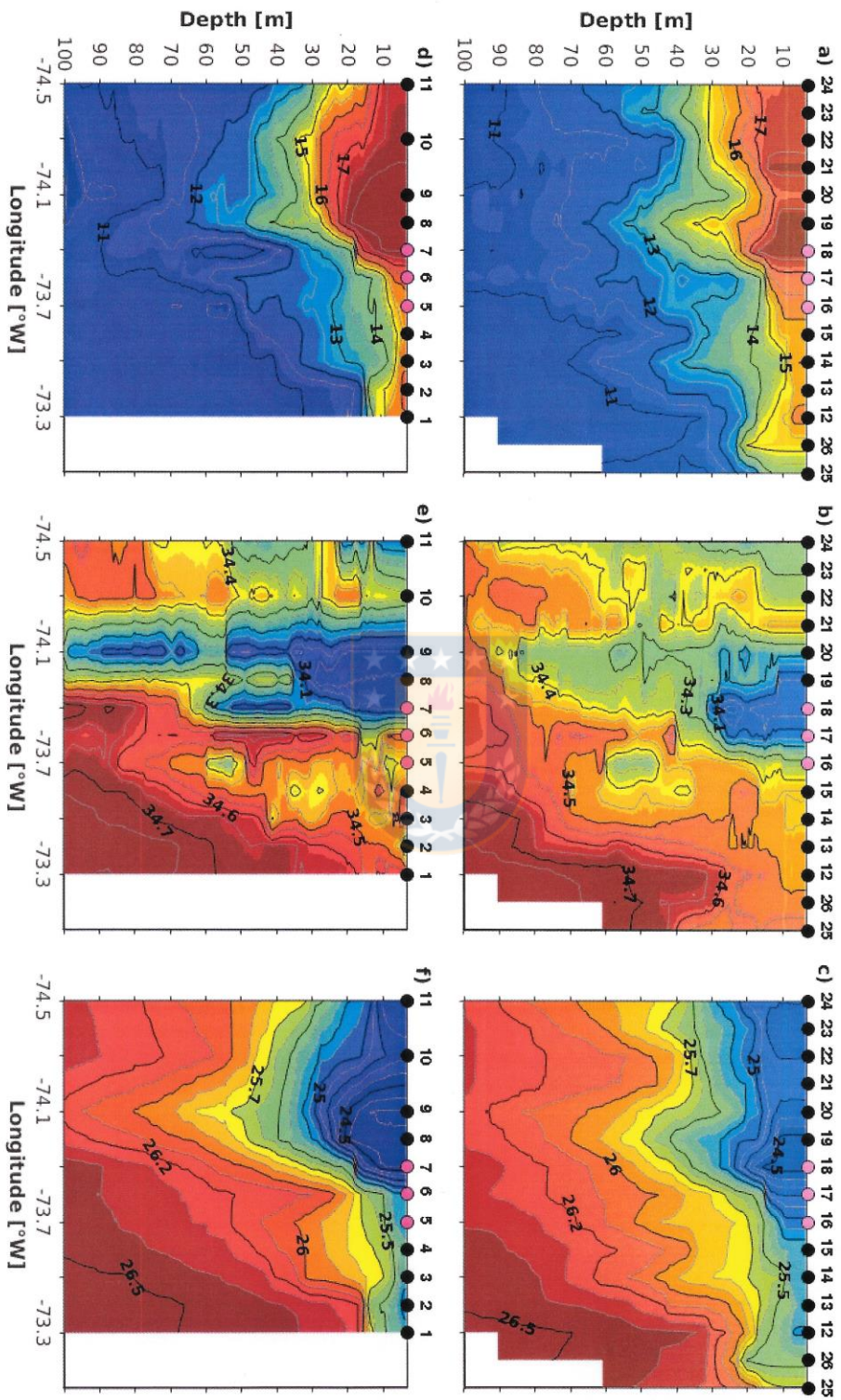


FIGURA 3

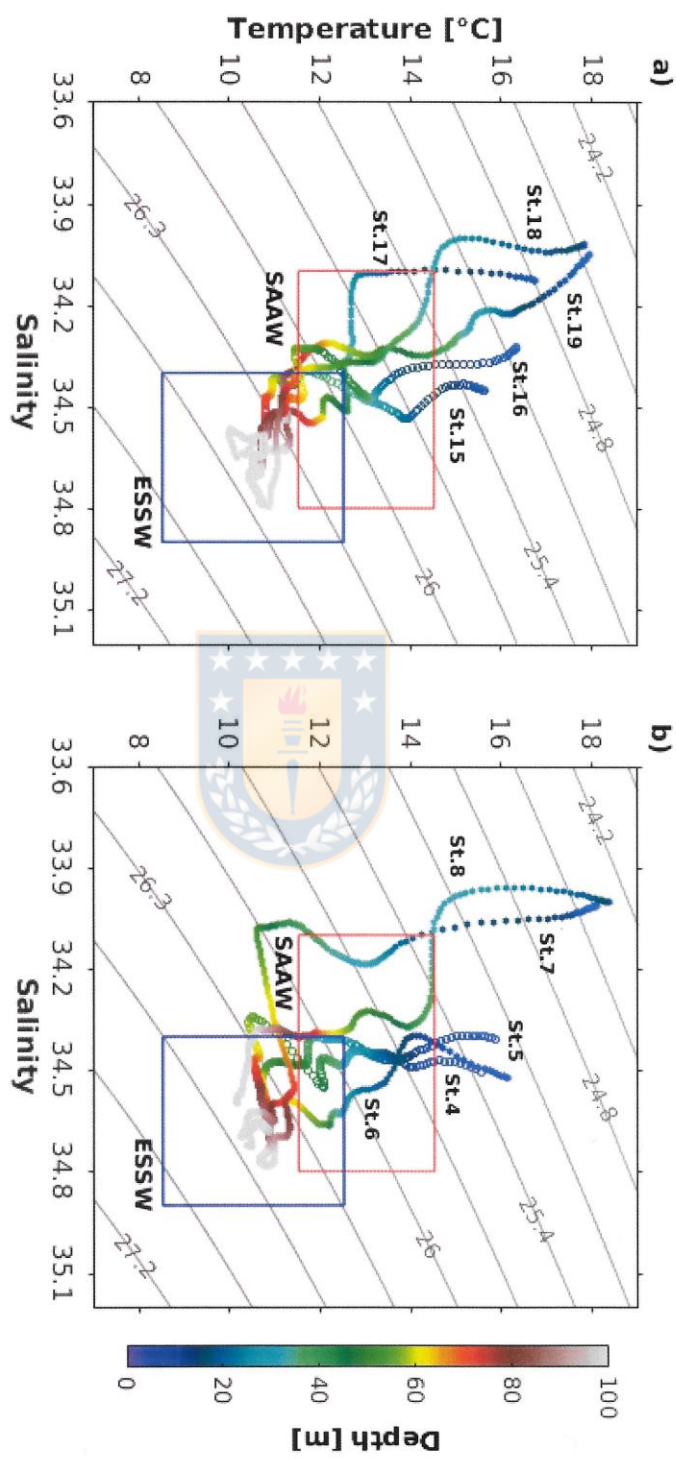


FIGURA 4

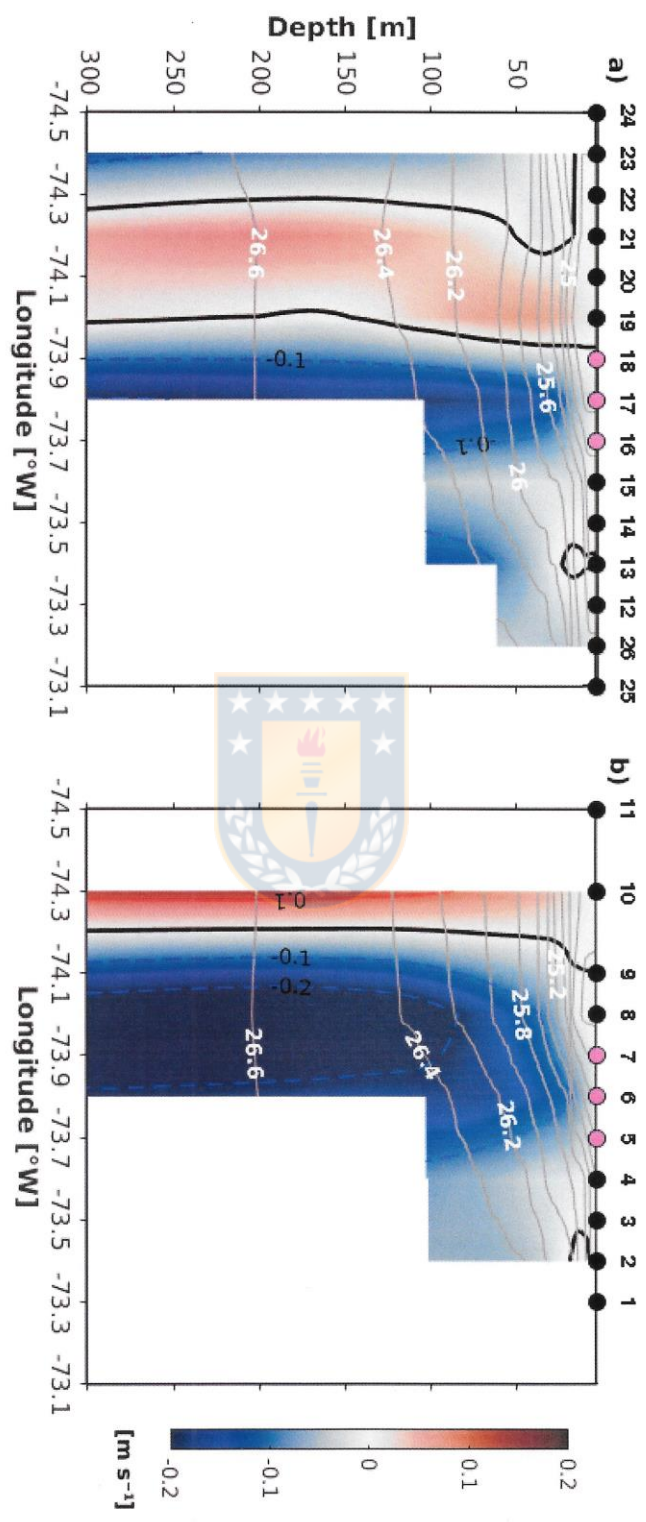


FIGURA 5

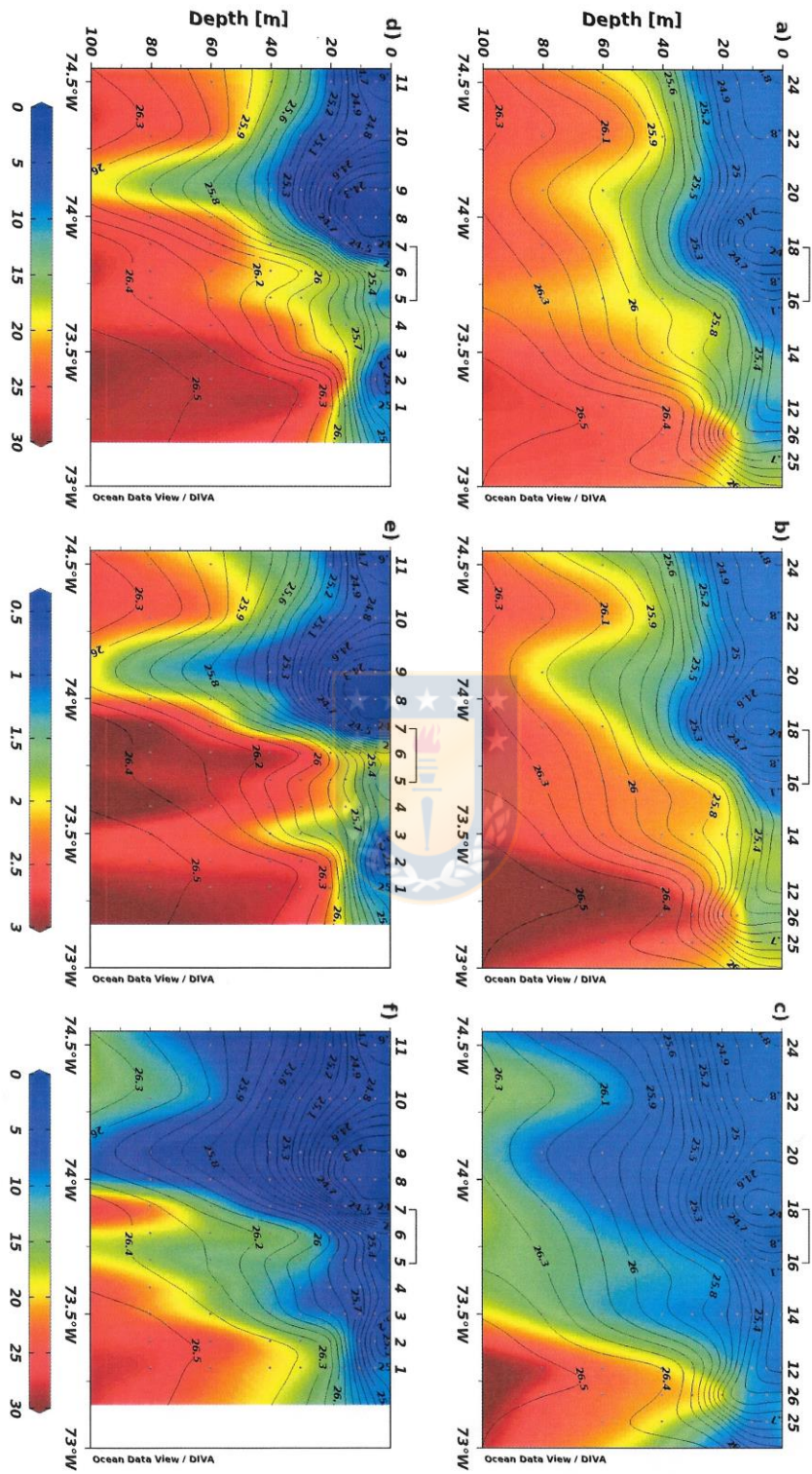


FIGURA 6

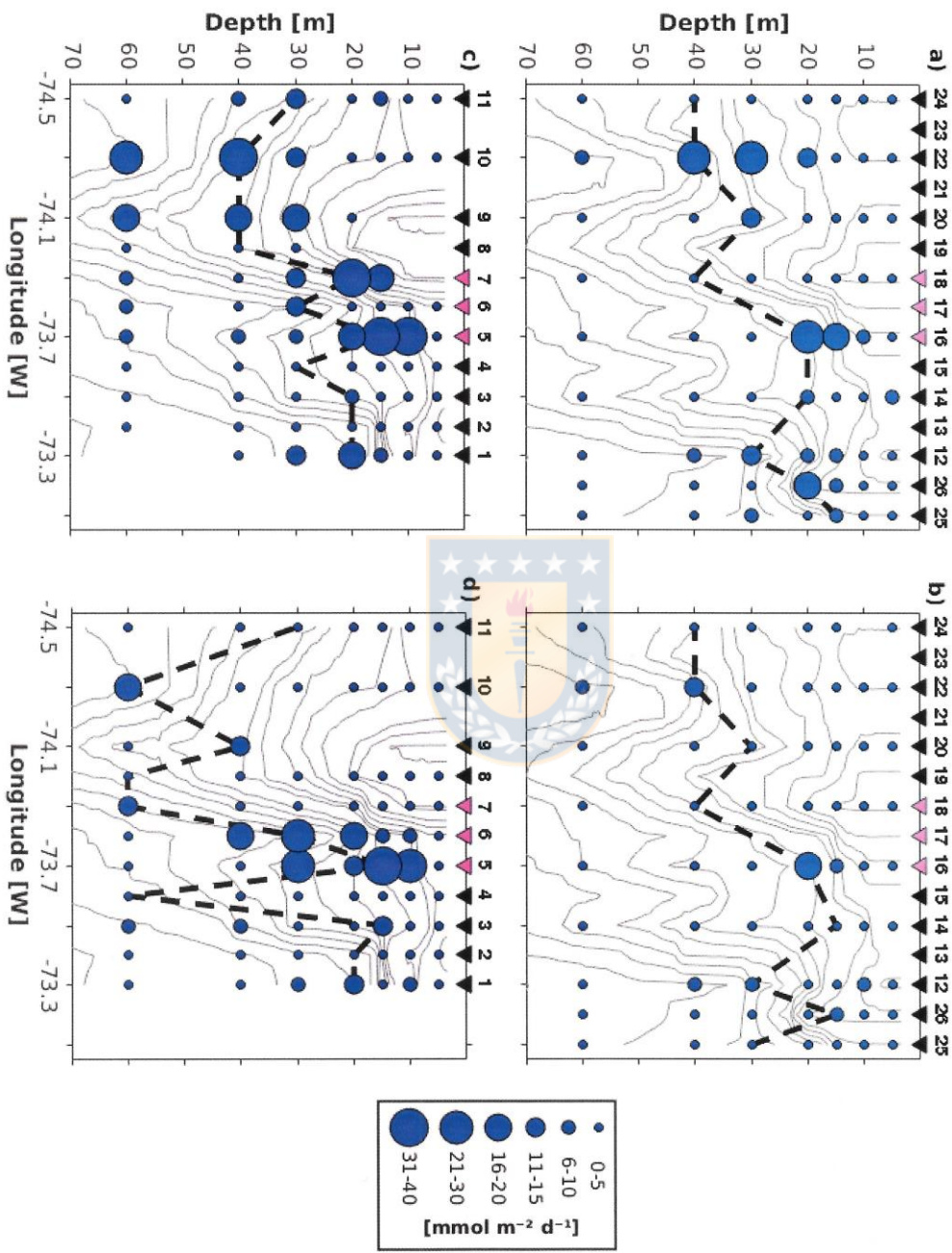


FIGURA 7

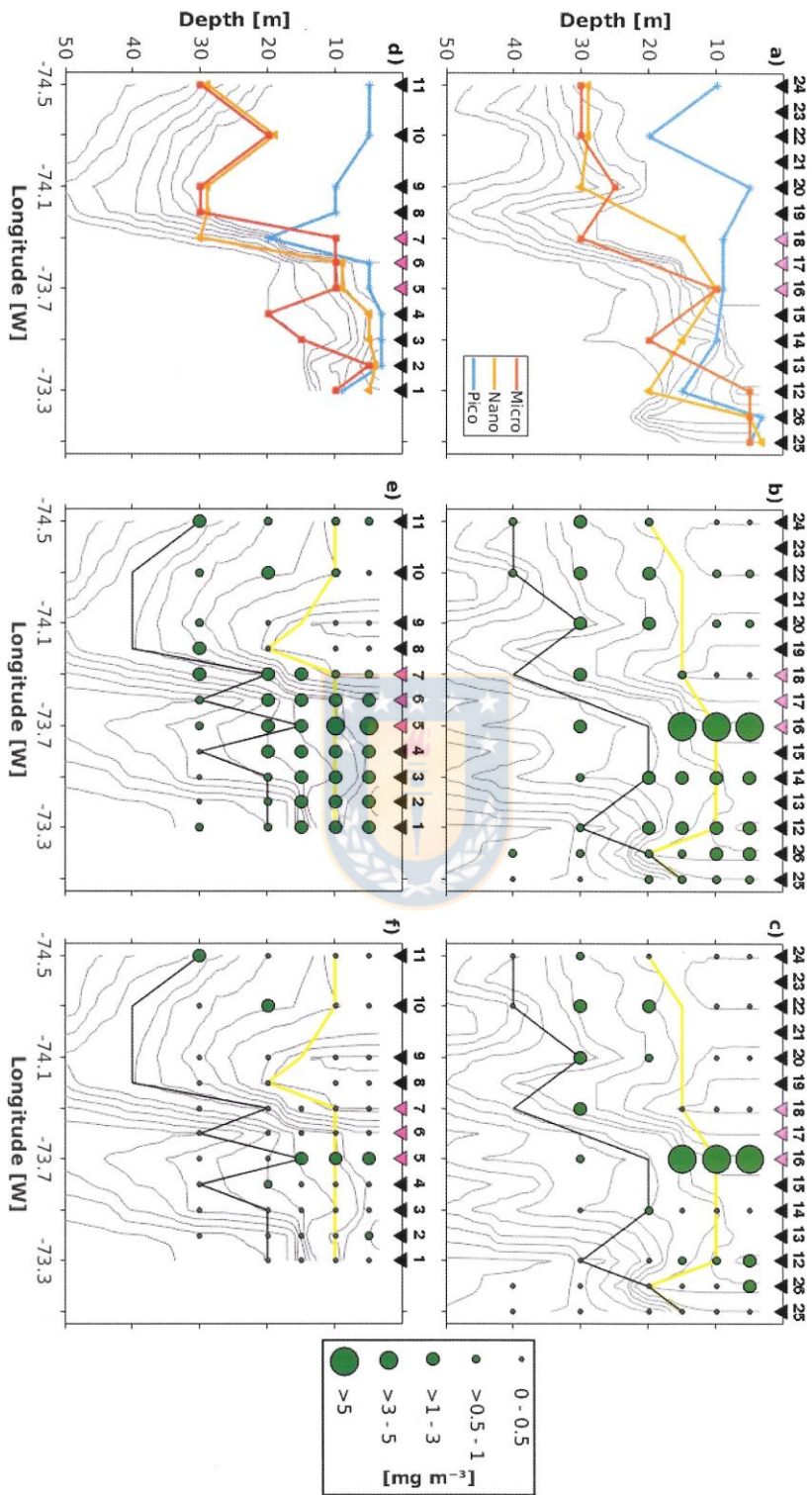
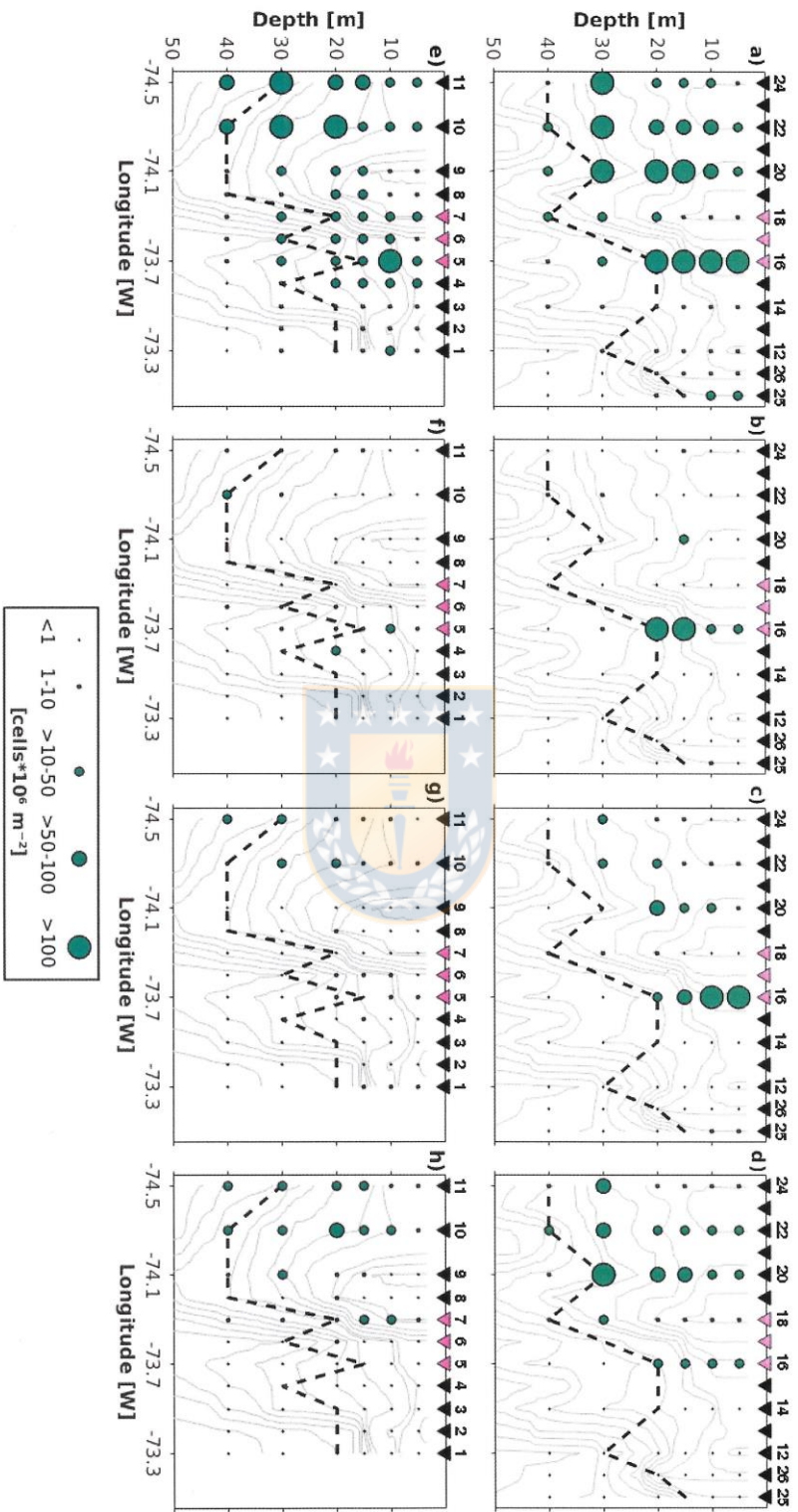


FIGURA 8



5. DISCUSIÓN

En la última década, se ha dado mayor énfasis al desarrollo de aproximaciones que permitan usar los productos satelitales de color del océano (ej. Clo-a total) para obtener datos con alta resolución espacio-temporal del fitoplancton por tamaño, debido a la importancia de la estructura de la comunidad fitoplanctónica como indicador del estado del ecosistema pelágico, su influencia en los ciclos biogeoquímicos marinos, las tasas de utilización de los nutrientes, la producción primaria y la transferencia de energía a los niveles tróficos superiores (Guidi et al., 2009; Finkel et al., 2009; Ward et al., 2012; Marañón, 2015). La mayoría de estas aproximaciones han sido implementadas en aguas oceánicas abiertas, siendo este estudio el primero en parametrizar un modelo de tres componentes (micro-, nano- y picoplancton) en aguas costeras (ZC) y de transición costera (ZTC) para un sistema altamente productivo, como es el caso de la región centro-sur de Chile.

Las diferencias en la parametrización obtenida en este estudio y aquellas previamente reportadas para otras zonas, se basaron principalmente en las características regionales (costa vs. océano) y/o en la técnica utilizada para obtener los datos *in situ* de Clo-a total y fraccionada por tamaño. De acuerdo a esto, las diferencias en los parámetros de concentración máxima asintótica alcanzada por las células fitoplanctónicas pequeñas (C_{NP}^m y C_P^m) estuvieron más influenciadas por el sesgo en las mediciones *in situ* debido a las incertidumbres de la técnica utilizada (filtración, HPCL y/o espectros de absorción). Por otra parte, las diferencias en los parámetros de porcentaje de contribución de las clases de tamaño más pequeñas a la Clo-a total cuando ésta última tiende a cero (D_{NP} y D_P), fueron asociadas con las características regionales debido a la dominancia de la fracción picoplanctónica en aguas oceánicas y de las fracciones nano- y microplanctónica en aguas costeras.

En términos de los estimados satelitales y su comparación con los datos *in situ* en la región centro-sur de Chile, los valores de Clo-a para la fracción microplanctónica mostraron valores de incertidumbre moderados, los cuales pueden estar relacionados con: i) la alta dispersión de las mediciones de concentración de Clo-a por el picoplancton a lo largo del rango completo de Clo-a total, siendo difícil ajustar una función monotónica para esta fracción; ii) los errores en

los estimados satelitales para el picoplancton afectan directamente a la fracción microplanctónica dado que esta última se obtiene al sustraer la concentración de Clo-a por las fracciones nano- y picoplancton de la Clo-a total; iii) la alta dispersión en los valores de Clo-a por el microplancton cuando la Clo-a total es $<1 \text{ mg m}^{-3}$; iv) mayores desviaciones en la relación de la Clo-a por tamaños y la Clo-a total en aguas costeras ópticamente complejas; v) la incertidumbre al comparar datos con diferente escala espacial (píxeles satelitales de 4 km vs. muestras *in situ* de ~250-300 ml de agua); vi) algoritmos regionales de Clo-a total que se basan en mediciones de reflectancias las cuales varían con el tamaño celular; y vii) la profundidad óptica.

Si bien los valores de incertidumbre para este estudio son similares a los reportados en otros estudios al usar el mismo modelo (ej. Brotas et al., 2013; Lin et al., 2014; Brewin et al., 2015; 2017; Ward, 2015), la incertidumbre asociada a la fracción microplanctónica podría representar una limitación para la aplicación de este modelo en la región centro-sur de Chile. Sin embargo, la distribución espacial del fitoplancton por tamaño en la ZC y ZTC es consistente con estudios previos para esta región, en donde a través de mediciones *in situ* han reportado la dominancia del microplancton en la ZC y del nanoplancton en la ZTC (ej. Anabalón et al., 2007; Morales et al., 2007; Morales y Anabalón, 2012). No obstante, al ser esta la primera aproximación para un sistema de surgencia altamente productivo, futuras investigaciones podrían enfocarse en la implementación de diferentes técnicas en las mediciones *in situ* de Clo-a total y fraccionada que conlleven a un menor sesgo al momento de discretizar el fitoplancton por tamaño, además de campañas oceanográficas que permitan incluir un mayor rango de Clo-a tanto en el tiempo (estacionalidad) como en el espacio (eje costa-océano).

5.1. Estructura de la comunidad fitoplanctónica por tamaños al interior de los remolinos de mesoescala

De acuerdo con los resultados presentados en el capítulo 4.1, se acepta la *Hipótesis I*: La variabilidad temporal de la comunidad fitoplanctónica por clases de tamaño al interior de los

remolinos de mesoescala depende de las fases de éstos durante su periodo de vida, las que implican cambios en la concentración de nutrientes en la capa superficial.

Dos fases han sido propuestas para el periodo de vida y desarrollo de los remolinos las cuales son la fase de formación e intensificación y la fase de decaimiento o relajación. A nivel de Clo-a total superficial se ha propuesto que durante la fase de formación-intensificación, los procesos físicos dominantes que modulan la biomasa fitoplanctónica al interior de los remolinos son: i) los procesos de advección horizontal desde y hacia la ZC, y ii) el desplazamiento vertical de las isopícnas por el bombeo según el tipo de remolino (Gaube et al., 2014). En términos de la variabilidad temporal de la estructura de la comunidad fitoplanctónica o ECF en los remolinos evaluados en este estudio (ciclón superficial (sC), anticiclón superficial (sAC) y anticiclones intratermoclina (ssAC1 y ssAC2)), los cambios parecen estar asociados en mayor medida a procesos de surgencia/subsistencia local durante la fase de formación-intensificación (~10 primeras semanas) dependiendo de la naturaleza del remolino, y a los procesos de advección y atrapamiento de nutrientes y plancton durante todo el periodo de vida de estas estructuras de mesoescala.

De acuerdo con el sentido de giro, se espera que los remolinos ciclónicos (anticiclónicos) advecten y atrapen aguas costeras (oceánicas) con alto (bajo) contenido de nutrientes y alta (baja) biomasa fitoplanctónica durante la fase de formación-intensificación del remolino. Además, se espera que estos procesos de advección sean similares en los anticiclones superficiales e intratermoclina, dada su similitud en el sentido de giro (Gaube et al., 2014). Sin embargo, durante esta primera fase y en comparación con los valores encontrados en la ZC, no se observó un aumento de la fracción microplanctónica en el sAC, pero si en los intratermoclina ssAC1 y ssAC2; a pesar de la similitud en el sentido de giro. Por tanto, el aumento del microplancton en ssAC1 y ssAC2, estaría asociado en mayor medida con el desplazamiento local de las isopícnas hacia la capa superficial, promoviendo el flujo de nutrientes y crecimiento de células fitoplanctónicas grandes, similar a lo observado en sC; mientras que, la disminución del microplancton en el sAC estaría asociada con el desplazamiento vertical hacia abajo de las isopícnas, transportando nutrientes y plancton hacia afuera de la capa fótica (Sweeney et al., 2003; Mouriño-Carballido y McGillicuddy, 2006;

McGillicuddy, 2016). Adicionalmente, las proporciones nitrato:silicato (N:Si) cercanas a 1:1 típicas de la ZC para la región de estudio, estarían favoreciendo el crecimiento de microdiatomeas y por tanto el aumento de la fracción microplanctónica cuando los remolinos se encuentran más cerca de la costa (Anabalón et al., 2016).

No obstante, dos criterios permiten también sugerir que los procesos de advección horizontal y atrapamiento de nutrientes y plancton estarían sucediendo a lo largo del periodo de vida completo de los distintos remolinos: i) no se observaron mayores diferencias en la contribución de las distintas fracciones de tamaño a la Clo-a total entre la periferia y el centro de los remolinos, y ii) no se observaron mayores diferencias en ECF durante la fase de relajación-decaimiento (posterior a las primeras ~10 semanas) entre los distintos tipos de remolinos evaluados, es decir, en todos los casos la fracción microplanctónica tiende a disminuir, mientras que, las fracciones nano- y picoplanctónica tienden al aumento y/o a mantenerse casi constante. En relación al primer criterio, para que los remolinos puedan atrapar fluido en su interior se espera que las velocidades rotacionales (periferia) sean mayores que su velocidad de propagación (Flierl, 1981), una condición que ha sido generalmente reportada para los remolinos de mesoescala subtropicales (Chelton et al., 2011). Esta condición implicaría un rápido intercambio de nutrientes y plancton entre la periferia del remolino y las aguas circundantes, facilitando un rápido atrapamiento de estos nutrientes y plancton en el interior del remolino, y por tanto, disminuyendo las diferencias en ECF entre la periferia y el centro de éstos. De igual forma, es importante considerar que los criterios escogidos para delimitar el centro y la periferia de los remolinos pueden implicar que se vean o no diferencias en ECF o que no se aíse completamente la señal del remolino de las aguas circundantes, y por tanto, futuras aproximaciones podrían basarse en distintos radios de muestreo y/o en contornos de velocidad.

En relación al segundo criterio, debido a la naturaleza diferente de los tipos de remolinos evaluados, se espera que durante la fase de relajación-decaimiento el sentido de las isopícnas hacia subducción (surgencia) local en los remolinos ciclónicos e intratermoclina (anticiclónico) generen diferencias en la ECF. En contraste, la similitud observada estaría asociada a la advección y atrapamiento de aguas de la ZTC caracterizadas por bajas

concentraciones de silicato, razones N:Si mayores ($>3:1$) y células fitoplanctónicas pequeñas principalmente nanoplancton (Morales et al., 2012; 2017), independientemente del sentido de giro de los remolinos. Si bien en este estudio los mecanismos físicos no fueron evaluados, la advección y atrapamiento como mecanismo constante de variabilidad temporal de la Clo-a total al interior de los remolinos ha sido previamente reportado en otros SSBO (Gaube et al., 2014) y recientemente en aguas subtropicales del Pacífico Sur (Frenger et al., 2018).

Dado que esta es la primera aproximación en seguir los cambios temporales en la estructura de la comunidad fitoplanctónica al interior de los remolinos de mesoescala en la región centro-sur de Chile, futuras investigaciones deben enfocarse en: i) evaluar los mecanismos por los cuales los distintos tipos de remolinos influyen la variabilidad temporal de la ECF y cómo se relaciona dicha variabilidad con la estacionalidad climática de la región principalmente durante la fase de formación-intensificación de los remolinos, ii) incluir análisis de comparación entre las velocidades de rotación y traslación de los remolinos que permitan inferir cuánto material biológico (plancton) es adveccionado y transportado al interior de éstos, a qué distancia y por cuánto tiempo, iii) analizar otros mecanismos por los cuales los remolinos permiten sostener un determinado grupo de fitoplancton principalmente a mayores distancias de la ZC y que facilitan el acceso de nutrientes a la capa superficial, por ejemplo por mezcla vertical de acuerdo al desplazamiento de estas estructuras de mesoescala. Adicionalmente, es importante tener en cuenta que dado que el modelo satelital utilizado asocia la Clo-a fraccionada con un rango de valores en la Clo-a total, esto podría generar un sesgo en la discretización de la ECF a nivel superficial y por tanto es necesario complementar las observaciones satelitales superficiales con mediciones *in situ* y modelos físicos-biogeoquímicos regionales.

5.2. Distribución del fitoplancton en un área de interacción entre un remolino intratermoclina y el frente de surgencia costera

De acuerdo con los resultados presentados en el capítulo 4.2, se acepta la *Hipótesis II*: La variabilidad espacial de la comunidad fitoplanctónica en la zona costera y de transición costera

depende de la magnitud del flujo vertical de nutrientes por procesos de mezcla diapicna turbulenta, lo que implica una ventaja competitiva para las células fitoplanctónicas grandes cuando estos flujos son máximos hacia la capa fótica.

Las condiciones de temperatura superficial del mar, circulación geostrófica y Clo-a total, en conjunto con la distribución del fitoplancton por tamaño, nutrientes (nitrato, fosfato y silicato) y propiedades físicas (temperatura, salinidad y densidad) de la columna de agua durante un crucero corto en la ZC y ZTC frente a Concepción (36-37°S), indicaron la ocurrencia de un evento de interacción entre un remolino intratermoclina (ITE) y el frente de surgencia costera (FSC). En ambas áreas, en el ITE y en el FSC, se encontró una alta proporción (~40-70%) de la fracción microplanctónica en respuesta a valores máximos de flujo diapicno (es decir entre isopicnas) de nutrientes hacia la capa fótica. Estos flujos fueron máximos por debajo de la capa de mezcla, producto de las inversiones turbulentas en la parte estratificada de la columna de agua (Park et al., 2014). Estos procesos turbulentos facilitan la mezcla diapicna y pueden ser generados por múltiples mecanismos físicos, tales como el cizalle vertical del flujo geostrófico, el rompimiento de ondas internas, inestabilidades ageostróficas y/o por inestabilidades baroclínicas asociadas a los gradientes laterales característicos de las zonas frontales, entre otros (Boccaletti et al., 2007; Gargett y Garner, 2008; Mahadevan y Archer, 2000; Li et al., 2012; Mahadevan, 2016). Adicionalmente, la elevación de las isopicnas por acción del viento en el FSC y por acción de la dinámica física del ITE, facilitan el transporte de masas de agua con alto contenido de nutrientes a la capa superficial, siendo esta distribución un factor clave para la mezcla diapicna dado que esta última depende del gradiente vertical de los nutrientes en la columna de agua.

Considerando que hay dos factores importantes que modulan en mayor medida el crecimiento y la producción primaria del fitoplancton a nivel de sub- y mesoescala en la ZC y ZTC, los cuales son luz y nutrientes, las células fitoplanctónicas en el caso estudiado no habrían estado limitadas por luz. Aunque no se tuvieron datos de este tipo durante el crucero, Testa et al. (2018) reportaron que la profundidad de la capa fótica para la región de estudio durante febrero (periodo del crucero) oscila entre los primeros ~10-30 m de la columna de agua, profundidad en la cual se encontraron los máximos de Clo-a por el microplancton. Estos

resultados son consistentes con estudios que en otras regiones han reportado la presencia de microdiatomeas en zonas frontales, ITEs y alrededor de la picnoclina, en relación con la mezcla turbulenta y el contenido de nutrientes, favoreciendo el crecimiento del microplancton y la acumulación de biomasa (ej. Ledwell et al., 2008; Li et al., 2012; Zhang et al., 2015). No obstante, son pocos los estudios que evalúan la distribución y cambios en la comunidad fitoplanctónica cuando este tipo de estructuras físicas interactúan en los SSBO (ej. Morales et al., 2017).

Dado que la dinámica del océano implica una cascada de energía que fluye desde la circulación de gran escala a escalas más pequeñas, la interacción ITE-FSC puede aumentar la mezcla diapicna turbulenta a nivel de submesoescala, erosionando la estabilidad de la columna de agua y llevando nutrientes a la capa superficial. Recientemente, Lévy et al. (2018) mediante observaciones y modelación numérica, indican que el forzamiento físico de submesoescala afecta directamente las tasas de crecimiento del fitoplancton y la estructura de la comunidad fitoplanctónica. Sin embargo, este es un tema de investigación actual debido a: i) la dificultad de adscribir un único mecanismo físico a los cambios en la estructura del fitoplancton por tamaño; ii) la interrelación de distintos procesos físicos con escalas espacio-temporales similares; y iii) la limitación de mediciones continuas de alta resolución para procesos de submesoescala y pequeña escala (ej. mediciones de microperfilador). Por tanto, esta tesis doctoral es un aporte en este sentido, al asociar la distribución del fitoplancton por tamaño con la variabilidad de submesoescala y el flujo diapicno de nutrientes en la ZC y ZTC durante un evento de interacción ITE-FSC en el SSBO en la región centro-sur de Chile.

Los resultados aquí obtenidos además implican: (i) que en el escenario de cambio climático donde se prevé la intensificación de los vientos favorables a la surgencia en la región centro-sur de Chile y con esto la intensificación del FSC (Garreaud y Falvey, 2008; Oerder et al., 2018), la mezcla turbulenta en la zona frontal estaría favoreciendo el incremento en la producción primaria local por la fracción microplanctónica y la eficiencia de la bomba biológica para esta región en relación con los procesos turbulentos de pequeña escala, y (ii) que si bien a escala interanual se ha visto una débil asociación entre las fases cálida (El Niño) y fría (La Niña) de El Niño Oscilación del Sur (ENSO) con la Clo-a total y la producción

primaria a nivel superficial para esta región (ej. Corredor-Acosta et al., 2015; Testa et al., 2018), el incremento en el número de ITEs durante la fase fría de ENSO propuesto por Combes et al. (2015) implicaría el aumento de Clo-a por la fracción microplanctónica a nivel subsuperficial durante años con eventos La Niña, en respuesta al potencial incremento del flujo diapicno de nutrientes por procesos de mezcla turbulentos en la fase de formación e intensificación de los ITEs cerca de la ZC.



6. CONCLUSIONES

Esta tesis doctoral es una contribución al entendimiento del impacto de la dinámica física de sub- y mesoescala en la distribución del fitoplancton en la región centro-sur de Chile. Los resultados muestran un cambio en la estructura de tamaños de la comunidad fitoplanctónica al interior de los remolinos de mesoescala a medida que éstos se desplazan entre la zona costera y de transición costera. Estos cambios fueron mayores durante los primeros ~2 meses de formación e intensificación de los remolinos, en donde una mayor (menor) contribución de la fracción microplanctónica fue asociada con los remolinos tipo ciclónico e intratermoclina (tipo anticiclónico), en relación con la elevación (hundimiento) de las isopícnas y la entrada (salida) de nutrientes a la capa superficial. Sin embargo, los procesos de advección y atrapamiento de nutrientes y plancton al interior de los remolinos evaluados, estarían sucediendo a lo largo del periodo de vida completo de los distintos remolinos dado que no se observaron mayores diferencias en la contribución de las distintas fracciones de tamaño a la Clo-a total entre la periferia y el centro de los remolinos, ni tampoco mayores diferencias en ECF durante la fase de relajación-decaimiento (posterior a las primeras ~10 semanas) entre los distintos tipos de remolinos evaluados. En consecuencia, los cambios en ECF durante la fase de formación-intensificación de los remolinos, estaría influenciada en mayor medida por la entrada o salida de nutrientes de la capa fótica de acuerdo al bombeo tipo remolino, mientras que los procesos de advección y atrapamiento de nutrientes y plancton sería un mecanismo constante durante el periodo de vida completo de los remolinos, principalmente durante la fase de relajación-decaimiento de éstos.

No obstante, los cambios en ECF durante la fase de formación-intensificación cuando los remolinos se encuentran cerca de la ZC, también están influenciados por la interacción de éstos con otras estructuras físicas tales como el frente de surgencia costera. En este sentido, los resultados obtenidos en un caso de interacción entre un remolino intratermoclina (ITE) y el frente de surgencia costera (FSC) frente a Concepción (36-37°S), muestran flujos verticales máximos de nutrientes en ambas áreas, en respuesta al gradiente vertical de nutrientes en la columna de agua y la alta mezcla diapícnica (entre isopícnas) por procesos turbulentos de

pequeña escala. Estos flujos máximos estuvieron correlacionados con valores máximos de Clo-a por parte del microplancton y máxima abundancia de microdiatomeas, demostrando la importancia de la variabilidad de submesoescala en los nutrientes y de los procesos de mezcla diapicna turbulenta en la configuración de la ECF, al favorecer la entrada de nutrientes a la capa fótica y por ende la ventaja competitiva de las células fitoplanctónicas grandes.

Adicionalmente, esta tesis presenta la aplicación de un modelo de tres componentes (micro-, nano- y picoplancton) para obtener estimados satelitales superficiales de Clo-a por tamaño para la región de estudio. Si bien se encontraron valores de incertidumbre moderados en los estimados satelitales para la fracción microplanctónica, asociados con la alta dispersión de las mediciones *in situ* de Clo-a por el picoplancton para el rango completo de la Clo-a total y del microplancton cuando la Clo-a total tiende a cero, los resultados muestran que el modelo logra capturar la tendencia de las observaciones *in situ* y que los supuestos del modelo se ajustan para esta región altamente productiva. En este sentido, futuras investigaciones deben enfocarse en coleccionar datos *in situ* de Clo-a total y fraccionada por tamaño incluyendo un mayor rango de Clo-a y preferiblemente sin dependencia de las fracciones con la Clo-a total de forma tal que se puedan mejorar este tipo de herramientas de observación satelital, y que puedan ser utilizadas para el forzamiento y validación de modelos biogeoquímicos regionales.

7. REFERENCIAS

- Agustí, S. (2004). Viability and niche segregation of *Prochlorococcus* and *Synechococcus* cells across the Central Atlantic Ocean. *Aquat. Microb. Ecol.* 36: 53–59.
- Aiken, J., N. Hardman-Mountford, R. Barlow, J. Fishwick, T. Hirata, and T. Smyth. 2008. Functional links between bioenergetics and bio-optical traits of phytoplankton taxonomic groups: an overarching hypothesis with applications for ocean colour remote sensing. *J. Plankton Res.* 30(2): 165–181.
- Aiken, J., Y. Pradhan, R. Barlow, S. Lavender, A. Poulton, P. Holligan, and N. Hardman-Mountford. 2009. Phytoplankton pigments and functional types in the Atlantic Ocean: A decadal assessment, 1995–2005. *Deep-Sea Res. II.* 56: 899–917.
- Anabalón, V., C.E. Morales, R. Escribano, and M.A. Varas. 2007. The contribution of nano- and micro-planktonic assemblages in the surface layer (0–30 m) under different hydrographic conditions in the upwelling area off Concepción, central Chile. *Prog. Oceanogr.* 75: 396-414.
- Anabalón, V., C.E. Morales, H.E. González, E. Menschel, W. Schneider, S. Hormazabal, and R. Escribano. 2016. Micro-phytoplankton community structure in the coastal upwelling zone off Concepción (central Chile): Annual and inter-annual fluctuations in a highly dynamic environment. *Prog. Oceanogr.* 149: 174-188.
- Arístegui, J., E.D. Barton, P. Tett, M.F. Montero, M. García-Muñoz, G. Basterretxea, and D. de Armas. 2004. Variability in plankton community structure, metabolism, and vertical carbon fluxes along an upwelling filament (Cape Juby, NW Africa). *Prog. Oceanogr.* 62: 95–113.
- Ascani, F., K.J. Richards, E. Firing, S. Grant, K.S. Johnson, Y. Jia, R. Lukas, and D.M. Karl. 2013. Physical and biological controls of nitrate concentrations in the upper subtropical North Pacific Ocean. *Deep Sea Research Part II: Topical Studies in Oceanography.* 93: 119-134.
- Atlas, E., S. Hager, L. Gordon, and P. Park. 1971. A practical manual for use of the Technicon Autoanalyser in sea water nutrient analyses (Tech. Rep. 215), Corvallis, OR: Department of Oceanography, Oregon State University.
- Barceló-Llull, B., P. Sangrà, E. Pallàs-Sanz, E.D. Barton, S.N. Estrada-Allis, A. Martínez-Marrero, and A. Marrero-Díaz. 2017. Anatomy of a subtropical intrathermocline eddy. *Deep-Sea Res. I.* 124: 126–139.
- Barth, J.A., S.D. Pierce, and T.J. Cowles. 2005. Mesoscale structure and its seasonal evolution in the northern California Current System. *Deep Sea Res. II.* 52(1-2): 5-28.
- Boccaletti, G., R. Ferrari, and B. Fox-Kemper. 2007. Mixed layer instabilities and restratification. *J. Phys. Oceanogr.* 37: 2228-2250.

Brewin, R.J.W., S. Sathyendranath, T. Hirata, S.J. Lavender, R. Barciela, N. Hardman-Mountford. 2010. A three-component model of phytoplankton size class for the Atlantic Ocean. *Ecol. Model.* 221: 1472–1483.

Brewin, R.J., S. Sathyendranath, T. Hirata, S.J. Lavender, R.M. Barciela, and N. Hardman-Mountford. 2012. A three-component model of phytoplankton size class for the Atlantic Ocean. *Ecol. Model.* 221: 1472–1483.

Brewin, R.J.W., S. Sathyendranath, T. Jackson, R. Barlow, V. Brotas, R. Airs, and T. Lamont. 2015. Influence of light in the mixed-layer on the parameters of a three-component model of phytoplankton size class. *Remote Sens. Environ.* 168: 437-450.

Brewin, R.J., S. Ciavatta, S. Sathyendranath, T. Jackson, G. Tilstone, K. Curran, R.L. Airs, D. Cummings, V. Brotas, E. Organelli, et al. 2017. Uncertainty in ocean-color estimates of chlorophyll for phytoplankton groups. *Front. Mar. Sci.* 4, 104.

Bricaud, A., H. Claustre, J. Ras, and K. Oubelkheir. 2004. Natural variability of phytoplanktonic absorption in oceanic waters: Influence of the size structure of algal populations. *J. Geophys. Res.* 109: C11010.

Brink, K.H., and T.J. Cowles. 1991. The coastal transition zone program. *J. Geophys. Res.* 96: 14637-14647.

Brito, A.C., C. Sá, V. Brotas, R.J.W. Brewin, T. Silva, J. Vitorino, T. Platt, and S. Sathyendranath. 2015. Effect of phytoplankton size classes on bio-optical properties of phytoplankton in the Western Iberian coast: Application of models. *Remote Sens. Environ.* 156: 537-550.

Brotas, V., R.J.W. Brewin, C. Sá, A.C. Brito, A. Silva, C.R. Mendes, T. Diniz, M. Kaufmann, G. Tarran, S.B. Groom, et al. 2013. Deriving phytoplankton size classes from satellite data: Validation along a trophic gradient in the eastern Atlantic Ocean. *Remote Sens. Environ.* 134: 66-77.

Bruland, K.W., E.L. Rue, and G.J. Smith. 2001. Iron and macronutrients in California coastal upwelling regimes: Implications for diatom blooms. *Limnol. Oceanogr.* 46: 1661–1674.

Chaigneau, A., G. Eldin, and B. Dewitte. 2009. Eddy activity in the four major upwelling systems from satellite altimetry (1992–2007). *Prog. Oceanogr.* 83, 117–123.

Chelton, D.B., P. Gaube, M.G. Schlax, J.J. Early, and R.M. Samelson. 2011. The influence of nonlinear mesoscale eddies on near-surface oceanic chlorophyll. *Science.* 334: 328–332.

Ciotti, A.M., M.R. Lewis, and J.J. Cullen. 2002. Assessment of the relationships between dominant cell size in natural phytoplankton communities and the spectral shape of the absorption coefficient. *Limnol. Oceanogr.* 47(2): 404–417.

Ciotti, A.M., and A. Bricaud. 2006. Retrievals of a size parameter for phytoplankton and spectral light absorption by coloured detrital matter from water-leaving radiances at SeaWiFS channels in a continental shelf off Brazil. *Limnol. Oceanogr. Methods.* 4: 237–253.

Claustre, H., P. Kerhervé, J.C. Marty, and L. Prieur. 1994. Phytoplankton photoadaptation related to some frontal physical processes. *J. Mar. Syst.* 5(3): 251-265.

Combes, V., S. Hormazabal, and E. Di Lorenzo. 2015. Interannual variability of the subsurface eddy field in the Southeast Pacific. *J. Geophys. Res. Oceans.* 120(7): 4907-4924.

Correa-Ramirez, M.A., S. Hormazabal, and G. Yuras. 2007. Mesoscale eddies and high chlorophyll concentrations off central Chile (29°–39°S). *Geophys. Res. Lett.* L12604.

Correa-Ramirez, M.A., S. Hormazabal, and C.E. Morales. 2012. Spatial patterns of annual and interannual surface chlorophyll-a variability in the Peru-Chile Current System. *Prog. Oceanogr.* 92-95: 8-17. doi:10.1016/j.pocean.2011.07.008.

Corredor-Acosta, A., C.E. Morales, S. Hormazabal, I. Andrade, and M.A. Correa-Ramirez. 2015. Phytoplankton phenology in the coastal upwelling region off central-southern Chile (35° S–38° S): Time-space variability, coupling to environmental factors, and sources of uncertainty in the estimates. *J. Geophys. Res. Oceans.* 120(2): 813-831.

Cotti-Rausch, B.E., M.W. Lomas, E.M. Lachenmyer, E.A. Goldman, D.W. Bell, S.R. Goldberg, and T.L. Richardson. 2016. Mesoscale and sub-mesoscale variability in phytoplankton community composition in the Sargasso Sea. *Deep-Sea Res. I.* 110: 106–122.

Chisholm, S. 1992. Phytoplankton size. In: Falkowski, P.G., Woodhead, A.D. (Eds.), *Primary productivity and biogeochemical cycles in the sea.* Plenum Press, New York, pp. 213–237.

Cullen, J.J., P.J.S. Franks, D.M. Karl, and A. Longhurst. 2002. Physical influences on marine ecosystem dynamics, p. 297-336. In: *The Sea*, Robinson, A.R., McCarthy, J.J., Rothschild, B.J. (Eds.), Volume 12, John Wiley & Sons.

Davis, R.E., M.D. Ohman, D.L. Rudnick, and J.T. Sherman. 2008. Glider surveillance of physics and biology in the southern California Current System. *Limnology and Oceanography.* 53(5part2), 2151-2168.

de Boyer Montégut, C., G. Madec, A.S. Fischer, A. Lazar, and D. Iudicone. 2004. Mixed layer depth over the global ocean: An examination of profile data and a profile-based climatology. *J. Geophys. Res. Oceans.* 109(C12).

Devred, E., S. Sathyendranath, V. Stuart, H. Maas, O. Ulloa, and T. Platt. 2006. A two-component model of phytoplankton absorption in the open ocean: Theory and applications. *J. Geophys. Res.* 111: C03011.

Devred, E., S. Sathyendranath, V. Stuart, and T. Platt. 2011. A three component classification of phytoplankton absorption spectra: Applications to ocean-colour data. *Remote Sens. Environ.* 115(9): 2255–2266.

Finkel, Z.V., J. Beardall, K.J. Flynn, A. Quigg, T.A.V. Rees, and J.A. Raven. 2009. Phytoplankton in a changing world: Cell size and elemental stoichiometry. *J. Plankton Res.* 32: 119–137.

Finkel, Z.V., J. Beardall, K.J. Flynn, A. Quigg, T.A.V. Rees, and J.A. Raven. 2010. Phytoplankton in a changing world: cell size and elemental stoichiometry. *J. Plankton Res.* 32: 119–137.

Flierl, G.R. 1981. Particle motions in large-amplitude wave fields. *Geophysical & Astrophysical Fluid Dynamics.* 18(1-2): 39-74.

Flierl, G.R., and D.J.Jr. McGillicuddy. 2002. Mesoscale and submesoscale physical-biological interactions. In *The Sea, Vol 12: Biological-physical interactions in the sea*, ed. AR Robinson, JJ McCarthy, BJ Rothschild, pp. 113-185. New York: Wiley & Sons.

Franks, P.J.S., and L. Walstad. 1997. Phytoplankton patches at fronts: A model of formation and response to wind events. *J. Marine Res.* 55: 1-29.

Frenger, I., M. Münnich, and N. Gruber. 2018. Imprint of Southern Ocean mesoscale eddies on chlorophyll. *Biogeosciences.* 15: 4781-4798.

Furnas, M.J. 1990. In situ growth rates of marine phytoplankton: approaches to measurement, 646 community and species growth rates. *J. Plankton Res.* 12(6): 1117-1151.

Gargett, A., and T. Garner. 2008. Determining Thorpe scales from ship-lowered CTD density profiles. *Journal of Atmospheric and Oceanic Technology.* 25(9): 1657-1670.

Garreaud, R.D., and M. Falvey. 2009. The coastal winds off western subtropical South America in future climate scenarios. *International Journal of Climatology.* 29(4): 543-554.

Gaube, P., D.J. McGillicuddy, D.B. Chelton, M.J. Behrenfeld, and P.G. Strutton. 2014. Regional variations in the influence of mesoscale eddies on near-surface chlorophyll. *J. Geophys. Res. Oceans.* 119: 8195–8220.

Girault, M., H. Arakawa, A. Barani, H.J. Ceccaldi, F. Hashihama, and G. Gregori. 2015. Heterotrophic prokaryote distribution along a 2300 km transect in the North Pacific

subtropical gyre during a strong La Niña conditions: relationship between distribution and hydrological conditions. *Biogeosciences*. 12(11): 3607-3621.

Goldman, J.C., and D.J.Jr. McGillicuddy. 2003. Impact of large marine diatoms growing at low light on episodic new production. *Limnol. Oceanogr.* 48: 1176–1182.

Grachev, Y., M. Koshlyakov, T. Tikhomirova, and Y. Yenikejev. 1979. Synoptic eddy field in the POLYMODE area. *Polymode News* (69).

Gruber, N., Z. Lachkar, H. Frenzel, P. Marchesiello, M. Münnich, J.C. McWilliams, and G.K. Plattner. 2011. eddy-induced reduction of biological production in eastern boundary upwelling systems. *Nat. Geosci.* 4: 787–792.

Guidi, L., L. Stemann, G.A. Jackson, F. Ibanez, H. Claustre, L. Legendre, M. Picheral, and G. Gorsky. 2009. Effects of phytoplankton community on production, size and export of large aggregates: A world-ocean analysis. *Limnol. Oceanogr.* 54(6): 1951–1963.

He, Q., H. Zhan, S. Cai, and G. Zha. 2016. On the asymmetry of eddy-induced surface chlorophyll anomalies in the southeastern Pacific: The role of eddy-Ekman pumping. *Prog. Oceanogr.* 141: 202–211.

Hirata, T., N. Hardman-Mountford, R.J.W. Brewin, J. Aiken, R. Barlow, K. Suzuki, et al. 2011. Synoptic relationships between surface chlorophyll-a and diagnostic pigments specific to phytoplankton functional types. *Biogeosciences*. 8: 311–327.

Hormazabal, S., G. Shaffer, and O. Leth. 2004. Coastal transition zone off Chile. *J. Geophys. Res. Oceans*. 109.

Hormazabal, S., V. Combes, C.E. Morales, M.A. Correa-Ramirez, E. Di Lorenzo, and S. Nuñez. 2013. Intrathermocline eddies in the coastal transition zone off central Chile (31-41°S). *J. Geophys. Res. Oceans*. 118: 4811-4821.

IOCCG (2014). *Phytoplankton Functional Types from Space*. Sathyendranath, S. (ed.), Reports of the International Ocean-Colour Coordinating Group, No. 15, IOCCG, Dartmouth, Canada.

Johnston, T.M.S., D.L. Rudnick, and E. Pallàs-Sanz. 2011. Elevated mixing at a front. *J. Geophys. Res.* 116: C11033. doi:10.1029/2011JC007192.

José, Y.S., H. Dietze, and A. Oschlies. 2017. Linking diverse nutrient patterns to different water masses within anticyclonic eddies in the upwelling system off Peru. *Biogeosciences*. 14(6): 1349-1364.

Kara, A.B., P.A. Rochford, and H.E. Hurlburt. 2000. An optimal definition for ocean mixed layer depth. *J. Geophys. Res. Oceans*. 105(C7): 16803-16821.

Karl, D.M., M.J. Church, J.E. Doreb, R.M. Letelier, and C. Mahaffey. 2012. Predictable and efficient carbon sequestration in the North Pacific Ocean supported by symbiotic nitrogen fixation. *PNAS*. 109, doi:10.1073/pnas.1120312109.

Karrasch, B., H.G. Hoppe, S. Ullrich, and S. Podewski. 1996. The role of mesoscale hydrography on microbial dynamics in the northeast Atlantic: Results of a spring bloom experiment. *J. Mar. Res.* 54: 99-122.

Landeira, J.M., B. Ferron, M. Lunven, P. Morin, L. Marié, and M. Sourisseau. 2014. Biophysical interactions control the size and abundance of large phytoplankton chains at the Ushant tidal front. *PloS ONE*. 9(2): e90507, doi: 10.1371/journal.pone.0090507.

Lamont, T., R. Barlow, and R. Brewin. 2018. Variations in Remotely-Sensed Phytoplankton Size Structure of a Cyclonic Eddy in the Southwest Indian Ocean. *Remote Sensing*. 10(7): 1143.

Ledwell, J.R., A.J. Watson, and C.S. Law. 1998. Mixing of a tracer in the pycnocline. *J. Geophys. Res. Oceans*. 103(C10): 21499-21529.

Ledwell, J.R., D.J.Jr. McGillicuddy, and L.A. Anderson. 2008. Nutrient flux into an intense deep chlorophyll layer in a mode-water eddy. *Deep Sea Research Part II: Topical Studies in Oceanography*. 55(10-13): 1139-1160.

Le Queré, C., S.P. Harrison, C.I. Prentice, E.T. Buitenhuis, O. Aumont, L. Bopp, H. Claustre, et al. 2005. Ecosystem dynamics based on plankton functional types for global ocean biogeochemistry models. *Global Change Biol.* 11, doi:10.1111/j.1365-2486.2005.1004.x.

Letelier, J., O. Pizarro, and S. Nuñez. 2009. Seasonal variability of coastal upwelling and the upwelling front off central Chile. *J. Geophys. Res.* 114: C12009. <http://dx.doi.org/10.1029/2008JC005171>.

Lévy, M., P.J. Franks, and K.S. Smith. 2018. The role of submesoscale currents in structuring marine ecosystems. *Nature communications*. 9(1), 4758.

Li, Q.P., P.J. Franks, M.D. Ohman, and M.R. Landry. 2012. Enhanced nitrate fluxes and biological processes at a frontal zone in the southern California current system. *J. Plankton Res.* 34(9): 790-801.

Lima, I.D., D.B. Olson, and S.C. Doney. 2002. Biological response to frontal dynamics and mesoscale variability in oligotrophic environments: Biological production and community structure. *J. Geophys. Res.* 107, doi:10.1029/2000JC000393.

- Lin, J., W. Cao, G. Wang, and S. Hu. 2014. Satellite-observed variability of phytoplankton size classes associated with a cold eddy in the South China Sea. *Mar. Pollut. Bull.* 83: 190-197.
- Macías, D., A. Rodríguez-Santana, E. Ramírez-Romero, M. Bruno, J.L. Pelegrí, P. Sangrà, B. Aguiar-González, B., and C.M. García. 2013. Turbulence as a driver for vertical plankton distribution in the subsurface upper ocean. *Sci. Mar.* 77: 541-549, doi: 10.3989/scimar.03854.03A.
- Mahadevan, A., and D. Archer. 2000. Modeling the impact of fronts and mesoscale circulation on the nutrient supply and biogeochemistry of the upper ocean. *J. Geophys. Res.* 105: 1209-25.
- Mahadevan, A., and A. Tandon. 2006. An analysis of mechanisms for submesoscale vertical motion at ocean fronts. *Ocean Model.* 14: 241–256.
- Mahadevan, A. 2016. The impact of submesoscale physics on primary productivity of plankton. *Annu. Rev. Mar. Sci.* 8: 161-84.
- Marañón, E., and E. Fernández. 1995. Changes in phytoplankton ecophysiology across a coastal upwelling front. *J. Plankton Res.* 17(10): 1999-2008, doi: 10.1093/plankt/17.10.1999.
- Marañón, E. 2015. Cell size as a key determinant of phytoplankton metabolism and community structure. *Ann. Rev. Mar. Sci.* 7: 241–264.
- Margalef, R. (1978). Life forms of phytoplankton as survival alternatives in an unstable environment. *Oceanologica Acta* 1: 439–509.
- Mason, E., A. Pascual, and J.C. McWilliams. 2014. A new sea surface height–based code for oceanic mesoscale eddy tracking. *J. Atmos. Ocean. Technol.* 31: 1181-1188.
- McDougall, T.J., and P.M. Barker. 2011. Getting started with TEOS-10 and the Gibbs Seawater (GSW) Oceanographic Toolbox, 28pp. SCOR/IAPSO WG127, ISBN 978-0-646-55621-5.
- McGillicuddy, D.J.Jr., A.R. Robinson, D.A. Siegel, H.W. Jannasch, R. Johnson, T.D. Dickey, J. McNeil, A.F. Michaels, and A.H. Knap. 1998. Influence of mesoscale eddies on new production in the Sargasso Sea. *Nature.* 394: 263–266.
- McGillicuddy, D.J.Jr., L.A. Anderson, N.R. Bates, T. Bibby, K.O. Buesseler, et al. 2007. Eddy/wind interactions stimulate extraordinary mid-ocean plankton blooms. *Science.* 316: 1021–1026.

McGillicuddy, D.J.Jr. 2016. Mechanisms of physical-biological-biogeochemical interaction at the oceanic mesoscale. *Annu. Rev. Mar. Sci.* 8: 125–159.

Moore II, T.S., R.J. Matear, J. Marra, and L. Clementson. 2007. Phytoplankton variability off the Western Australian Coast: Mesoscale eddies and their role in cross-shelf exchange. *Deep-Sea Res. II.* 54: 943–960.

Morales, C.E., H.E. González, S. Hormazabal, G. Yuras, J. Letelier, and L.R. Castro. 2007. The distribution of chlorophyll-a and dominant planktonic components in the coastal transition zone off Concepción, central Chile, during different oceanographic conditions. *Prog. Oceanogr.* 75: 452–469.

Morales, C.E., and V. Anabalón. 2012. Phytoplankton biomass and microbial abundances during the spring upwelling season in the coastal area off Concepción, central-southern Chile: Variability around a time series station. *Prog. Oceanogr.* 92: 81-91.

Morales, C.E., S. Hormazabal, M.A. Correa-Ramírez, O. Pizarro, N. Silva, C. Fernandez, V. Anabalón, and M.L. Torreblanca. 2012. Mesoscale variability and nutrient-phytoplankton distributions off central-southern Chile during the upwelling season: The influence of mesoscale eddies. *Prog. Oceanogr.* 104: 17-29. doi:10.1016/j.pocean.2012.04.015.

Morales, C.E., V. Anabalón, J.P. Bento, S. Hormazabal, M. Cornejo, M.A. Correa-Ramírez, and N. Silva. 2017. Front-Eddy Influence on Water Column Properties, Phytoplankton Community Structure, and Cross-Shelf Exchange of Diatom Taxa in the Shelf-Slope Area off Concepción (36–37°S). *J. Geophys. Res. Oceans.* 122: 8944–8965.

Morel, A., and A. Bricaud. 1981. Theoretical results concerning light absorption in a discrete medium, and application to specific absorption of phytoplankton. *Deep-Sea Res.* 28: 1375–1393.

Mouriño-Carballido, B., and D.J. McGillicuddy. 2006. Mesoscale variability in the metabolic balance of the Sargasso Sea. *Limnol. Oceanogr.* 51: 2675–2689.

Oerder, V., J.P. Bento, C.E. Morales, S. Hormazabal, and O. Pizarro. 2018. Coastal Upwelling Front Detection off Central Chile (36.5–37°S) and Spatio-Temporal Variability of Frontal Characteristics. *Remote Sensing.* 10(5): 690; doi:10.3390/rs10050690.

Osborn, T.R. 1980. Estimates of the local rate of vertical diffusion from dissipation measurements. *Journal of Physical Oceanography.* 10(1): 83-89.

Park, Y.H., J.H. Lee, I. Durand, and C.S. Hong. 2014. Validation of Thorpe-scale-derived vertical diffusivities against microstructure measurements in the Kerguelen region. *Biogeosciences.* 11(23): 6927-6937.

Pegliasco, C., A. Chaigneau, and R. Morrow. 2015. Main eddy vertical structures observed in the four major Eastern Boundary Upwelling Systems. *J. Geophys. Res. Oceans.* 120: 6008-6033.

Pelegrí, J.L., J. Arístegui, L. Cana, M. González-Dávila, A. Hernández-Guerra, S. Hernández-León, and S. Santana-Casiano. 2005. Coupling between the open ocean and the coastal upwelling region off northwest Africa: Water recirculation and offshore pumping of organic matter. *J. Mar. Syst.* 54: 3–37.

Platt, T., H. Bouman, E. Devred, C. Fuentes-Yaco, and S. Sathyendranath. 2005. Physical forcing and phytoplankton distributions. *Sci. Mar.* 69: 55–73.

Platt, T., and S. Sathyendranath. 2008. Ecological indicators for the pelagic zone of the ocean from remote sensing. *Remote Sens. Environ.* 112: 3426-3436. doi:10.1016/j.rse.2007.10.016.

Pond, S., and G.L. Pickard. 2013. *Introductory dynamical oceanography*. 2nd edition. Elsevier.

Reul, A., V. Rodríguez, F. Jiménez-Gómez, J.M. Blanco, B. Bautista, et al. (2005). Variability in the spatio-temporal distribution and size-structure of phytoplankton across an upwelling area in the NW-Alboran Sea, (W-Mediterranean). *Cont. Shelf Res.* 25(5-6): 589-608.

Rodríguez, J., J. Tintoré, J.T. Allen, J.M. Blanco, D. Gomis, et al. 2001. Mesoscale vertical motion and the size structure of phytoplankton in the ocean. *Nature.* 410: 360-363.

Sangrà, P., C. García-Muñoz, C.M. García, A. Marrero-Díaz, C. Sobrino, and B. Mouriño-Carballido. 2014. Coupling between upper ocean layer variability and size-fractionated phytoplankton in a non-nutrient-limited environment. *Mar Ecol Prog Ser.* 499: 35-46.

Sathyendranath, S., G. Cota, V. Stuart, H. Maass, and T. Platt. 2001. Remote sensing of phytoplankton pigments: A comparison of empirical and theoretical approaches. *Int. J. Remote Sens.* 22: 249-273.

Sathyendranath, S., and T. Platt. 2007. Spectral effects in bio-optical control on the ocean system. *Oceanologia.* 49(1): 5–39.

Shaffer, G., S. Hormazabal, O. Pizarro, and S. Salinas. 1999. Seasonal and interannual variability of currents and temperature off central Chile. *J. Geophys. Res. Oceans.* 104: 29951-29961.

Sieburth, J.M., V. Smetacek, and J. Lenz. 1978. Pelagic ecosystem structure: Heterotrophic compartments of the plankton and their relationship to plankton size fractions. *Limnology and oceanography.* 23(6): 1256-1263.

Sobarzo, M., L. Bravo, D. Donoso, J. Garcés-Vargas, and W. Schneider. 2007. Coastal upwelling and seasonal cycles that influence the water column over the continental shelf off central Chile. *Prog. Oceanogr.* 75: 363–382.

Sweeney, E.N., D.J.Jr. McGillicuddy, and K.O. Buesseler. 2003. Biogeochemical impacts due to mesoscale eddy activity in the Sargasso Sea as measured at the Bermuda Atlantic Time-series Study (BATS). *Deep-Sea Res. II.* 50: 3017–3039.

Testa, G., I. Masotti, and L. Farias. 2018. Temporal Variability in Net Primary Production in an Upwelling Area off Central Chile (36°S). *Frontiers in Marine Science.* 5, 179.

Uitz, J., H. Claustre, A. Morel, and S.B. Hooker. 2006. Vertical distribution of phytoplankton communities in open ocean: an assessment based on surface chlorophyll. *J. Geophys. Res.* 111: C08005.

Uitz, J., Y. Huot, F. Bruyant, M. Babin, and H. Claustre. 2008. Relating phytoplankton photophysiological properties to community structure on large scales. *Limnol. Oceanogr.* 53(2): 614–630.

Wang, L., B. Huang, K.P. Chiang, X. Liu, B. Chen, Y. Xie, Y. Xu, J. Hu, and M. Dai. 2016. Physical-biological coupling in the western South China Sea: The response of phytoplankton community to a mesoscale cyclonic eddy. *PLoS ONE.* 11, e0153735.

Ward, B.A., S. Dutkiewicz, O. Jahn, and M.J. Follows. 2012. A size-structured food-web model for the global ocean. *Limnol. Oceanogr.* 57: 1877–1891.

Ward, B.A. 2015. Temperature-correlated changes in phytoplankton community structure are restricted to polar waters. *PLoS ONE.* 10, e0135581.

Zhang, Y., J. Bellingham, J. Ryan, and M. Godin. 2015. Evolution of a physical and biological front from upwelling to relaxation. *Cont. Shelf Res.* 108: 55-64. <http://dx.doi.org/10.1016/j.csr.2015.08.005>.